

The quest for the solar g modes

T.Appourchaux · K. Belkacem ·
A.-M. Broomhall · W.J. Chaplin ·
D.O. Gough · G. Houdek · J. Provost ·
F. Baudin · P. Boumier · Y. Elsworth ·
R.A. García · B.Andersen · W.Finsterle ·
C.Fröhlich · A.Gabriel · G.Grec ·
A.Jiménez · A.Kosovichev · T.Sekii ·
T.Toutain · S.Turck-Chièze

November 26, 2024, *Revision : Final*

T. Appourchaux · F. Baudin · P. Boumier · A. Gabriel
Institut d'Astrophysique Spatiale, UMR8617, Bâtiment 121, 91045 Orsay Cedex, France
E-mail: Thierry.Appourchaux@ias.u-psud.fr

K. Belkacem
Institut d'Astrophysique et Géophysique, Université de Liège, Allée du 6 Août 17-B 4000 Liège,
Belgium

A.-M. Broomhall · W.J. Chaplin · Y. Elsworth
School of Physics and Astronomy, University of Birmingham, Edgbaston, Birmingham B15
2TT, UK

D.O. Gough
Institute of Astronomy and Department of Applied Mathematics and Theoretical Physics,
University of Cambridge, Cambridge CB30HA, UK

G. Houdek
Institute of Astronomy, University of Vienna, Türkenschanzstraße 17, A-1180 Vienna, Austria
Institute of Astronomy, University of Cambridge, Cambridge CB30HA, UK

J. Provost and G. Grec
Université de Nice Sophia-Antipolis, CNRS, Laboratoire Cassiopée, Observatoire de la Côte
d'Azur, BP4229, 06304 Nice Cedex4, France

R.A. García · S. Turck-Chièze
Laboratoire AIM, CEA / DSM - CNRS, Université Paris Diderot, IRFU / SAp, Centre de
Saclay, 91191 Gif-sur-Yvette, France

B.N. Andersen
Norwegian Space Centre, N-0212 Oslo, Norway

W.Finsterle · C.Fröhlich
Physikalisch-Meteorologisches Observatorium Davos, World Radiation Center, 7260 Davos
Dorf, Switzerland

A. Jiménez
Instituto de Astrofisica de Canarias, E-38205 La Laguna, Tenerife, Spain.

A. Kosovichev
W.W. Hansen Experimental Physics Laboratory, Stanford University, Stanford, CA 94305,
USA

T. Sekii
National Astronomical Observatory of Japan, 2-21-1 Osawa, Mitaka, Tokyo 181-8588, Japan

”A ce compte, toutes les sciences ne seraient que des applications inconscientes du calcul des probabilités ; condamner ce calcul, ce serait condamner la science tout entière.”

”From this point of view all the sciences would only be unconscious applications of the calculus of probabilities. And if this calculus be condemned, then the whole of the sciences must also be condemned.”

Henri Poincaré, 1914, *La Science et l'hypothèse*

Abstract Solar gravity modes (or g modes) – oscillations of the solar interior for which buoyancy acts as the restoring force – have the potential to provide unprecedented inference on the structure and dynamics of the solar core, inference that is not possible with the well observed acoustic modes (or p modes). The high amplitude of the g-mode eigenfunctions in the core and the evanescence of the modes in the convection zone make the modes particularly sensitive to the physical and dynamical conditions in the core. Owing to the existence of the convection zone, the g modes have very low amplitudes at photospheric levels, which makes the modes extremely hard to detect. In this paper, we review the current state of play regarding attempts to detect g modes. We review the theory of g modes, including theoretical estimation of the g-mode frequencies, amplitudes and damping rates. Then we go on to discuss the techniques that have been used to try to detect g modes. We review results in the literature, and finish by looking to the future, and the potential advances that can be made – from both data and data-analysis perspectives – to give unambiguous detections of individual g modes. The review ends by concluding that, at the time of writing, there is indeed a consensus amongst the authors that *there is currently no undisputed detection of solar g modes.*

Keywords Sun · theory · data analysis · g modes

1 Introduction

The detection of solar oscillations by Leighton et al. (1962) marked the start of a memorable era for solar physics, and the birth of a new field, helioseismology. The oscillatory motions detected in the solar atmosphere had typical periods of about five minutes, and Deubner (1975) subsequently verified observationally that the oscillations were the visible manifestation of acoustic (p) modes trapped in cavities in the solar interior. Later in the 1970s, Claverie et al. (1979) showed that the Sun supported truly global modes of oscillation. The low-angular-degree (low- l) modes observed by Claverie et al. (1979) penetrated the solar core, and had therefore opened a window on the structure of the deep interior of the Sun. Grec et al. (1980) subsequently made long-duration observations of the Sun from the South Pole, providing the very first clean power spectrum free from day-night interruptions.

While inference on the internal structure of the Sun made using high-quality data on the p modes has gone from strength to strength over the intervening 30 years, attempts to detect g modes have proven altogether more elusive. This is in stark contrast with the ubiquitous detection of stellar g modes across the Hertzsprung-Russell diagram such as in white dwarfs (Winget & Kepler 2008), in subdwarfs B stars (Green et al.

T. Toutain
Center for Information Technology, University of Oslo, P.O. Box 1059 Blindern, N-0316 Oslo, Norway

2003), in B stars (Waelkens 1991) and in γ Dor stars (Aerts et al. 1998). The detection, and subsequent exploitation, of data on the solar g modes would provide much more precise inference on the structure and dynamics of the solar core than is possible with p modes. This is because the g modes are trapped in cavities in the radiative interior, and they may have much higher displacement amplitude in the radiative zone / core than their acoustic counterparts. However, this high sensitivity to the core properties comes at a price. Because the g modes are trapped beneath the convective envelope they have very low amplitudes at the photospheric level where the perturbations due to the oscillations are detected; hence their elusive nature.

The first attempt to detect long-period oscillations date back to the mid 1970s, e.g., Severnyi et al. (1976). Further claims, from ground-based Doppler velocity observations, were made in the 1980s, e.g., Delache & Scherrer (1983). It was realized very early on in the development of helioseismology as a field that a space mission would be ideally suited not only for observing the p modes but also for detecting g modes (in principle providing the long-term stability needed to detect the low-frequency g modes). The DISCO¹ mission was proposed by Bonnet et al. (1981) primarily as an irradiance mission to which helioseismology was added later on. The initial design was subsequently modified to accommodate several in-situ instruments and spectrographs, and finally matured into the SOHO² mission (Domingo et al. 1995).

One of the goals of the helioseismology instruments on SOHO was to detect g modes. Following its launch in 1995 December, initial analyses of the helioseismology data failed to uncover evidence for the modes. By 1997, it was realized that the searches would benefit greatly from an internationally coordinated effort comprised of the principal observational and theoretical scientists involved in g-mode research. This led to the formation of the Phoebus Group, which has been working since to use all available high-quality helioseismic data, and to develop the analysis techniques that are required, to detect g modes.

In this review we collect and summarize the knowledge accumulated by the Phoebus group over more than a decade of g-mode research. Our review is broken down as follows. In Section 2 we review the theoretical properties of the solar oscillations. [A complete presentation of the properties of solar and stellar oscillations may be found for example in Unno et al. (1989), Christensen-Dalsgaard & Berthomieu (1991), and Christensen-Dalsgaard (2002a).] We also consider the accuracy of the theoretical computations of the g mode frequencies, and detail the various factors that contribute to the uncertainties (i.e., the accuracy of the oscillation computations themselves, and the sensitivity of the frequencies to the structure and dynamics of the solar models).

In Section 3 we discuss the excitation and damping of the g modes, again from a theoretical perspective. We consider the different physical mechanisms that can potentially contribute to the stability of g modes, and present theoretical estimates of the amplitudes of g modes excited stochastically by convection in the convective envelope.

In Section 4, we turn to the observations. We begin by considering the different detection techniques that are available to observers, and discuss in detail the constituent elements required to “build” a front-to-end analysis algorithm. Our presentation quite naturally includes an in-depth discussion of frequency-domain analysis, and hypothesis testing (frequentist versus Bayesian). We finish this section by reviewing (from the literature) attempts to apply these techniques to detect g modes.

¹ Dual Spectral Irradiance and Solar Constant Orbiter

² SOLar and Heliospheric Observatory

Finally, in Section 5, we conclude with some remarks on the current state of play. Our view is that, at the time of writing, there is no unambiguous evidence for the detection of solar g modes, although some of the most recent theoretical predictions suggest a positive result may be attainable in the near future. We therefore finish by looking to the future prospects for finally detecting g modes.

2 Eigenfrequencies for the solar model

The Sun can show oscillations whose restoring forces are due either to compressibility or to buoyancy. Compressibility gives rise to acoustic waves: resonant pressure (p) modes in the high-frequency range (typically about 3000 μ Hz). The effects of buoyancy can give rise to internal gravity (g) modes, which have very low frequencies, and are the focus of this review. The so-called f modes (surface gravity waves) and mixed modes (having dual p- and g-mode characteristics) occur at frequencies around the transition between g modes and p modes.

2.1 Properties of gravity modes

2.1.1 General properties (adiabatic)

The Sun, as a mass of compressible self-gravitating gas, can oscillate around its equilibrium state. The small-amplitude oscillations displayed by the Sun may be described by spherical harmonic functions, $Y_l^m(\theta, \phi)$, of degree l and order m where (θ, ϕ) are spherical polar co-ordinates, θ being colatitude (i.e., the angle from the polar axis) and ϕ longitude. For example, for a singlet, the perturbation of a thermodynamical quantity like the Eulerian pressure perturbation p' can be written:

$$p' = \tilde{p}(r)Y_l^m(\theta, \phi)e^{-2\pi i\nu_{n,l,m}t}, \quad (1)$$

where $\nu_{n,l,m}$ is the cyclic oscillation frequency (which may be related to the angular frequency by $\omega = 2\pi\nu$). The displacement vector of the material from its equilibrium position ξ may be written, in the frame of polar spherical coordinates, as:

$$\xi = \left(\xi_r(r)Y_l^m, L^{-1}\xi_h(r)\frac{d}{d\theta}Y_l^m, imL^{-1}\xi_h(r)\frac{Y_l^m}{\sin\theta} \right) e^{-2\pi i\nu_{n,l,m}t}, \quad (2)$$

ξ_r and ξ_h being related to the radial and horizontal components of the displacement and $L = \sqrt{l(l+1)}$. Each mode is characterized by three numbers, n, l, m : the radial order n is essentially the number of nodes³ of the radial displacement eigenfunction from centre to surface in the radial direction, the degree l is related to the horizontal wavelength of a mode, and corresponds to the number of nodal lines on the solar surface, and the magnitude of the azimuthal order m , where m satisfies $-l \leq m \leq l$, is twice the number of nodes in longitude (e.g. Unno et al. 1989; Christensen-Dalsgaard & Berthomieu 1991; Gough 1993). If the Sun were spherically symmetric (no rotation and no magnetic fields) the frequency $\nu_{n,l,m}$ of a mode would not depend on the azimuthal order m .

³ At the limit of low and high frequency, the radial order n is essentially the number of nodes of the radial displacement in a solar model. But the classification of modes, i.e. the assignment of a radial order to them, may be more complicated depending on the frequency range (case of mixed modes) and on the model (e.g. Eckart 1960; Scuflaire 1974; Osaki 1975; Takata 2006).

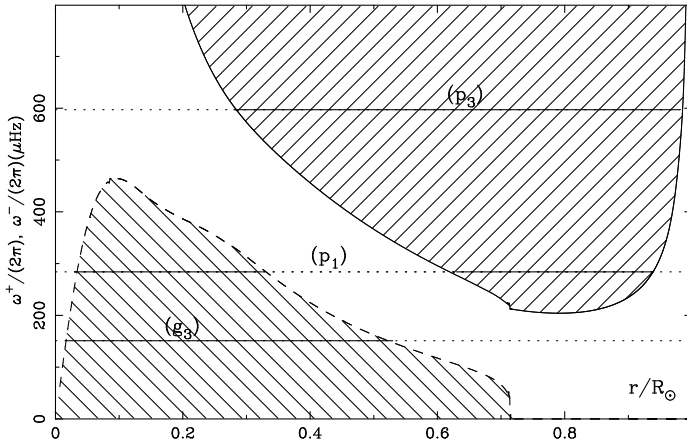


Fig. 1 Propagation diagram for a reference solar model. The solid and dashed curves represent, respectively, the real values $\omega^+/2\pi$ and $\omega^-/2\pi$ corresponding to zero values of $K^2(r)$, and are plotted as a function of the radius, for $l=1$. The hatched areas indicate p-mode and g-mode propagation regions for this degree. The full horizontal lines indicate the propagation regions of three modes of degree $l=1$: a p mode of frequency $\nu \simeq 600\mu\text{Hz}$ (p_3), a g mode of frequency $\nu \simeq 150\mu\text{Hz}$ (g_3), and a mixed mode of frequency $\nu \simeq 280\mu\text{Hz}$ (p_1). The corresponding eigenfunctions of these modes are shown in Figure 2.

The solar oscillations have two restoring forces, compressibility and buoyancy, characterized respectively by the sound speed c and the buoyancy (Brunt-Väisälä) frequency N :

$$c^2 = \frac{\gamma_1 p}{\rho}, \quad N^2 = g \left[\frac{1}{\gamma_1 p} \frac{dp}{dr} - \frac{1}{\rho} \frac{d\rho}{dr} \right], \quad (3)$$

Here, g , p and ρ are, respectively, the gravity acceleration, the pressure, and the density of the solar model, r is the radius, and γ_1 is the adiabatic exponent. In order to have an insight into the relation between the oscillations and the structure of the model, one may consider a simplified wave equation, which provides an approximate description of the oscillations (Deubner & Gough 1984). If the wavelength is much less than the solar radius, the local effects of spherical geometry on the dynamics can be ignored. This equation is then derived under the local wave-like approximation JWKB⁴, and under the Cowling approximation, i.e. where the perturbation to the gravitational potential by the waves is neglected. The equation is

$$\frac{d^2\Psi}{dr^2} + K(r)\Psi = 0 \quad (4)$$

with

$$K(r) \equiv k_r^2 = \frac{1}{c^2} \left[\omega^2 - \omega_c^2 - S_l^2 \left(1 - \frac{N^2}{\omega^2} \right) \right] \quad (5)$$

The quantity Ψ is related to the displacement of the wave, via $\Psi = c^2 \rho^{1/2} \text{div}\xi$. ω_c and H are, respectively, the Lamb and the acoustic cut-off angular frequencies, and

⁴ JWKB stands for Jeffreys-Wentzel-Kramers-Brillouin (Jeffreys 1925). See also Gough (2007) in the asteroseismic context.

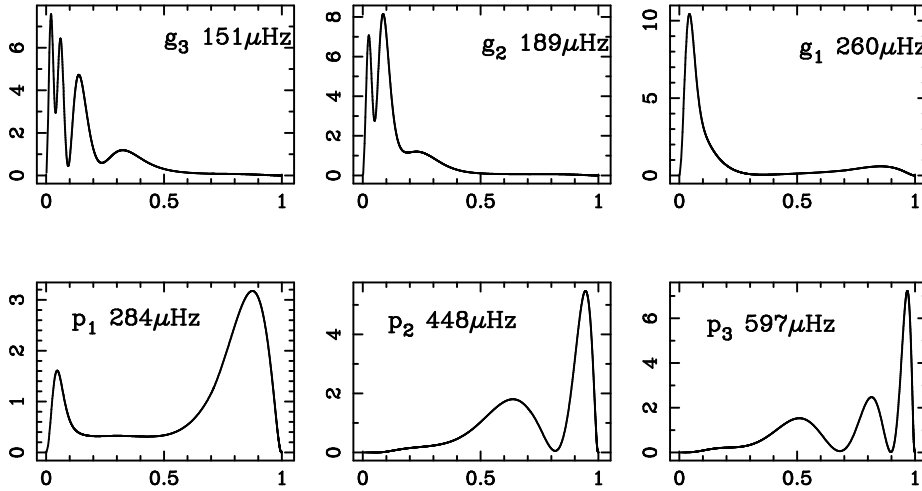


Fig. 2 Kinetic energy density (i.e. $\rho r^2 |\xi|^2$ normalized by the inertia $\mathcal{I}_{n,l}$), as function of the radius for modes g_3 , g_2 , g_1 , p_1 , p_2 and p_3 of degree $l=1$, as computed for a reference solar model. From Provost et al. (2000).

the density scale height:

$$S_l = \sqrt{l(l+1)} \frac{c}{r} \quad \omega_c^2 = \frac{c^2}{4H^2} \left(1 - 2 \frac{dH}{dr} \right) \quad H = - \left(\frac{1}{\rho} \frac{d\rho}{dr} \right)^{-1} \quad (6)$$

In this plane-wave approximation, k_r represents a local radial wave number, which may be associated with a local horizontal wave number, $k_h = L/r$. In the wave equation, the term in N^2 is the signature of the buoyancy, which acts as restoring force only in the radiative regions (where $N^2 > 0$). The stratification in density close to the solar surface induces an acoustic cut-off angular frequency, ω_c , which corresponds to an upper limit to the frequencies of trapped, radial modes ($l = 0$).

Equation (4) shows that a mode will oscillate as a function of r in regions where $K(r) > 0$. Such regions are called regions of propagation. In contrast, a mode will be evanescent, i.e. its energy will vary exponentially, in regions where $K(r) < 0$. $K(r)$ is positive either for $\omega > (\omega^+, \omega^-)$ or $\omega < (\omega^+, \omega^-)$, the angular frequencies ω^+ and ω^- corresponding to the zeros of $K(r)$. ω^+ and ω^- are close to S_l and N respectively, except in the external layers where ω^+ is close to ω_c and ω^- is very small. The frequencies ω^+ and ω^- are plotted, as functions of the radius, in the so-called propagation diagram, for a solar model (Figure 1). The horizontal lines represent modes; they are continuous in the propagating regions and dotted in the evanescent regions. There are two possible regions of propagation, according the frequency of the modes: a high frequency region ($\omega \gtrsim S_l, \omega_c$) corresponding to pressure modes (or p modes) resulting from the compressibility, and a low frequency region ($\omega \lesssim N$) corresponding to internal gravity modes caused by the buoyancy. In between, some modes, called mixed modes, can experience a substantial restoring force from both the gradient of pressure and buoyancy.

In the high-frequency range, which corresponds to observed solar oscillations, the modes are acoustic modes, and their properties depend mainly on the variation of the

sound speed $c(r)$. Their radial wave number k_r is

$$k_r \sim \sqrt{\frac{\omega^2}{c^2} \left(1 - \frac{S_l^2}{\omega^2}\right)}. \quad (7)$$

Thus these modes obey the classical dispersion relation $k_r^2 + k_h^2 \sim \frac{\omega^2}{c^2}$, and the frequencies increase with the radial order n . Owing to the increase of the sound speed towards the solar interior, the p modes are refracted at the level where $\omega = S_l$. Thus, they are trapped in a cavity between that level and the surface. The lower the degree of the mode, the more deeply it penetrates the solar interior. An example of a trapping region is indicated in Figure 1 for the p mode with $n = 3$ and $l = 1$. Figure 2 shows how the amplitudes of various modes vary within the solar interior.

In the low frequency range, we are dealing with gravity modes (g modes), for which buoyancy in radiative zones (N^2 positive) provides the restoring force. Their radial wave number is given by:

$$k_r \sim k_h \frac{N}{\omega}. \quad (8)$$

The properties of these modes therefore depend principally on N , and the frequencies decrease with increasing radial order n . Because g modes oscillate in regions where their frequencies are smaller than the Brunt-Väisälä frequency, g modes are confined in the solar radiative zone and core (see Figure 1 and Figure 2). Low-degree gravity modes have much larger displacements in the horizontal than the vertical, the opposite of what is shown by p modes.

The g modes are attenuated in the convection zone with a factor proportional to r_{cz}^L , r_{cz} being the radius at the base of the convection zone (Christensen-Dalsgaard 1980; Berthomieu & Provost 1990), so that low-degree g modes may be easier to detect than their higher-degree cousins. We shall see in the next subsection that the frequency spectrum shown by the g modes is manifested as a pattern of roughly equidistant periods for modes of given degree l .

In an intermediate frequency range between 200 and 400 μHz , there are low radial-order g modes, f modes (surface gravity oscillations that have no radial nodes) and p₁ modes (a mode with one radial node). Some of the modes, called mixed modes, have a pronounced mixed character, i.e. they have amplitude both in the central layers, like g modes, and in the external layers, like p modes (e.g. mode p₁ ($l = 1$) in Figure 2). The properties of mixed modes have been studied in detail by Provost et al. (2000). The mixed character of these modes appears very clearly when we look at their inertiae, $\mathcal{I}_{n,l}$. The inertia may be written

$$\mathcal{I}_{n,l} = \int_V \rho \boldsymbol{\xi} \cdot \boldsymbol{\xi} dV, \quad (9)$$

where the eigenfunctions $\boldsymbol{\xi}$ are normalized at the surface of the Sun and where the integral is taken over the whole volume of the Sun. Figure 3 plots the normalised kinetic energy of the modes, which is proportional to the mode inertia, as a function of frequency. Under the assumption of equipartition of the energy in the modes, the surface amplitudes would be approximately inversely proportional to the square root of the mode energy (e.g. Berthomieu & Provost 1990).

For g modes with frequencies less than 200 μHz , the lower the degree, the smaller is the energy, and the higher is the surface amplitude. Around 280 μHz , modes of mixed character have smaller energies and therefore higher surface amplitudes than modes

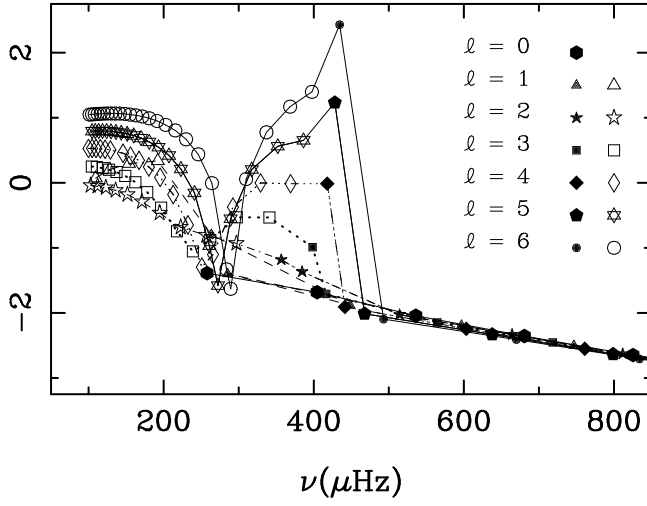


Fig. 3 Logarithm of the normalized energy $\omega^2 \mathcal{I}_{n,l}$ of low-frequency g and mixed modes (open symbols) and low-frequency p modes (filled symbols) for a reference solar model M1 of Provost et al. (2000), plotted as a function of frequency, for modes of degree $l=0, 1, 2, 3, 4, 5$ and 6 . (The normalization is taken assuming that the modes have equal amplitudes at the photospheric level, where the temperature equals the effective temperature level). Note the transition from p to g modes around $450 \mu\text{Hz}$, and the existence of a set of modes of mixed character around $280 \mu\text{Hz}$, having lower energies than modes in the neighbouring frequency regions Provost et al. (2000).

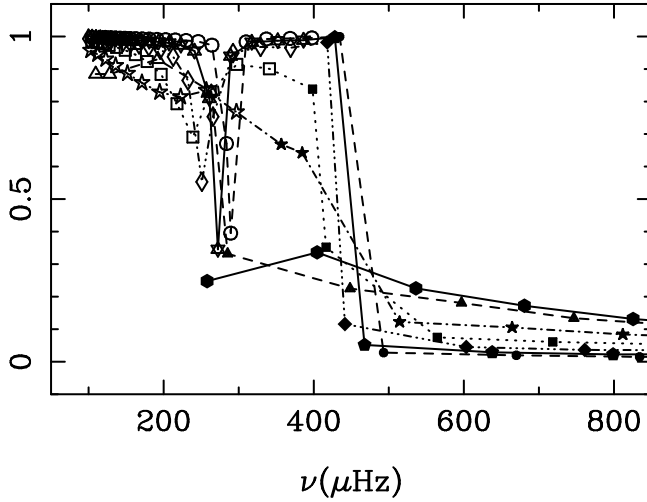


Fig. 4 Relative contribution of the buoyancy restoring force to the frequency, $\mathcal{K}_2/(\mathcal{K}_1 + \mathcal{K}_2)$. \mathcal{K}_1 and \mathcal{K}_2 are defined in Eq. (10), for the same modes, model, and symbols in Figure 3. From Provost et al. (2000).

adjacent in frequency. We discuss the excitation and damping mechanisms of g modes in detail in Section 3.

The frequencies of the oscillation modes may be expressed using a variational principle (e.g. Unno et al. 1989). Neglecting surface terms and the perturbation of the gravitational potential, we have:

$$(2\pi\tilde{\nu})^2 \sim \frac{1}{\mathcal{I}_{n,l}} \int \left(\frac{\tilde{p}^2}{\gamma_1 p} \right) dr + \frac{1}{\mathcal{I}_{n,l}} \int N^2 \xi_r^2 \rho r^2 dr \equiv \frac{(\mathcal{K}_1 + \mathcal{K}_2)}{\mathcal{I}_{n,l}}, \quad (10)$$

where the Eulerian pressure perturbation, \tilde{p} , is given by $\tilde{p} = \rho r \omega^2 L^{-1} \xi_h$. The quantities \mathcal{K}_1 and \mathcal{K}_2 correspond, respectively, to the contributions to the frequency of pressure and buoyancy forces.

Figure 4 shows the variation of $\mathcal{K}_2/(\mathcal{K}_1 + \mathcal{K}_2)$ as a function of the frequency, for the modes of a reference solar model. As expected, for p modes there is a dominant contribution to the frequency from the “acoustic” term \mathcal{K}_1 , while for g modes it is the the “buoyancy” term, \mathcal{K}_2 , which dominates. Mixed modes, between 200 and 450 μHz , have frequencies defined by significant contributions from both terms.

2.1.2 Asymptotic approximation

Low-degree g modes with cyclic frequencies less than $\nu_{n,l} \leq 200 \mu\text{Hz}$ may be described by an asymptotic relation (Vandakurov 1968; Tassoul 1980; Olver 1956). For small frequency, the second-order asymptotic expression for the period $P_{n,l}$ ($P_{n,l} = 1/\nu_{n,l}$) can be represented by:

$$P_{n,l} \sim \bar{P}_{n,l} = \frac{P_0}{L} \left(n + l/2 - \frac{1}{4} + \vartheta \right) + \frac{P_0^2}{\bar{P}_{n,l}} \frac{L^2 V_1 + V_2}{L^2}, \quad (11)$$

$$\text{with } P_0 = \frac{2\pi^2}{\int_0^{r_{cz}} (N/r) dr}, \quad (12)$$

$$V_1 = \frac{1}{P_0} \lim_{r_\varepsilon \rightarrow 0} \left(\int_{r_\varepsilon}^{r_{cz}} \frac{dr}{N(r)} - \frac{1}{N(\varepsilon)} \right) \quad \text{and} \quad L^2 = l(l+1). \quad (13)$$

Here, ϑ is a phase factor sensitive to the properties of the layers lying below the convection zone (Provost & Berthomieu 1986; Ellis 1986). If N^2 is assumed to vanish proportionally to $(r_{cz} - r)^p$ for some power p at the base of the convection zone, ϑ tends at low-frequency to a constant $-0.5/(p+2)$ (see also for details Berthomieu & Provost 1991). For the standard solar model, a linear behaviour of N^2 may be assumed and ϑ tends to $-1/6$. The second-order coefficient V_1 depends on the Brunt-Väisälä frequency. V_2 depends in a more complicated way on the stratification (Berthomieu & Provost 1991).

In sum, the above tells us that the frequencies of g modes are related closely to the Brunt-Väisälä frequency, particularly through P_0 and V_1 . Typical values of P_0 , V_1 , and V_2 for a reference solar model are, $P_0 \sim 35$ to 36 min, $V_1 \sim 0.4$ and $V_2 \sim 5.7$.

The periods of g modes of a given degree l are proportional, in the first order, to P_0/L . The separation in period between modes adjacent in n is therefore almost equidistant. In the low-frequency asymptotic limit, the relative frequency difference of

two modes of the same degree, l , and same radial order, n , from two different models is equal to:

$$\frac{\delta\nu_{n,l}}{\nu_{n,l}} = -\frac{\delta P_{n,l}}{P_{n,l}} \sim -\frac{\delta P_0}{P_0}. \quad (14)$$

Detailed comparisons of the numerical periods and the asymptotic periods (Provost & Berthomieu 1986; Christensen-Dalsgaard & Berthomieu 1991) have allowed checks to be made of the validity of the asymptotic formula. A least-squares fit minimising $\Sigma_{n,l}(P_{n,l}-\bar{P}_{n,l})^2$, for g modes of degrees $l = 1, 2, 3, 4$ and radial order $n_{\min} \leq n \leq n_{\max}$, allows the values of P_0 , V_1 , V_2 , and ϑ , to be estimated. It has been shown that by varying the values of n_{\min} and n_{\max} – for example n_{\min} from 10 to 15 and n_{\max} from 27 to 35 – and by taking the mean values of the results for the global quantities, it is possible to determine from a set of numerical periods the quantities P_0 and V_1 , related to the structure of the inner radiative zone. The values of P_0 and V_1 are then shown to be very close to their asymptotic values.

Similar good agreement is shown between the numerical periods $P_{n,l}$ and the asymptotic periods $\bar{P}_{n,l}$. The fractional agreement is of order 10^{-3} or less for radial orders larger than 10, that is for frequencies less than $60 \mu\text{Hz}$ at $l = 1$, and for frequencies less than $100 \mu\text{Hz}$ at $l = 2$. At lower radial orders, the effects of the third-order terms and of the non-constant ϑ , which are neglected here, may account for fractional differences of up to $5 \cdot 10^{-3}$.

These asymptotic properties of g modes may be exploited in attempts to detect the modes, i.e., by searching for signatures of near-regular patterns in period, as we shall discuss in detail in Section 4.

2.1.3 Effect of rotation : splittings, rotation kernels

The rotation of the Sun induces a splitting of each multiplet frequency $\nu_{n,l}$ into $2l+1$ separate singlet frequencies $\nu_{n,l,m}$, where m is the azimuthal order of the oscillation ($-l \leq m \leq l$). We define the splitting as:

$$\sigma_{n,l,m} = (\nu_{n,l,m} - \nu_{n,l,0}). \quad (15)$$

The effects of the Coriolis force and distortions of the model must also be considered. The angular velocity Ω is small compared with the characteristic frequency $\Omega_g = \sqrt{GM/R^3}$ ($\Omega/\Omega_g \sim 5 \times 10^{-3}$), so that the distortion of the model, which depends on $(\Omega/\Omega_g)^2$, may usually be neglected. Generally a first-order analysis in the ratio Ω/ω is adequate to compute the rotational splittings (Cowling & Newing 1949; Ledoux 1951). In this first-order approximation, the splittings in an inertial frame are related to the rotation by

$$\sigma_{n,l,m} = \frac{m \int \Omega \xi \cdot \xi^* \rho dV - i \int (\xi \times \xi^*) \cdot \Omega \rho dV}{\int 2\pi \xi \cdot \xi^* \rho dV}, \quad (16)$$

where the integrals are taken over the whole solar volume, dV being an element volume. Moreover, it is sufficient to adopt the corresponding (unperturbed) eigenfunctions ξ of the nonrotating stellar model to evaluate the integrals. If the magnitude Ω of the angular velocity Ω is constant on spheres the splitting can be represented by the simple weighted averages:

$$\sigma_{n,l,m} = m \int \Omega_0(r) \mathcal{K}_0^{n,l}(r) dr, \quad (17)$$

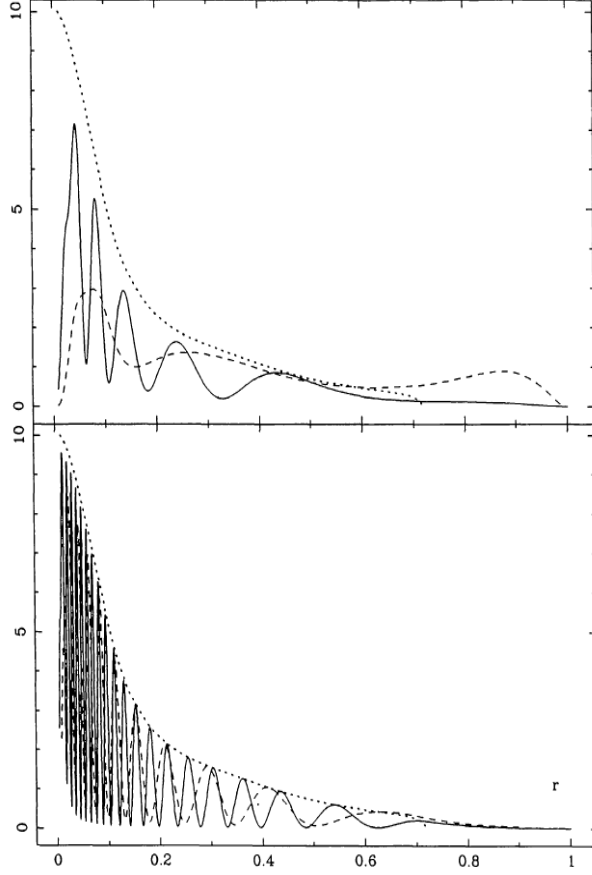


Fig. 5 Rotational kernels $\mathcal{K}_0^{n,l}$, caused by a rotation constant on spheres (cf. Eq. 17), plotted as a function of radius r/R_\odot . The quantity $R_\odot \times \mathcal{K}_0^{n,l}$ is plotted for modes $l = 2$ with radial order $n = 5$ (full line) and $n = 1$ (dashed line) in the upper panel and $n = 20$ (full line) and $n = 10$ (dashed line) in the lower panel. The dotted lines represent the asymptotic envelope given by the function $(P_0/\pi^2)(1 - 1/L^2)N/r$ (from Berthomieu & Provost 1991).

with

$$\mathcal{K}_0^{n,l} = \rho r^2 \frac{\xi_r^2 + \xi_h^2 - 2L^{-1}\xi_r\xi_h - L^{-2}\xi_h^2}{\int_0^{R_\odot} (\xi_r^2 + \xi_h^2) \rho r^2 dr}, \quad (18)$$

Some typical examples of $\mathcal{K}_0^{n,l}$ are plotted in Figure 5; they have large amplitudes in the solar core, implying a high sensitivity to core rotation.

As noted previously, low-frequency g modes of low degree have much larger displacements in the horizontal direction than in the radial direction, so that the simplified expression for the rotational kernels depends only on ξ_h^2 . Using the asymptotic expressions for the eigenfunctions (e.g. Tassoul 1980; Provost & Berthomieu 1986),

Berthomieu & Provost (1991) have shown that the asymptotic kernels have a sensitivity envelope in the radiative zone that is proportional to $(1 - 1/L^2)N/r$. This demonstrates the sensitivity of the frequency splittings of the gravity modes to the solar core rotation (Fig 5).

We know from the inversion of observed p-mode frequency splittings that the solar rotation is not dependent only on radius, but that the rotation in the convective zone varies with latitude as much as the rotation observed at the solar surface (Thompson et al. 1996).

If we take a simple law that reflects this differential rotation namely $\Omega = \Omega_0(r) + \Omega_1(r) \cos^2(\vartheta)$, we may then express the frequency splittings $\sigma_{n,l,m}$ of the g modes by

$$\sigma_{n,l,m} = m \left[\overline{\Omega_0} \left(1 - \frac{1}{L^2} \right) + \overline{\Omega_1} \left(C_{l,m} \left(1 - \frac{6}{L^2} \right) + \frac{1}{L^2} \right) \right], \quad (19)$$

with

$$C_{l,m} = \frac{1}{2l+1} \left[\frac{(l+1)^2 - m^2}{2l+3} + \frac{l^2 - m^2}{2l-1} \right], \quad (20)$$

where $\overline{\Omega_0}$ and $\overline{\Omega_1}$ are mean values of the rotation coefficients seen by g modes, and

$$\overline{\Omega_{0,1}} = \frac{\int \Omega_{0,1}(r)(N/r)dr}{\int (N/r)dr}. \quad (21)$$

An important point to be made about the equations above is that $\sigma_{n,l,m} \sim m\overline{\Omega_0}(1 - \frac{1}{L^2})$, so that, at low frequencies, the splittings of $l = 1$ g modes are about half the size of the splittings of $l = 2$ g modes. This must be taken into account when attempts are made to identify g modes in the low-frequency range. When g modes with very low frequencies are considered, the ratio Ω/ω is no longer small and another asymptotic analysis has to be made to take into account the fact that Coriolis effects cause the oscillation eigenfunctions to be no longer described by a single spherical harmonic (e.g. Berthomieu et al. 1978; Dziembowski & Kosovichev 1987; Dintrans & Rieutord 2000; Mathis et al. 2008). These modes can be expanded in terms of a hierarchy of unperturbed eigenfunctions ξ , a procedure which is valid because Ω/Ω_g is small even though Ω/ω is not. However the usual first-order expression for the frequency splittings is relevant for modes of frequency larger than about $20\mu\text{Hz}$ (Berthomieu & Provost 1991).

2.2 g-mode frequency predictions and their reliability

In order to aid observational attempts to detect and identify low-frequency p and g modes in the frequency spectrum, several groups have computed theoretical g-mode frequencies (e.g. Provost et al. 2000; Couvidat et al. 2003; Mathur et al. 2007; Cox & Guzik 2004). The reliability of these predicted frequencies depends first on the uncertainties of the solar modelling and on the sensitivity of the low-frequency oscillations to these uncertainties, and second on the numerical precision of the frequency calculations. Another important uncertainty lies in the estimation of the frequency splittings of the g modes, because these splittings depend of course on the rotation close to the centre of the Sun, which is not well constrained observationally.

2.2.1 Modern solar models and their uncertainties

The large number of p-mode frequencies already detected lead to a *seismic* model of the Sun (e.g. Gough 2004) that is found to have a structure that is very close to the structures shown by modern solar models (e.g. Christensen-Dalsgaard et al. 1996; Gough et al. 1996). The only regions where the structure inferred by p-mode observations of the p modes remains uncertain is in the central few percent of the solar core. (Uncertainty in the angular velocity, as inferred from the frequency splittings of p modes extends through a large part of the solar core.)

Standard solar models are assumed to be spherically symmetric, in hydrostatic equilibrium with no macroscopic motion except convection, no mass loss nor accretion, no rotation and no magnetic field. The structures are determined by the assumed microscopic properties of the solar material (equation of state, opacity, nuclear reaction rates etc.), and by the description of energy transport by convection usually (mixing-length prescription, e.g. Böhm-Vitense 1958; Canuto & Mazzitelli 1991; Gough et al. 1996; Turck-Chièze et al. 1993). The numerical codes leading to these solar models have been carefully compared (Monteiro 2009). Solar models are calibrated by adjusting the initial abundances Y_i and Z_i of helium and heavy elements, and (usually only a single) mixing-length parameter which determines the efficacy of the convective transport in a mixing-length description, to obtain, for a one-solar-mass model, the solar radius and the solar luminosity at the solar age, and the observed surface metallicity $(Z/X)_\odot$, where $X = 1 - Y - Z$ is the abundance of hydrogen. Antia & Basu (2006) attempted to determine the solar heavy-element abundance without reference to spectroscopy by using helioseismic data.

The introduction into the models of microscopic diffusion and settling of chemical elements decreases the surface helium content, reducing the discrepancy between the observed and modelled sound-speed profiles, and also bringing the surface helium content, and the convection zone depth, of the models into better agreement with the observations. (e.g. Burgers 1969; Cox et al. 1989; Proffitt & Michaud 1991; Michaud & Proffitt 1993; Christensen-Dalsgaard et al. 1993; Thoul et al. 1994; Morel 1997; Brun et al. 1998). But what of the heavy-element abundances?

The quantity of heavy elements assumed in the models is extremely important, because these elements dominate the radiative opacities. Usually one considers only the total heavy element abundance Z_\odot or the so-called metallicity $(Z/X)_\odot$. Until 2004, the solar abundances were taken from results given by two rather close spectroscopic analyses, namely Grevesse & Noels (1993) (GN) and Grevesse & Sauval (1998) (GS). However, since then new heavy element abundances have been inferred using a 3D, NLTE analysis of the spectroscopic data, which takes hydrodynamics into account in the transfer calculations as in Asplund et al. (2005, 2009, hereafter AGS) and Caffau et al. (2009).

Amongst other differences, the AGS abundances of C, N, O, Ne are substantially lower than the older GN and GS abundances, by 0.16 dex, 0.19 dex, 0.21 dex and 0.24 dex. The reduction lowers the total surface metallicity of $(Z/X)_\odot$ (0.0166, compared to 0.0245 for GN and 0.023 for GS abundances). These changes have led to an extensive discussion in the literature on the robustness of the new results, which is beyond the scope of this paper, (e.g. Basu & Antia 2008; Caffau et al. 2008). In particular, it led to an attempt by Antia & Basu (2006) to determine the heavy-element abundance seismologically without reference to spectroscopy, by calibrating the average effect of ionization on γ_1 . However, Antia & Basu (2006) simply adopted a particular

equation of state which, like all others, was known not to be exact (cf. Baturin et al. 2000), so their result cannot be relied upon.

Solar models constructed with the GN or GS abundances in the generally accepted opacity formulae are in good agreement with helioseismic constraints. For example, the agreement for the sound-speed profile is within 0.2 percent, as shown in Figure 6 (e.g. Christensen-Dalsgaard et al. 1996; Gough et al. 1996). In attempts to account for the discrepancies that remain, several non-standard physical processes have been included in the solar modelling, in particular processes to improve the description of the layers located just beneath the convection zone where the most marked differences between the observations and the models occur. We know from helioseismology that the transition from differential rotation in the convection zone to almost uniform rotation in the radiative zone below occurs in a shallow layer called the tachocline (e.g. Spiegel & Zahn 1992; Kosovichev 1996; Thompson et al. 1996; Corbard et al. 1999). The shear of the rotational velocity necessarily induces mixing (Hughes et al. 2005). Various descriptions of this mixing have been included in some models, leading to reductions in the differences between the observations and models. (e.g. Richard et al. 1996; Gabriel 1997; Morel et al. 1998; Brun et al. 1999; Elliott & Gough 1999).

Other non-standard processes, such as overshoot of convective elements at the boundary of the convective core which appears at the end of the pre-main-sequence evolution, or mass-loss occurring during the initial stages of solar evolution, have been studied, with special emphasis placed on the changes induced in the most central parts of the models which are not well constrained by observations of p modes (see below).

The AGS abundances have caused considerable concern. This issue is simple to state: Except in the near-surface layers, which are of no import to this discussion, we already know from seismology the sound speed and the density stratification throughout the Sun to a precision easily good enough to be confident in the inference. If one then accepts the basic tenets of solar evolution theory - namely that a helium-abundance augmentation has occurred in the core due to nuclear transmutations on the main sequence and that the Sun is in thermal balance, energy being transported throughout the entire region beneath the convection zone by radiative transfer - and if one accepts also the equation of state (which we surely know to well within the limits set by the abundance change) and the nuclear reaction, then one can infer the absolute value of the hydrogen-helium abundance ratio and hence the temperature stratification (by demanding that the energy-generation rate in the core is equal to the luminosity observed at the surface) from which can be inferred the *value* of the opacity beneath the convection zone (Gough 2004). The issue, therefore, is simply how to reconcile that value with the photospheric abundances. At first sight, the apparently most straightforward resolution is that the abundances in the convection zone differ from these in the radiative interior, presumably as a results of accretion of metal-deficient material after the Sun has (almost) reached the main sequence and had a relatively shallow convection zone, which is contrary to standard assumptions. We should point out, however, that Guzik (2006) and Castro et al. (2007) have failed to construct such a model that is in adequate agreement with helioseismology.

It follows that using the AGS abundances in the accepted opacity formulae leads to solar models which disagree with the helioseismically determined constraints on the solar interior properties (e.g. Turck-Chièze et al. 2004; Montalbán et al. 2004; Bahcall et al. 2005; Guzik et al. 2005; Zaatari et al. 2006, 2007). There is a large discrepancy in the sound speed (e.g. Figure 6). The surface helium content of these new models is too low, and the convection zone is too thin, compared to the observed (helioseismic) values.

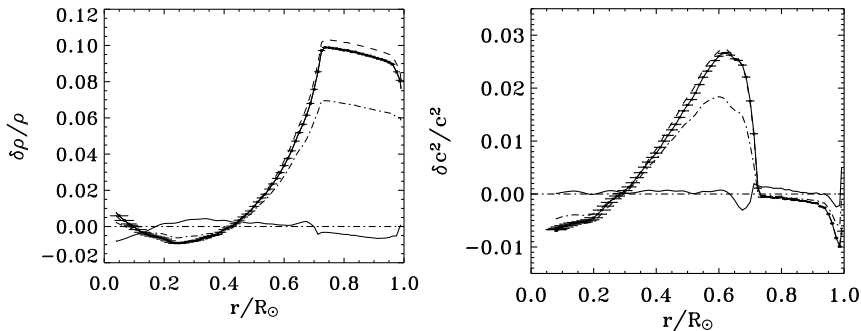


Fig. 6 Relative density profile and relative squared sound-speed differences between standard models using a new estimate of the CNO composition proposed by Asplund et al. (2005) (full line with seismic error bar) and the helioseismic observations. The dot-dash line corresponds to a model computed with abundances from Holweger (2001), intermediate between AGS and GN. The seismic model (thin line) is a model which reproduces properly the observed sound speed and is used to predict gravity modes and neutrino fluxes (After Turck-Chièze et al. 2004).

Many other attempts, and suggestions, have been made to try to reconcile the AGS abundances with the helioseismic results (e.g. Guzik 2006). Evidently, increasing the radiative opacities below the convection zone (e.g. Serenelli et al. 2004; Montalbán et al. 2004; Bahcall et al. 2004) decreases the discrepancies if one insists on lowering the heavy-element abundances to the AGS values. Using artificially enhanced diffusion rates for He and heavy elements (Basu & Antia 2004; Montalbán et al. 2004; Guzik et al. 2005; Yang & Bi 2007), does improve the agreement with seismic sound speed, though such changes by the amount required have not been justified. Rotational mixing, acting in the tachocline just beneath the convection zone can lead to models with acceptable values of the surface helium abundance, but their convection zones are too shallow (e.g. Turck-Chièze et al. 2004). Taking account of tachocline mixing (perhaps calling it convective overshoot) helps to bring the convection zone depth closer into line, but the discrepancies shown in the sound-speed profile are not necessarily reduced in size (e.g. Montalbán et al. 2006).

In sum, at the time of writing the solar abundances remain a major source of uncertainty in solar modelling (e.g. Basu & Antia 2008, and references therein).

Finally in this section we consider mechanisms to describe transport of angular momentum and chemical elements which are not fully accounted for in solar and stellar evolution codes. The respective rôles in angular momentum transport of dynamical processes involving rotation, magnetic fields (e.g. Gough & McIntyre 1998; Garaud 2002) and gravito-inertial waves have been much discussed in the solar context (Schatzman 1993, 1996; Talon & Zahn 1998; Talon et al. 2002; Mathis et al. 2008; Gough 2009). When only the meridional circulation and the “classical” hydrodynamic instabilities are invoked, models predict a Sun with a radiative interior and core rotating much faster than the surface (e.g. Pinsonneault et al. 1989), which is incompatible with p-mode helioseismology (e.g. Thompson et al. 1996). Mathis & Zahn (2005) have recently derived, in a self-consistent manner, a formalism to describe the effects of an axisymmetric magnetic field on the meridional circulation and the turbulence generated by

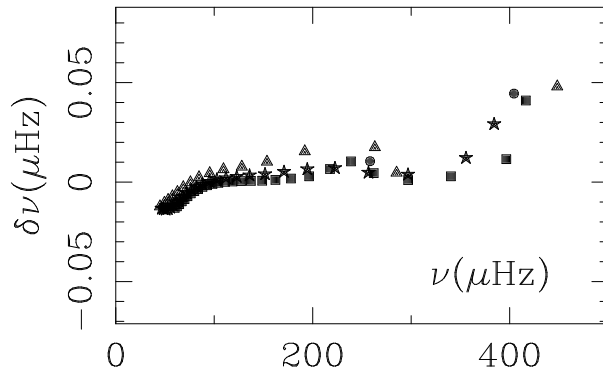


Fig. 7 Differences $\delta\nu = \tilde{\nu}_{n,l} - \nu_{n,l}$ between eigenfrequencies $\nu_{n,l}$ computed by an oscillations code, and predictions of the frequencies given by the integral expressions for a reference solar model, $\tilde{\nu}_{n,l}$ [cf. Eq. (10)] for modes of degree $l=0$ (dots), 1 (triangles), 2 (full stars) and 3 (squares).

the shear of differential rotation. This formalism is now implemented in some evolution codes.

2.2.2 Numerical precision

The numerical precision of the frequencies depends both on the physical and numerical accuracy of the evolutionary models and on the algorithms used to compute the oscillation frequencies themselves. Many evolution codes have been compared, in the 1990s for the Sun (GONG solar model comparison) and more recently in a stellar context as part of the CoRoT Evolution and Seismic Tools Activity (ESTA) (Lebreton et al. 2008; Monteiro 2009). The numerical precision of the frequencies may be estimated for a given stellar model by considering the range of values obtained from different oscillations codes, which compute the mode frequencies (Moya et al. 2008).

For a given oscillations code, an internal accuracy may also be estimated by comparing a numerical eigenfrequency $\nu_{n,l}$ with its integral value, as obtained from Eq. (10) (e.g. Provost 2008). Any inconsistency, either in the computation of the oscillation frequencies or in the equilibrium models, gives rise to a non-zero value of $\tilde{\nu}_{n,l} - \nu_{n,l}$ as, of course, does the neglect of the surface term in Eq. (10) which are actually negligible only at low frequency.

For g-mode calculations one also needs a solar model with a sufficiently large number of mesh points (where the model quantities are given explicitly), well distributed in solar radius, in particular close to the centre of the model where g modes have large amplitudes (e.g. Christensen-Dalsgaard & Berthomieu 1991). Figure 7 shows that, for a reference solar model, a numerical precision of g-mode frequencies – as measured by $\tilde{\nu}_{n,l} - \nu_{n,l}$ – better than $0.01 \mu\text{Hz}$ for frequencies lower than $200 \mu\text{Hz}$ has been achieved. This difference is much larger than uncertainties we expect to obtain from observations (should the g modes be detected). Therefore the numerical procedures should be improved. However, as we shall show below, this error is much smaller than errors introduced by uncertainties in the theoretical structure and the dynamics of the models. Therefore g modes have diagnostic potential.

Table 1 Asymptotic coefficients of g modes, i.e., P_0 , V_1 , V_2 , and ϑ . Plotted are mean values of the coefficients for n_{\min} from 10 to 15 and n_{\max} from 27 to 35, as computed for models M1 to M8 from Provost et al. (2000) (1), M-GN & M-AGS from Zaatari et al. (2007) (2). The estimation of the uncertainty, in percent, was obtained from the scatter of the least-squares fit values around their mean values. In this table the following differences show the following effects (for details see Provost et al. (2000)): (M6-M1) shows the effect of increasing age from 4.65 to 4.75 Gyr; (M2-M1) shows the effect of increasing the surface metallicity from 0.0245 to 0.0260; (M3-M1) and (M8-M1) show the effects of mass loss, set to a rate of $\dot{M} = -5 \times 10^{-10} M_{\odot} y^{-1}$, occurring for 200 Myr at the beginning of the evolution, with additional turbulent mixing below the convection zone in model M8, according to Montalbán & Schatzman (2000); (M4-M1) and (M5-M1) show the effects of overshoot of, respectively, 0.2 and 0.25 pressure scale heights at the edge of the convective core which appears at the end of the pre-main sequence evolution; (M1-M7) shows the effects of improved nuclear reaction rates; (M-AGS - M-GN) shows the effects of changing the chemical abundances from GN to AGS (see text); and finally (M-AGS - M-GN) shows the effects of changing the chemical abundances from GN to AGS (see text).

	P_0 (min)	%	V_1	%	V_2	%	ϑ	%	
M1	35.08	0.04	0.437	1.6	5.69	4	-0.160	11	(1)
M2	34.94	0.04	0.439	1.6	5.67	4	-0.161	11	–
M3	34.63	0.04	0.444	1.6	5.72	4	-0.161	11	–
M4	35.39	0.04	0.430	1.6	5.64	4	-0.161	11	–
M5	36.75	0.03	0.399	1.4	5.46	3	-0.164	8	–
M6	34.77	0.04	0.440	1.6	5.71	4	-0.161	11	–
M7	35.42	0.04	0.433	1.6	5.61	4	-0.162	11	–
M8	34.78	0.07	0.437	1.3	6.12	6	-0.217	14	–
M-GN	35.09	0.03	0.442	1.5	5.77	3	-0.166	9	(2)
M-AGS	35.69	0.04	0.433	1.4	5.96	3	-0.157	11	–

2.2.3 Sensitivity of low-frequency g- and mixed mode frequencies to solar models

As a first step, the sensitivity of g-mode frequencies to uncertainties in the solar models may be studied by taking advantage of the asymptotic properties of g modes. As noted previously, the three global coefficients P_0 , V_1 , V_2 , and the phase factor ϑ , which characterize the frequency may be obtained by a least-squares fit to a set of numerical frequencies. The values of P_0 and V_1 are typically very close to those derived directly from the integrals (cf. Eq. (11)), and results for some models are given in Table 1. In this table one can see the effects of changing some fundamental model parameters, such as the age to which the model is evolved, the metallicity, and also some important physics such as the nuclear reaction rates.

We find that the values of the asymptotic coefficients are very similar for models with slightly different fundamental parameters and different physics, including changes between the old and new metallicities. Ignoring gravitational settling increases P_0 by about 0.7 min (Morel et al. 1997). Mathur et al. (2007) have found that the theoretical value of P_0 changes by no more than 1 min when models with plausible differences in treatments of microscopic diffusion, turbulence in the tachocline, and the chemical composition, are considered. The results give an idea of the possible range of values for these asymptotic coefficients.

The sensitivity of the frequencies to uncertainties in the models can also be studied in more detail by looking at the relative frequency differences computed for two different evolutionary models (e.g. Provost et al. 2000; Mathur et al. 2007). Some general properties can be seen in Figures 8, 9, and 10: (i) at low frequencies, the frequency dif-

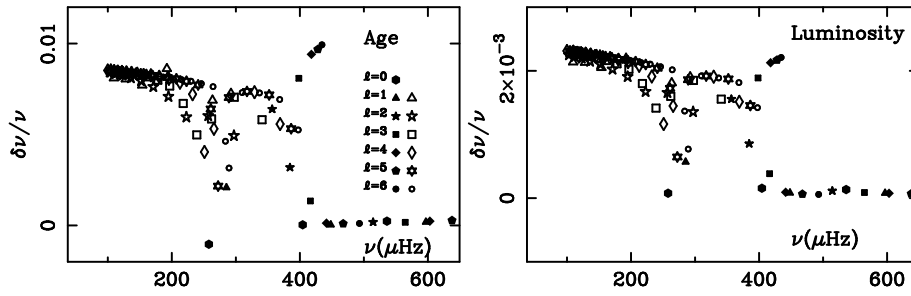


Fig. 8 Relative frequency differences, $\delta\nu/\nu$, between a solar model and the reference model M1. Results are shown for g modes (open symbols) and low-frequency f and p modes (full symbols) with degrees $l = 1$ to 6, to test the sensitivity to the solar parameters: age (model M6 - $\delta t = 0.1Gy$), and luminosity ($\delta L/L = 3.6 \cdot 10^{-3}$). Adapted from Provost et al. (2000).

ferences between two models obey approximately the asymptotic relation of Eq. (14); (ii) the largest frequency differences appear in the range 200 to 300 μHz , where there are mixed modes, and the behaviour is more irregular as a function of frequency than the behaviour shown at very low frequencies; and (iii) in contrast, the sensitivity of the low-frequency p-mode frequencies to changes in the solar models is much smaller than for the g modes.

The sensitivity of low-degree g-mode frequencies to changes in the age and luminosity of solar models is shown in Figure 8. The frequencies are seen to increase with increasing age, increasing metallicity, Z/X , and increasing luminosity. For instance, an increase of either 1% in age, 6% in metallicity increases the frequencies by about 0.4%. An increase in luminosity of 3.5%, which corresponds to the upper value reported in Guenther et al. (1992), increases the g-mode frequencies by 0.2%. A frequency augmentation of about 1% arises from augmenting the nuclear reaction rates above the values in the tables of Caughlan & Fowler (1988) to the most recent tables of Adelberger et al. (1998).

A reduction in the solar abundances from the old (GN/GS) to the new (AGS) values reduces the frequencies of the order of 1.5% or more, as shown in see Figure 9 (Mathur et al. 2007; Zaatri et al. 2007). This effect is in agreement with the global asymptotic parameter results shown in Table 1 for models M-AGS and M-GN. We also note that Zaatri et al. (2007) have reported that the characteristic low-frequency g-mode period P_0 decreases by increasing the neon abundance in the new solar mixture (Figure 9) which is consistent with inferences from the work of Mathur et al. (2007).

The effects of different descriptions of mixing in the tachocline have been considered by Mathur et al. (2007), who showed that the introduction of horizontal diffusion, as suggested by Spiegel & Zahn (1992), would decrease the g-mode frequencies by about 0.25%. Core overshooting and mass loss during initial stages of evolution decreases and increases the g-mode frequencies, respectively, by about 1% (Figure 10).

In conclusion, the sensitivity of the g-mode frequencies to uncertainties in the solar models appears to be of order at least 1% for the cases considered here, which corresponds to frequency differences of the order 1 μHz around 100 μHz and 2 μHz around 200 μHz , i.e. much larger than the numerical precision of the frequency computations (down to 100 μHz).

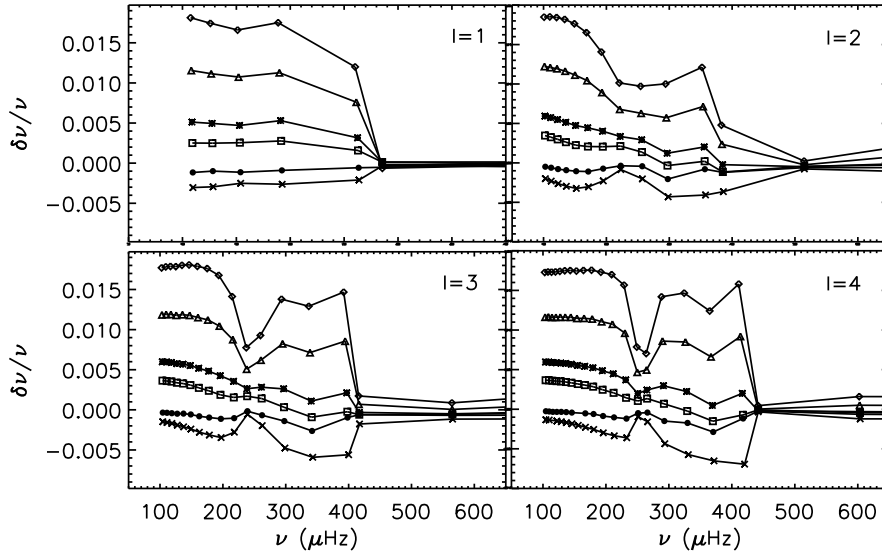


Fig. 9 Relative frequency differences between the g modes and the gravest low-frequency p modes of a calibrated solar model computed with the old GN abundances (M-GN) and a model computed with the AGS abundances (\diamond). The other symbols, (\triangle , $*$, \square , \times , \bullet) correspond to models computed with increasing changes to the neon abundance of the models with a dex of 8.10, 8.29, 8.35, 8.47 and 8.35, respectively. From Zaatri et al. (2007).

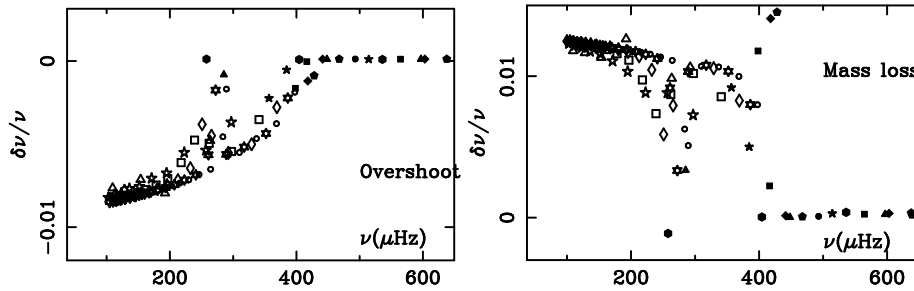


Fig. 10 Relative frequency differences, $\delta\nu/\nu$, between a solar model and the reference model M1, shown to test the sensitivity to the following physics (see caption of Table 1): overshoot of 0.2 pressure scale heights (model M4); and strong mass loss rates (model M3) (same symbols as in Figure 8). Adapted from Provost et al. (2000)

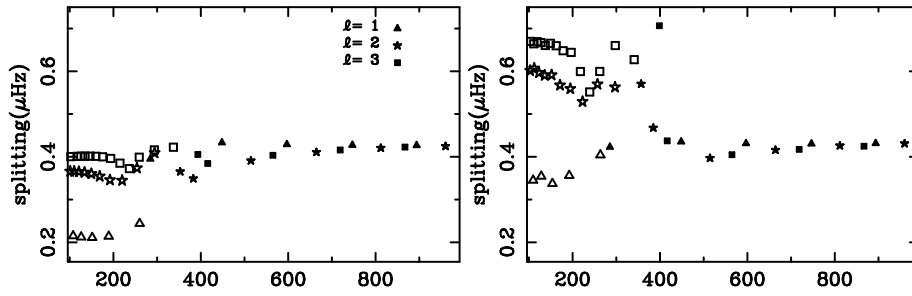


Fig. 11 Splittings of low-degree, low-frequency sectoral $m = l$ modes as a function of the frequency for a reference model and for a simplified rotation law, which mimics for $r > 0.2 R_{\odot}$ the solar rotation inferred by inversion of the observed p-mode frequency splittings. Shown are predictions for different values of the rotation Ω_c below $0.2 R_{\odot}$. Left panel: $\Omega_c = 0.433 \mu\text{Hz}$. Right panel: $\Omega = 2\Omega_c$ for $r < 0.2R_{\odot}$ (open symbols: g modes; full symbols: f and p modes). From Provost et al. (2000).

2.2.4 Sensitivity to the rotation and dynamics in the core

The sensitivity of g-mode frequency splitting to the dynamics of the solar core may be investigated by the forward method, using a solar rotation law, which, for $r \geq 0.2 R_{\odot}$, mimics the rotation rate obtained by inversion of the p-mode frequency splittings, i.e. rigid rotation below the convection zone and latitudinal differential rotation inside the zone (see e.g. Corbard et al. 1997; Dikpati et al. 2002). Since the core rotation is very uncertain, analyses of this type assume a constant rotation in the core $r < 0.2 R_{\odot}$ equal to Ω_c (e.g. Provost et al. 2000; Mathur et al. 2008). Figure 11 shows the variation with the frequency of the model-predicted splittings, $\sigma_{n,l,l}$, of sectoral g modes, for two different values of Ω_c : either the core rotation is assumed the same as in the radiative zone ($\Omega_c = 0.433 \mu\text{Hz}$; left panel), or it is assumed to be twice this value (right panel). At low frequencies, the splittings depend on the degree l , with a behaviour close to the asymptotic behaviour of g modes, i.e. a splitting proportional to $1 - 1/L^2$. At high frequencies the splittings instead tend to the asymptotic p-mode values, with a very weak dependence on the degree l arising from differential rotation in the convection zone. As expected, if the core rotation is increased by a factor of two, the g-mode splittings are increased significantly by a factor of about 1.75, while the p-mode splittings are almost unchanged. The splittings of the mixed modes have a complicated dependence on degree, frequency and the shape of the rotation law below $0.2 R_{\odot}$. If the rotation of the solar core differs notably from that of the radiative zone, such behaviour will make their detection and identification in the observed spectrum harder.

The internal magnetic field, which is often neglected, can also split the frequencies into several components and thus it can affect the reliability of predicted g-mode frequencies. Rashba et al. (2007) attempt to estimate analytically the effect of a magnetic field in the radiative zone on the g-mode frequencies, using a MHD perturbative correction (e.g. Unno et al. 1989). They show that a 1-per-cent g-mode frequency shift can be obtained for magnetic field as low as 300kG in the radiative zone, for modes of radial order $n=20$ and degree $l=1$ ($\nu \sim 33 \mu\text{Hz}$), and they argue that a similar shift

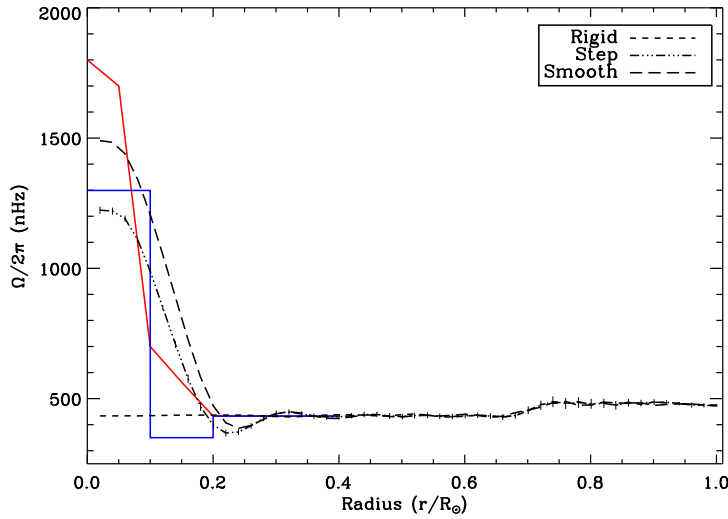


Fig. 12 Equatorial rotation profiles below $0.4 R_{\odot}$ reconstructed by inversion of artificial data, using eight g modes, each with an assumed frequency splitting uncertainty of 7.5 nHz. Results are shown for three different rotation laws in the solar core (dashed line rigid, full line step profile, long dashed line smooth profile). The continuous blue, red and dotted lines represent, respectively, the input step, smooth and rigid artificial rotation profiles. From Mathur et al. (2008).

for the case of low-order g-mode frequency cannot result from a central magnetic field unless its strength exceeds 8 MG which would be a very large magnetic field.

The rotational kernels would help to infer the core rotation by inversion, once the splitting of g modes could be measured. Preliminary work using inverse methods has been carried out to try to know how measured splittings of some g modes would influence our knowledge of the rotation of the solar core (Mathur et al. 2007; García et al. 2008b). Numerical inversions using artificial data, corresponding to different laws of rotation in the solar core (see Figure 12) were performed. It was shown that the introduction of only one g mode gives a much better idea of the rotation profile. The introduction of eight g-mode frequencies with an error bar of 7.5 nHz in the data allows one to recover the rotation profile in the core quite well, with the low-degree p modes contributing to constrain the solar rotation profile down to $0.2 R_{\odot}$. As expected, without g modes, it is not possible to distinguish between the three assumed core rotation laws

2.3 Conclusion

It appears that g-mode frequency predictions are affected by two sorts of uncertainty. First, the faults in the solar modelling induce uncertainties in the solar stratification, hence in the Brunt-Väisälä frequency which determines mainly the g-mode frequencies. Some contributions have been estimated to 1% (see subsection 2.2.3), but the consequences of the lack of a reliable description of the dynamical and magnetic effects

remains to be estimated. Second, the prediction of the splittings depends on the core rotation, which remains poorly known. A rotation twice larger below $0.2R_{\odot}$ would increase the low-frequency g-mode splittings by a factor about 1.75.

3 Excitation and damping of g modes

In the past, several attempts have been made to estimate solar g-mode amplitudes (Gough 1985; Berthomieu & Provost 1990; Andersen 1996; Kumar et al. 1996). The common result of these predictions is that g-mode amplitudes are not larger than a few mms^{-1} (Elsworth et al. 2006).

The investigations of g-mode amplitudes first focused on the linear stability of the modes so as to determine whether or not they could be excited by overstability (i.e. thermal instabilities). Results published to date suggest that g modes are most likely linearly stable (Section 3.2). Consequently most of the theoretical efforts have therefore assumed that g modes are intrinsically damped and excited stochastically by turbulent convection (Section 3.4), as it is also believed to be the case for p modes, whether the excitation is predominantly in the body of the convection zone (Gough 1985; Berthomieu & Provost 1990; Kumar et al. 1996; Belkacem et al. 2009), or in the lower overshooting layers (e.g., Andersen 1996; Dintrans et al. 2005). Note also that other mechanisms such as mode coupling (e.g., Dziembowski 1983; Guenther & Demarque 1984; Ando 1986; Wentzel 1987; Wolff & O'Donovan 2007), or excitation by magnetic torques (Dziembowski et al. 1985) have been investigated.

The resulting amplitudes are determined by a balance between the intrinsic linear stability of the modes, which are characterised by the damping rates η , and the energy input via nonlinear interactions with the turbulence. These will be discussed separately in Section 3.2 and 3.4.

3.1 The separation of the oscillation modes from the convection

Before describing some of the details of what has appeared in the astrophysical literature, it is instructive first to ask just what the question is that we wish to ask. The glib response is simply: to what amplitudes does the turbulence drive the modes? But before we can address that matter, we should try to be clear in our minds how to separate the motion into convection and modes of oscillation. There have been several attempts to accomplish that task, mainly unpublished because unfortunately unambiguous success has never been achieved. Therefore we shall be brief.

In the case of radial (p) modes, superficially the issue is reasonably clear: the modes are horizontally uniform, and convection, which is motion driven by buoyancy, is intrinsically horizontally nonuniform. Therefore one simply takes a horizontal average, and regards the average motion as the oscillation mode and the remainder as convection. This is a fairly safe procedure, at least for isolating radial modes (and was justified to some degree by Gough 1969), provided that one takes the horizontal average of ρw , where ρ is density and w is the vertical (radial) Eulerian component of the convective velocity, rather than w , to define the oscillation mode. Incidentally, convection, even when approximated by a mixing-length-type theory of eddies (e.g. Gough 1965, 1977a,b; Unno 1967), is most naturally described in (local) Eulerian coordinates; since

the eddies maintain a degree of integrity, they are advected by the large-scale pulsational flow, which is therefore most appropriately described in Lagrangian coordinates.

Separating nonradial modes from convection is a more difficult task. It can be accomplished only approximately, and that only when there is a good separation of scales. Modes of low degree have horizontal scales comparable with the radial coordinate r , and because most of the energy in the convective motion is in scales rather smaller than that (at least on timescales comparable with the periods of the p modes and grave ($n \leq 3$) g modes) one can at least separate the motion, this time by taking appropriate large-scale spatial and temporal averages. In this way, a mixed Eulerian-Lagrangian coordinate system can be set up (Gabriel et al. 1975; Unno et al. 1989) similar to that defined originally for radial pulsations (Gough 1969). However, such a separation cannot be achieved for the very-high-order g modes that resonate with the turbulence at the base of the convection zone. In that case it is necessary to resort to more involved procedures. For example, one may try, following Poyet (1983), to decompose the motion into a superposition of linear p modes and g modes, regarding the function space spanned by the direct, so-called g^+ , modes as convection; that procedure suffers from ambiguity when trying to estimate the overlap integrals that couple the two kinds of motion, because there can remain some freedom in how the decomposition is carried out. Most of the analytically based studies simply separate the motion by fiat. And now, having issued our warning, we shall do likewise.

Before proceeding, a word concerning the analysis of numerical simulations is in order. Simulations have been carried out to shed light directly on the mode-excitation issue, although in some cases also with the intention of calibrating analytical approximations to the energy-input rate (Rosenthal 1998; Stein & Nordlund 2001; Rogers & Glatzmaier 2005; Rogers et al. 2008). Because convective motion cannot be unambiguously separated from what we imagine to be the oscillation modes, the details of what one envisages to be energy conversion cannot be isolated. But what one can do is to look in the far field where convection is ignorable, provided the domain of the simulation is extensive enough, and there determine the spectrum of the g-wave and p-wave radiation by projection onto linearized wave functions (e.g., Dintrans et al. 2005).

3.2 Linear g-mode stability

The discussion of the stability of g modes in a star has a long history. Ledoux & Sauvenier-Goffin (1950) were probably the first to address the general problem, although they limited their discussion to white dwarfs. As is the case for acoustic modes, the stability of gravity modes depends on the integrated effect of various physical mechanisms which can either drive or damp the oscillations. The excitation and damping processes usually take place in layers with rather small radial extent: these are the ionisation regions of hydrogen and helium where the Eddington valve can operate, the energy-generating core where temperature-sensitive nuclear reactions can feed energy into the oscillatory motion, and also the highly superadiabatic upper convective boundary layer and, for g modes, the vicinity of the boundaries of convection zones where dynamical interaction between the convection and the oscillations is relatively strong. In the following section we review these mechanisms.

3.2.1 Linearized equations governing g-mode oscillations

One first takes a statistical (temporal) average of the governing equations (which determines the basic, background state of the star) and subtracts it from the full equations to yield the fluctuation equations. Having separated the fluctuating variables into an oscillatory mode contribution and convection, one linearizes the fluctuation equations in the mode variables, and then typically arranges the outcome with the mode variables on the left and the fluctuating terms associated with the convection on the right. In all studies to date the mode amplitudes are regarded as being so small that they do not influence the inhomogeneous convective driving term on the right. Therefore each mode can be treated separately. The equation of motion can then be written formally as

$$\mathcal{L}\xi = \mathfrak{F}(\mathbf{v}, T'), \quad (22)$$

where ξ is the displacement eigenfunction of the mode, with (\mathbf{v}, T') is the convective velocity and temperature fluctuation, and complex frequency $2\pi\nu_{n,l,m} \equiv \omega - i\eta$ (See Eq. 1), in which ω is real and positive, η is real. The term \mathfrak{F} represents inhomogeneous stochastic driving and damping terms that depend only on convective quantities (*i.e.* \mathbf{v} and T') unperturbed by the oscillations. The spatial differential wave operator \mathcal{L} (e.g., Unno et al. 1989, for details) depends upon $\omega - i\eta$ and the background state of the star, which itself depends on the convective fluxes of heat and momentum; it depends also on the perturbation to those fluxes that is produced by the oscillations. Ignoring the right-hand side of Eq. (22) yields the equation of free oscillation (*i.e.* free from the inhomogeneous damping and driving, but including in principle the linearized momentum and convective momentum flux perturbations that are induced by the oscillations), which in the adiabatic Cowling approximation can be approximated by Eq. (4).

3.2.2 Excitation by the ϵ mechanism

The first dynamical investigation of g-mode instability of the Sun in which the nuclear reactions were perturbed consistently was carried out in the quasiadiabatic approximation by Dilke & Gough (1972) who approximated the eigenfunctions in the radiative interior by those of a polytrope of index 3. Soon afterwards Rosenbluth & Bahcall (1973) discussed the thermal instability of hydrostatic disturbances. The aim in both papers was to question the assumptions upon which standard solar models are built with a view to addressing the still-existing solar neutrino problem. Dilke & Gough found that low-order g modes could have been dynamically unstable in the early evolutionary stages of the Sun owing principally to the strong temperature dependence of particularly the ${}^3\text{He}({}^3\text{He}, 2\text{p}){}^4\text{He}$ reaction which manifests itself in the energy budget when the reactions of the p-p chain are thrown out of balance by the dynamical oscillations, and also to the fact that the Sun has a convective envelope deep enough to provide an effective evanescent shield; earlier investigations confined to stars with radiative envelopes (e.g. Auré 1971) had indicated that g-mode amplitudes are so high in the surface layers that radiative damping would overwhelm any driving in the core. Rosenbluth & Bahcall found that their solar models are stable to non-radial thermal instability.

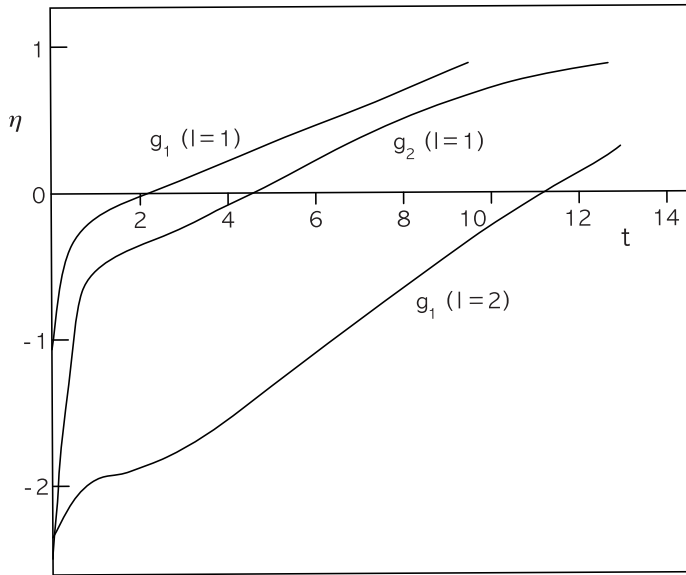


Fig. 13 Theoretical growth rates η of three low-order g modes as a function of age t in the early stages of the main-sequence evolution of the Sun. The units are 10^{-7}y^{-1} for η and the age is measured in units of 10^8y of the equilibrium models (Christensen-Dalsgaard et al. 1974). The current age of the Sun is about $4 \cdot 10^9$ years. Modes are found linearly unstable for $\eta < 0$ and stable for $\eta > 0$.

3.2.3 Radiative damping

Following Dilke & Gough (1972), Christensen-Dalsgaard et al. (1974), Boury et al. (1975), and Shibahashi et al. (1975) addressed the g-mode instability using eigenfunctions of solar models, although still in the quasi-adiabatic approximation. All authors found unstable low-order g modes in models younger than the present Sun. The instability arose because the temperature sensitivity of nuclear reactions perturbed on a g-mode timescale is substantially greater than it is on a stellar-evolution timescales – the latter is too weak to overcome radiative damping (e.g. Dziembowski & Sienkiewicz 1973). For the present Sun, however, all authors found all g modes to be stable, at least if the evolutionary consequence of earlier instability could be ignored. It is particularly so in the early stages of evolution when the star was less centrally condensed that the g-mode amplitudes are relatively large in the core (e.g. Noels et al. 1974), and are therefore more receptive to nuclear driving. Figure 13 shows low-order g-mode growth rates for an evolving $1 M_{\odot}$ star computed in the quasi-adiabatic approximation.

The first fully nonadiabatic stability computations of solar p and g modes were undertaken by Christensen-Dalsgaard & Gough (1975). The authors concluded that nonadiabatic processes in the very outer layers of the present Sun dominate over the destabilising influence of the temperature-dependent ${}^3\text{He}({}^3\text{He}, 2\text{p}){}^4\text{He}$ reactions in the core, suggesting that low-order g modes are very likely stable. An important deficiency in these computations, however, is that the modulation of the convective fluxes of heat and momentum were omitted. Kosovichev & Severny (1985) investigated the g-

mode instability for solar models with different metallicities and concluded that the instability is stronger in low metallicity models.

3.2.4 The κ mechanism

In stellar layers where partial ionisation of chemical elements takes place, opacity can increase with temperature during the compression phase of a stellar pulsation, tending to produce an Eddington valve that can lead to instability. The radiative (energy) flux through such a layer is then absorbed by the stellar matter more effectively than it would have been otherwise. After the subsequent expansion phase the previously absorbed excess energy is released, the net effect over the whole cycle being to feed energy into the pulsation. This mechanism is responsible for pulsations of some variable stars such as δ Scuti, β Cephei and Cepheids (e.g. Dziembowski & Pamiatnykh 1993; Gautschy & Saio 1995, 1996). This process is effective only if much of the heat flux in the relevant layer is carried by radiation, which in the Sun is not the case. However, the valve can operate also as a result of a perturbation to the convective heat flux. Irrespective of whether the flux is predominantly radiative or convective, in any star the valve is most effective if the thermal relaxation time of the material in and above the relevant layer is similar to that of the period of the pulsation. Because the thermal relaxation time increases with depth, low-period oscillation modes are driven in deeper layers than are corresponding short-period oscillations (e.g. Pamyatnykh 1999; Houdek 2003).

3.2.5 The effect of convection

Saio (1980) reported the first non-adiabatic solar g-mode stability computations that incorporated the modulation of the convection, adopting the treatment of convection by Gabriel et al. (1975), which is based on Unno's (1967) time-dependent mixing-length formalism. In these computations, only the heat flux was taken into account: the momentum fluxes (Reynolds stresses) were omitted from both the equilibrium structure and the stability analysis.

Saio (1980) confirmed the earlier findings by Christensen-Dalsgaard et al. (1974) of g-mode instability during the early evolutionary phases of the Sun. Interestingly, for solar models with an age of 4.5×10^9 y he found that some of the g modes are additionally driven by the hydrogen ionization zone in the very outer layers of the star. However, as discussed by Dilke & Gough (1972), the main agent driving grave low-degree g modes appears to be the $^3\text{He} - ^3\text{He}$ reaction in the energy-generating core.

It was reported by Gough (1965, 1980) that the dynamical effects arising from the turbulent momentum flux perturbations contribute significantly to the growth rates of solar oscillations. Stability computations of a star in which both the convective heat flux and the Reynolds stresses were included, in both the equilibrium structure and the pulsation calculations, using the time-dependent mixing-length formalism by Gough (1965, 1977a), were reported by Baker & Gough (1979) for acoustic oscillations in RR Lyrae stars. A subsequent detailed analysis of the Sun by Balmforth (1992b) revealed the manner in which the phases of the fluctuating Reynolds stresses and the density perturbations differ, causing radial p modes to be damped. Similar findings were reported also by Houdek et al. (1999) in other main-sequence stars. Different results were obtained from the computation of Dupret et al. (2006a), which suggest

that the perturbation of the convective heat flux is dominant. The formalism that was adopted is based on the approach of Unno (1967) generalized to non-radial modes by Grigahcène et al. (2005). In addition, Dupret et al. (2006a) found that the effect of the turbulent pressure modulation is partly compensated by the perturbation of the dissipation rate of turbulent kinetic energy into heat (see also Ledoux & Walraven 1958).

For high-order g modes ($\nu < 100\mu\text{Hz}$), Belkacem et al. (2009) have shown, using a partially non-adiabatic non-radial computation (Grigahcène et al. 2005), that the damping rates are dominated by radiative losses and are insensitive to the convection-pulsation interaction. This result is in agreement with previous findings of Kumar et al. (1996).

It is perhaps useful to point out the fundamental approximations that have been used to model the temporal modulation of the convection by the oscillations. Formulae for these modulations are needed when estimating the influence of convection on the frequencies and, more importantly, the growth rates of the oscillations. We limit ourselves here to those procedures that have been used for estimating solar g-mode amplitudes.

The most naive procedure is to presume that the convective fluxes simply relax exponentially on a timescale τ_c towards the time-independent formula evaluated for the current (time-varying) environment. Thus, if F_c is a component of a flux, be it of heat or momentum, it is taken to obey an equation of the type

$$\frac{dF_c}{dt} = \frac{F_{c0} - F_c}{\tau_c}, \quad (23)$$

where τ_c is a multiple of ℓ/w , ℓ being the mixing length and w a characteristic convective velocity, both of which are evaluated typically for the non-oscillating background state. The function F_{c0} is some chosen formula for the corresponding flux evaluated for the instantaneous state of the star as though that state were not pulsating. Evidently, there is some formal freedom in the choice of that formula, because it was derived under the assumption that the background state is in (statistical) hydrostatic equilibrium, whereas when the star is oscillating that is not the case. Therefore different representations that are equivalent in the non-oscillating state can differ for the oscillating star. It is also evident that the phase lag of the oscillatory perturbation F'_c to F_c behind that of the perturbation to F_{c0} , which controls the damping rate of the oscillations, is determined directly by the (arbitrary) value adopted for the constant of proportionality between τ_c and ℓ/w .

Other approaches address the dynamics of the turbulent perturbations. In the mixing-length approach, the fluid is considered to be composed of an ensemble of eddies, which somehow attain an existence, grow in the unstable environment and then break up, presumably through a cascade of scales. Two extreme approximations have been adopted. In one (Gough 1965, 1977a), the growth is estimated from linear theory, thereby ignoring nonlinear interactions, and eventually the nonlinearities are posited to act instantaneously to break up the eddy and destroy its correlations between velocity and temperature fluctuations. The instants of creation and breakup are determined statistically, with probability distributions that are determined solely by the background state. In the other extreme (Unno 1967), the nonlinear interactions are presumed to dominate that aspect of the dynamics that determines the turbulent fluxes. In a statistically steady state, the eddies are presumed to be steady too, the buoyancy driving being balanced by an algebraic representation of nonlinear transfer

to other scales. This obviates the need to discuss creation and destruction. Both approaches can easily be worked out for a statistically steady convection zone, and yield essentially the same formulae for the fluxes. And both can be perturbed for studying stellar oscillations, although now the resulting equations for the perturbed fluxes lead to very different results. A careful comparison of these two extreme approaches has never been undertaken.

One major deficiency resides in the reduction of the whole turbulent cascade into a single length-scale, as it is assumed in mixing-length approaches. As the physical link with the cascade is lost, no realistic and reliable predictions for the perturbation of the mixing-length can be obtained. Unfortunately, it appears to play a major role in mode driving and damping. In all the formulations it is necessary to make assumptions, either explicitly or implicitly, about the anisotropy of the convective motion, and how it is modulated by the oscillations. In so naive an approach as mixing-length theory, this inevitably entails the introduction of new parameters, which, together with the parameters in the theory for steady convection, should somehow be calibrated against astrophysical observations, laboratory convection or numerical simulation, where possible. This is a difficult task, partly because we do not have enough experience with modelling and analysing convection and partly because we probably do not have enough data in a form in which we can comprehend their implications. The manner in which the anisotropy is taken into account affects the formulae for the turbulent heat flux and Reynolds stress, and thereby influences the computed damping rates of the oscillations.

It is important to recognise that the form adopted for the anisotropy of the convective motion reappears in the evaluation of the excitation integral of Eq. (24) discussed in the next section, although it is rare for the formulation of the forcing term \mathfrak{F} in the integrand to be consistent with the calculation of the damping rate. The rationale, usually unstated, appears to be that because the calculations of both the damping and excitation are uncertain, consistency between the two is hardly called for.

All currently reported stability computations suggest that low-degree solar g modes of order $n > 3$ are stable. For these modes, the damping is dominated by radiative losses (Kumar et al. 1996) and is found to be insensitive to the pulsation-convection interaction (Belkacem et al. 2009). For the stability of g modes with $n \leq 3$, however, detailed agreement has not been achieved, largely because the balance between nuclear driving, radiative damping and energy exchange with the convection is quite delicate (Christensen-Dalsgaard et al. 1974; Boury et al. 1975; Shibahashi et al. 1975). If grave g modes were indeed unstable some nonlinear process must have limited their exponential growth.

3.3 Amplitude limitation

Dziembowski (1982, 1983) studied the effect of three-mode interactions on the g-mode amplitudes. In particular, Dziembowski (1983) considered the special case of parametric resonance, in which a parent linearly unstable mode is coupled with two linearly damped daughter modes. Once a mode is sufficiently mature, it spawns two resonating g-mode daughters who sap energy from their parent at a rate proportional to the product of the amplitudes of the three modes. The parent is thereby unable to continue to evolve unencumbered, and eventually her growth is stunted. There are various ways in which the interactions can proceed, but the most effective for grave low-degree parents appears to be a coupling with a pair of similar high-degree twins leading to a

state in which the amplitudes of all three modes are steady. The most intricate part of the calculation is the evaluation of the interactions. However, the basic overall limiting process is generic. Therefore we illustrate it with a much simpler, one-dimensional acoustic process described in Appendix A. In that discussion the structure of the background state was assumed not to vary with time. Yet to achieve amplitude limitation appears to require frequency mismatches $\Delta\omega$ of order $10^{-6}\omega_0$, which would need to be maintained for times of order η^{-1} . That could be several decades or centuries. Can such precise resonance be maintained in the face of solar-cycle variation, or any other change? And if not, what are the consequences regarding g-mode amplitudes? These questions have been addressed by Jordinson & Gough (2000), who merely reported that the reduction in the amplitude limitation caused by drifting out of resonance is offset by the increased probability of actually encountering a resonance, leaving Dziembowski's estimate unchanged.

Dziembowski estimated a likely actual mode amplitude for $g_1(l=1)$ in the photosphere to be about 20 cm s^{-1} . That value is considerably greater than the upper bounds set by observation. Of course that discrepancy presents no actual serious conflict, because the estimate is probabilistic: Eq. (51) does not necessarily preclude a precise resonance with daughters of moderate degree whose damping rates are somewhat smaller than those of the 'most likely' resonance. Moreover, provided solar-cycle activity is confined essentially to the convection zone, associated structure variations are unlikely to have a large impact on mode resonance, which is determined by conditions in the region in the radiative interior in which the daughters are trapped.

But perhaps instead it is more likely that there is no intrinsically unstable g mode. All calculations to date have found models of the present Sun to be stable to all g modes, although a consistent modern calculation, carried out since the solar structure was determined seismologically, appears not to have been reported. So the possibility of there being grave self-excited g modes should not yet be wholly abandoned.

What is it, one naturally might ask, that is so different in more massive stars, such as SPB stars or γ Doradus stars, that enables them to undergo g-mode oscillations at such higher amplitudes? The principal difference is that they have only shallow convection zones, and therefore daughter g modes extend much higher in the envelope and dissipate much more strongly, thus being limited themselves to much lower amplitudes and thereby being less able to extract energy from their parent.

If all g modes were indeed stable today, their amplitudes would be determined from a balance between stochastic driving by turbulent convection and damping. We therefore discuss in the coming sections the physical mechanisms responsible for solar g-mode damping and excitation, and the resulting theoretical amplitude estimates that have been published to date.

3.4 Stochastic excitation by turbulent convection

3.4.1 Amplitudes of oscillations

If the general solution to the homogeneous equation of free oscillation were known, then the solution of Eq. (22) for forced oscillations could be written down in terms of \mathfrak{F} . The general solution for free oscillations of realistic stellar models is not known, but because the adiabatic oscillation eigenfunctions computed in the absence of the interactions with convection form a complete set (Eisenfeld 1969; Dyson & Schutz 1979), they can be

used as a basis for what is probably a reasonable approximation to the spatial structure of the oscillatory motion. What then remains is to characterise the fluctuating driving term \mathfrak{F} on the right-hand side of Eq. (22).

The first serious attempt to address this general problem for the Sun was by Stein (1966, 1967). This pioneering work addressed the generation of acoustic waves based on the method developed by Lighthill (1952) to derive the acoustic radiation from an isolated unstratified free-turbulent region, a region in which no external body force is imposed on the fluid. Because acoustic waves can exist in and propagate from the turbulent region, the local wave-turbulent interaction can be estimated from the turbulent field in terms of simple waves. Lighthill showed that, in the relatively straightforward situation in which he applied his analysis, conservation conditions required that the basic wave emission is quadrupolar. But in a stellar envelope stratified under gravity, the situation is more complicated. First, one cannot even define universal multipole emission components in general circumstances, although in simple cases, such as an isothermal atmosphere under constant gravity, a multipolar decomposition is possible (Unno 1966): the stratification produces monopolar (mass fluctuations) and dipolar emission (force fluctuations), in addition to quadrupolar (shear fluctuations), although, as Unno (1966), Stein (1967) and subsequently Osaki (1990) pointed out, there is a tendency for the monopolar and dipolar components to cancel.

A direct generalisation of Lighthill's method is not possible, because gravity waves cannot propagate through a convectively unstable medium. Indeed, it is probably not most prudent even to work in terms of simple emitted waves, because one would still have to impose resonance conditions on them in order to represent the normal modes, which, as Stein appreciated, involves some subtle argument. Instead, it is more straightforward to solve Eq. (22) as a nonsingular perturbation, regarding \mathfrak{F} as a forcing term on a spatially unperturbed oscillation eigenfunction ξ of oscillation having angular frequency ω and (positive) damping rate η . Basically, one represents the forced motion as $A(t)\xi(\mathbf{r})\exp(-i\omega t - \eta t)$, where A varies slowly compared with $\exp(-i\omega t)$. Substituting this into the spatio-temporal wave operator from which \mathcal{L} was derived, and retaining only terms proportional to A and its first derivative, yields a differential equation for A whose solution can be written down explicitly as an integral depending on ξ and \mathfrak{F} (Goldreich & Keeley 1977b; Balmforth 1992a; Musielak et al. 1994; Samadi & Goupil 2001; Chaplin et al. 2005). For statistically stationary turbulence exciting modes having characteristic wavelengths much greater than the typical scale k^{-1} of all convective eddies and with $\eta \ll \omega$, the integral expression for the mean-square amplitude A reduces to

$$\overline{A^2} \simeq \frac{1}{4\eta\omega^2\mathcal{I}^2} \int_0^\infty G(\tau) e^{-\eta\tau} \cos(\omega\tau) d\tau \quad (24)$$

(Chaplin et al. 2005), where $G(\tau) = \overline{Q(t')Q^*(t'')}$ is a global correlation function with argument $\tau = t' - t''$, the overbar denoting ensemble (or temporal) average, and

$$Q(t) = \int_{\mathcal{V}} \xi^*(\mathbf{r}) \cdot \mathfrak{F}(\mathbf{r}, t) dV, \quad (25)$$

the integral being over the volume V of the star. The asterisk denotes complex conjugate, and $\mathcal{I} = \int \rho\xi \cdot \xi^* dV$ is the inertia of the mode. The ensemble average $\overline{Q(t')Q^*(t'')}$ can itself be written as a double integral over the volume of the star. $Q(t)$ depends on a two-point correlation function between (\mathbf{r}', t') and (\mathbf{r}'', t'') which can be represented by its (local) Fourier transform $\chi(\nu, \mathbf{k}; \mathbf{r})$ with respect to τ and $\mathbf{r}' - \mathbf{r}''$ referred to the mean position $\mathbf{r} = (\mathbf{r}' + \mathbf{r}'')/2$.

The principal uncertainties in the estimation of $\overline{A^2}$ lie in the evaluation of the damping rate η and the correlation function G . The mean-squared surface velocity is computed, for each mode, as

$$\overline{v_s^2(h)} = \overline{A^2} \left[v_r^2(h) + v_h^2(h) \right] \quad (26)$$

where h is the height in the atmosphere at which the complex oscillation velocity $(v_r, v_h) = i\omega_0(\xi_r, \xi_h)$ is observed (for details see Houdek et al. 1995; Baudin et al. 2005).

3.4.2 Application to g-mode amplitudes

There have been several attempts to estimate the stochastic excitation of g modes, all of which stem from the early formulation by Goldreich & Keeley (1977a,b) of the mechanism of the excitation of global p modes. This work was initially extended by Goldreich et al. (1994) and then by others. The analyses differ in detail, as do the results. The differences in the assumptions adopted in the analyses occur in several places, and it is not possible to determine from the published work just how they influence the conclusions. Therefore we shall only summarise very briefly the principles behind the work.

The intention of Goldreich and his colleagues was to improve the earlier work on the excitation of solar p modes. Subsequently Kumar et al. (1996) addressed the issue of g-mode observability. The first step in the endeavour was to derive an explicit form of the linearized momentum equation governing the oscillations in order to obtain an explicit expression for the forcing term in Eq. (22). Goldreich et al. (1994) approached that task by implicitly assuming that the convection also satisfies the linearized momentum equation. The outcome is

$$\mathfrak{F} = -\nabla \cdot \left[\left(\frac{\partial p}{\partial s} \right)_\rho s' - \overline{\left(\frac{\partial p}{\partial s} \right)_\rho s'} \right] - \nabla \cdot (\rho v v - \overline{\rho v v}) , \quad (27)$$

where p is pressure, although Goldreich et al. (1994) did not explicitly separate the fluctuations from the means. This result generalises a similar expression presented by Goldreich & Kumar (1990) for an isentropically stratified plane-parallel atmosphere of perfect gas. The function \mathfrak{F} was entered into the integrals in Eq. (25) and the terms estimated from mixing-length theory.

In deriving the inhomogeneous wave equation Goldreich et al. (1994) omitted terms containing the Eulerian density perturbation (even when coupled with the gravitational acceleration, a term that must not be neglected even in the Boussinesq approximation) and the inertia terms of the convection. Furthermore, the authors assumed that the effect of the oscillations is to destroy the balance of the convective momentum transfer in such a way that the linearized momentum equation is satisfied in the absence of Eulerian entropy fluctuations, leaving the unbalanced convective entropy fluctuations and nonlinear inertia terms to drive the oscillations. This assumption caused the entropy fluctuations to be an order of magnitude more effective than the fluctuating Reynolds stress in driving the oscillations. Goldreich et al. (1994) ignored products of oscillation variables and convective fluctuations, and the effect of the oscillations on the convection. Consequently an adiabatic linear wave equation (with homogeneous terms untrammelled by convection) is supplied just with an inhomogeneous forcing term to

account for all the effect of convection. The anisotropy of the convective motion was acknowledged merely by multiplying the entire inhomogeneous term \mathfrak{F} by a single constant scaling factor, which was determined by calibrating the energy supply rate to the oscillations against observation.

The theory was reformulated by Samadi & Goupil (2001), who combined aspects of the analyses by Stein (1967) and Goldreich & Keeley (1977b). Perturbations due to convection and global oscillations were separated in the equation of motion, and approximated according to their dominating dynamics, adopting a Boussinesq-like approximation for the convection. Samadi & Goupil (2001) have shown that the linear term due to entropy fluctuation [Eq. (27)] introduced by Goldreich et al. (1994) gives no significant contribution to the driving but the advection of Eulerian entropy fluctuations by turbulent velocity. The analysis represents what is probably the most careful recent attempt to generate a consistent forced wave equation. Unfortunately, however, there is subsequently an error in the treatment of the frequency correlations in the expression for the driving by the fluctuating Reynolds stress, corrected by Samadi et al. (2005).

The predictions for the maximum amplitude for ξ Hydrae made by Houdek & Gough (2002) and Samadi et al. (2007) are in good agreement with the observations by Frandsen et al. (2002), while their predicted maximum amplitude for Procyon are overestimated by a factor 2 to 4. This discrepancy for Procyon is serious and must be understood; the structure of Procyon is rather different from other stars that have been modelled, indicating that the theory, anchored by calibration against solar p modes, cannot not be extrapolated reliably to very different stars. By the same token the reliability of extrapolating from p modes to g modes even in the Sun must be exercised with due caution, and may not be as reliable as Kumar et al. (1996) suspect.

One of the controversial conclusions of the discussion by Goldreich et al. (1994) is that driving from the first term in Eq. (27) for \mathfrak{F} is an order of magnitude greater than driving from the fluctuations in the Reynolds stress, at least for acoustic emission. This contradicts the earlier findings of Goldreich & Kumar (1990) who concluded that, in a convection zone that appears to the oscillations (but not to the convection) to be adiabatically stratified, the contribution from the two terms are comparable. The latter conclusion had been drawn from the realisation that the emission from what Goldreich & Kumar (1990) termed the monopole and dipole sources (contributions which in a stratified envelope are not unambiguously defined, cf. Unno (1966) from the buoyancy (entropy fluctuation) terms largely cancel as a result of the manner in which the eddy motion is correlated with them. Such cancellation results in predominantly quadrupolar emission, as Osaki (1990, see also Houdek 2006) also pointed out, and is consistent with Stein's (1967) earlier findings. It is interesting to note that simulations by Stein & Nordlund (2001); Stein et al. (2004), and the model calculations by Belkacem et al. (2006b) and Samadi et al. (2007) indicate that emission is dominated by the fluctuating Reynolds stress and entropy fluctuations as had been implied by Balmforth's (1992b) discussion.

The treatment of the turbulent velocity spectrum in evaluating the correlation integral of Eq. (24) deserves some comment. In this context, Stein (1967) first adopted the quasi-normal approximation to relate the fourth-order correlation to a sum of three independent products of second-order correlations, as have others who have explicitly considered the velocity correlation after him, notwithstanding Kraichnan's (1957) warning of the danger of so doing. This decomposition would be correct if the probability distribution function of turbulent quantities were Gaussian, which is not what was

subsequently assumed (see Belkacem et al. 2006a; Kupka & Robinson 2007). Note that a decomposition of the fourth-order moment that takes the effect of plumes into account has been proposed by Belkacem et al. (2006a) and permits to better reproduce the observations (Belkacem et al. 2006b). The dominant term (a product of single-point correlations) is balanced by the Reynolds stress that appears as the last term in Eq. (27), leaving the forcing term \mathfrak{F} to depend only on two-point correlations. The next approximation adopted by Stein (1967) is to write the energy spectrum as a product of a function of local wavenumber and a function of frequency, relating the three-dimensional velocity correlation to the energy spectrum by the formula valid for incompressible, homogeneous isotropic turbulence (Batchelor 1953). This result is approximately valid for isotropic turbulence in the Boussinesq approximation - almost universally adopted, either explicitly or implicitly, in mixing-length theory - and which can be generalised to the axisymmetric case expected of convection in a nonrotating star (Chaplin et al. 2005), although the generalisation to anisotropic turbulence has been adopted (e.g. Belkacem et al. 2009). Similar approximations have been used in p-mode studies by Balmforth (1992a), Samadi & Goupil (2001) and Samadi et al. (2003b).

3.4.3 The energy-equipartition principle

A simple way of crudely estimating the mode amplitudes, without recourse to an explicit model for the excitation and damping of oscillation modes, is to adopt the equipartition ansatz discussed first by Goldreich & Keeley (1977b). It is obtained from a rough estimate of the integral in Eq. (24), which is proportional to the ratio of the rate of forcing to the energy lost by dissipation (cf Batchelor 1953). The energy supply rate was estimated from a mixing-length-like description of turbulence assuming that the motions of all the convective eddies are independent of one another, and that, as usual, the spatial scale of the eddies is the smallest of all scales, being less than both the scale height of the background state and the inverse wavenumber of the oscillation eigenfunction. The temporal spectrum of the turbulence was taken to be Gaussian, with variance proportional to the square of the characteristic timescale τ_c of the energy-bearing eddies (i.e. the largest eddies, with spatial scale equal to the mixing length ℓ), and with an autocorrelation that is significant only over the spatial scale of a single eddy. The intrinsic damping rate η was estimated by Goldreich & Keeley (1977) from a radial-pulsation calculation in which they presumed, as had Cox et al. (1966) previously, that the phase of the perturbed heat flux F'_c is determined by the equation $dF'_c/dt = -F'_c/\tau_c$, and that the Reynolds stress, whose influence dominates the energy loss, can be represented by a time-independent scalar turbulent viscosity ν_t whose value is either $v_c^2 \tau_c$, where v_c is a characteristic velocity of an energy-bearing eddy, provided $\omega \tau_c < 1$, or $v_\lambda^2 \tau_\lambda$, where v_λ is the velocity of an eddy in the turbulent cascade (assumed to satisfy Kolmogorov scaling) that resonates with the pulsation: $\omega \tau_\lambda = 1$. This discontinuous change in behaviour had been adopted previously by Goldreich & Nicholson (1977), and takes some account of the fact that eddies with timescales much greater than ω^{-1} contribute very little to the dissipation of the pulsational motion; more sophisticated mixing-length descriptions of convection (e.g. Gough 1965, 1977a; Unno 1967) predict a continuous transition.

From simple scaling arguments Goldreich & Keeley (1977b) concluded that the turbulent fluctuating momentum fluxes with timescales comparable with the pulsation period dominate the driving term Q [Eq. (25)], as had Stein (1967) before them,

and, because the dissipation is also dominated by the same fluxes, via ν_t , there is a cancellation of a squared turbulent velocity in the power-to-dissipation ratio, leading to an equipartition between the energy E_{osc} in a mode of oscillation and the energy $\rho \ell^3 v_c^2 / 2$ in a single resonating eddy satisfying $\omega \tau_c = 1$, if such an eddy exists, or the most energetic resonating eddy in the turbulent cascade if no such energy-bearing eddy exists. In the case where one does exist, this balance may be written

$$E_{\text{osc}} = \Lambda p_t \ell^3 \equiv E_c, \quad (28)$$

where p_t is the (r, r) component of the Reynolds stress (also known as the turbulent pressure), and Λ is a factor of order unity whose value depends on uncertain properties of the turbulent flow, and is therefore itself uncertain.

This equipartition principle was adopted by Christensen-Dalsgaard & Frandsen (1983) for estimating p-mode amplitudes in main-sequence stars, and was applied for estimating g mode amplitudes in the Sun by Gough (1985; see also Berthomieu & Provost 1990). In these calculations it was necessary to estimate the convective timescale τ_c , which in the Sun has a minimum in the superadiabatic boundary layer (see e.g. Chaplin et al. 2005). Hence, for a mode with a period Π that is longer than $\min(\tau_c)$ there are at least two radii in the convection zone where $\tau_c = \Pi$, because formally τ_c tends to infinity towards the boundaries of the convection zone. The kinetic energy in a mode is then balanced against the sum of the values of E_c at these points.

Because the value of Λ is uncertain, Gough (1985) calibrated the calculation by equating the maximum value of the amplitudes of the 5-minute p-mode oscillations with the value observed. He then obtained a maximum velocity amplitude of about 0.5 mm s^{-1} for the gravest quadrupole g mode and 1 mm s^{-1} for the gravest dipole g mode, and about 3 mm s^{-1} for gravest of low-degree p modes. The result is very nearly a function of frequency alone; it is depicted in Fig. 15.

3.4.4 The results of Kumar, Quataert and Bahcall

Kumar et al. (1996), motivated by a claim of g-mode detection in the solar wind (Thomson et al. 1995), carried out computations using the formalism developed by Goldreich et al. (1994) originally to estimate the amplitudes of p modes. In this formulation, Kumar et al. (1996) assumed a simplified description of turbulence in which the velocities, length scales and timescales cascade consistently according to the Kolmogorov spectrum. They assumed that the modes are driven solely by the fluctuating Reynolds stress. Their calculation was identical to that of Goldreich et al. (1994).

Of particular interest is the way in which the eddies and the standing waves are temporally correlated. In the Goldreich & Keeley (1977b) approach, from which was derived the procedures of Balmforth (1992a); Goldreich et al. (1994), it was assumed that the temporal correlation between eddies is Gaussian. As we shall see in the following sections, variations in the manner in which that function is chosen can lead to very different estimations of g-mode amplitudes.

Concerning the damping rates, both turbulent and radiative contributions to the damping rates were included as derived by Goldreich & Kumar (1991). Turbulent damping was approximated purely as a momentum-diffusion process, with a time-dependent scalar diffusion coefficient derived from mixing-length estimates of the motion of eddies with lengthscales smaller than the local wavelength of the oscillation. Temporal modulation of the Reynolds stresses, considered to be as important as momentum diffusion, if not more so, at least for grave p modes (e.g., Baker & Gough

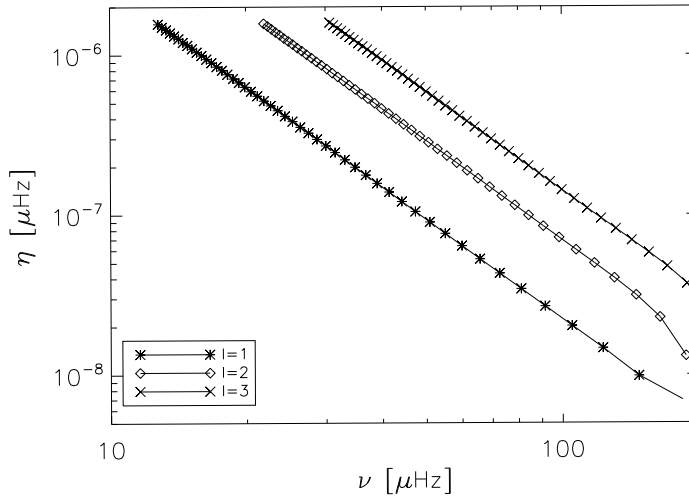


Fig. 14 Theoretical damping rate η of g modes of low degree plotted versus cyclic frequency ν according to the predictions by Belkacem et al. (2009).

1979; Balmforth 1992b), was ignored, as was the modulation of the energy generation in the core. For higher-order p modes of low degree, the diffusive contribution was estimated by Goldreich & Kumar (1991) to be comparable to the radiative losses, but for low-order p and g modes it is smaller (Goldreich & Kumar 1991; Balmforth 1992b).

Goldreich & Kumar (1991) found mode lifetimes of about 10^6 y, comparable with previous estimates. The resulting surface mode amplitude, based on Eq. (26), was found to be greatest, at about 1 mm s^{-1} , for $l = 1$ modes near $\nu = \omega/2\pi = 200 \mu\text{Hz}$; modes with $\nu < 100 \mu\text{Hz}$ were all found to have amplitudes less than $10^{-2} \text{ mm s}^{-1}$.

3.4.5 The results of Belkacem et al.

Belkacem et al. (2009) investigated the particular case of the amplitude of asymptotic g modes. The formalism used by Belkacem et al. (2009) to compute excitation rates of non-radial modes was developed by Belkacem et al. (2008) who extends to non-radial modes the work of Samadi & Goupil (2001). The turbulent-mean stresses were neglected since the excitation takes place in the innermost convective layers where the Mach number is very small. The driving is shown to be dominated by the Reynolds-stress fluctuations. In this formalism, the turbulent kinetic energy spectrum as well as the eddy-time correlation function are derived from 3D numerical simulation (see Belkacem et al. 2009, for details). The Lorentzian function (χ_k) is found to better reproduce the eddy-time correlation function from the 3-D numerical simulation than a Gaussian function in the frequency range $\nu \in [20 \mu\text{Hz}; 110 \mu\text{Hz}]$. In addition, the eddy-time correlation function is poorly represented by a Gaussian function, which underestimates χ_k by many order of magnitudes.

Damping rates are computed with a fully non-radial non-adiabatic pulsation code MAD (Dupret et al. 2006c,b,a), including a non-local treatment of convection based on Unno (1967) formalism extended to non-radial modes by Gabriel (1996); Grigahcène et al. (2005). It takes into account the role played by the variations of the convective flux, the

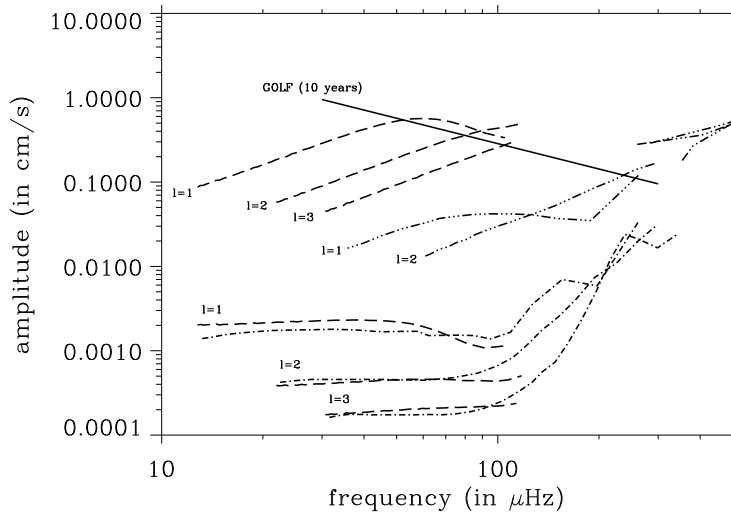


Fig. 15 Estimated amplitudes of stochastically excited g modes of low degree plotted against cyclic frequency ν . The estimates are rms surface values for singlet modes (single values of n , l and m), joined by lines: triple-dot-dashed for Gough (1985), dot-dashed for Kumar et al. (1996) and dashed for Belkacem et al. (2009). The continuous line is an estimated from 10 years GOLF data (García et al. 2007). For proper comparison, the effect of the spatial instrumental filter must be included, i.e. visibilities (See Belkacem et al. 2009) (See Section on Observables).

turbulent pressure and the dissipation rate of turbulent kinetic energy. Belkacem et al. (2009) have found that for high frequency g modes ($\nu > 110 \mu\text{Hz}$), the work integrals and thus the damping rates are sensitive to the convection/pulsation interactions because the role of the surface layers in the work integrals becomes important. In contrast, for low-frequency g modes ($\nu < 110 \mu\text{Hz}$), the work integral and then the damping rates are found to be *insensitive* to the convection/pulsation interactions as well as the non-local parameters. Eventually, the damping rates dominated by radiative losses behaves as ν^{-3} .

Taking visibility factors as well as the limb-darkening into account, Belkacem et al. (2009) finally found that the maximum of apparent surface velocities of asymptotic g -modes is $\approx 3 \text{ mm s}^{-1}$ for $\ell = 1$ at $\nu \approx 60 \mu\text{Hz}$ and $\ell = 2$ at $\nu \approx 100 \mu\text{Hz}$. Those results then put the theoretical g -mode amplitudes near the GOLF observational threshold.

The principal differences between the calculations Belkacem et al. (2009) and Kumar et al. (1996) stems from the turbulence spectra that were adopted. It would create enormous differences in g -mode amplitudes. They are produced by convection-oscillation interactions deep in the convection zone, which are off resonance, and whose intensity depends crucially on the assumed frequency dependence of the turbulent spectrum in the high-frequency tail. Stein (1967) and Goldreich & Keeley (1977b) had favoured a Gaussian distribution. A Gaussian was preferred also by Chaplin et al. (2005), for although the energy-bearing eddies of the convection theory they used (that of Gough 1965, 1977a) has a Lorentzian time-dependence. We discuss the disparity in Section 3.5.

3.4.6 High-order waves generated at the base of the convection zone

A series of papers using a wave-mechanical consistent numerical approach with a simplified two-dimensional solar model attempted to quantify the excitation of gravity waves in the solar interior as well the transmission of gravity waves through the solar convection zone (Press 1981; Zahn 1991; Andreassen et al. 1992; Andersen et al. 1993; Andersen 1994, 1996; Talon & Charbonnel 2003). The results indicate that the efficiency of generating gravity waves in the interior by convective overshoot is slightly less than 0.1% for waves with a horizontal extent equivalent to $l=6-18$. The overshoot layer where the excitation occurs is very shallow, 0.02-0.06 pressure scale heights. The energy transmission through the convection zone of a gravity wave equivalent to an $l=6$ mode is found to be $3-8 \cdot 10^{-4}$ in the 50-250 μHz . Combining these results indicate that the convective overshoot into the interior provides enough energy to sustain an amplitude of 1-5 mm s^{-1} at the surface of a single gravity mode. If the energy is distributed into more modes the amplitudes are reduced by the square root of the number of modes.

These results should not be taken as serious physical predictions of amplitudes of solar g-modes, but rather as a demonstration that there is enough energy available in the convective overshoot to maintain a single g-mode at an observable level at the solar surface. Assuming that a thousand modes are excited and scaling the amplitudes to an $l=1$ mode implies an amplitude of about 0.02-0.08 cm s^{-1} in the 50-250 μHz . As seen from Fig. 15, this is approximately the same values provided by Gough (1985).

3.4.7 Prediction of g-mode amplitudes

Amplitudes of singlet g modes (single values of n , l and m) predicted by Gough (1985), Kumar et al. (1996) and Belkacem et al. (2008, 2009) are depicted in Fig. 15. Shown are the root-mean-square total velocity amplitudes in the photosphere; instrumental filtering (e.g. Dziembowski 1977; Christensen-Dalsgaard & Gough 1982) must be taken into account when converting these values into observables.

3.5 Discussion

The principal difference between the calculations of Kumar et al. (1996) and Belkacem et al. (2009) stems from the turbulence spectra that were adopted and, in particular, the way the two lead to enormous differences in g-mode amplitudes. Those differences are produced by convection-oscillation interactions deep in the convection zone, which are off resonance, and whose strength depends critically on the assumed frequency dependence of the turbulent spectrum in the high-frequency tail⁵.

For solar p modes, Stein (1967) and Goldreich & Keeley (1977b) had used a Gaussian time-correlation function. A Gaussian was preferred also by Chaplin et al. (2005), for although the energy-bearing eddies of the convection theory they used (that of Gough 1965, 1977) has a Lorentzian time-dependence, Chaplin et al. (2005) reported

⁵ In this section, we denote by time-correlation function the Fourier transform χ_k of the local correlation function entering the evaluation of the global correlation function $G(\tau)$ appearing in Eq. (24) (see Samadi & Goupil 2001; Chaplin et al. 2005, for details). We discuss Gaussian and Lorentzian forms, both of which have characteristic widths that depend on the lengthscales and timescales of the convective eddies, and therefore vary with position \mathbf{r} in the star.

that there is experimental evidence for more rapid decline in the tail. However, Samadi et al. (2003a) had pointed out that the three-dimensional simulations by Stein & Nordlund (2001) were more nearly Lorentzian. Indeed, Samadi et al. (2003a) and Belkacem et al. (2006b) reported that the use of a Lorentzian function reproduces the observations for solar p modes better. A similar conclusion was reached by Samadi et al. (2008) in the case of the star α Cen A. In contrast, Chaplin et al. (2005) mention that a pure Lorentzian results in an over-estimation for the low-frequency modes. They explained that the over-estimation of the mode excitation rates at low frequency results from the Lorentzian function decreasing too slowly with depth compared to a Gaussian. Consequently, a substantial fraction of the excitation rate of the low-frequency modes arises from large eddies situated deep in the Sun. A Gaussian time-correlation function gives much less weight to the large off-resonance eddies. Which is more nearly correct remains an open issue.

Belkacem et al. (2009) favoured a Lorentzian modelling for solar g modes, on the ground that it reproduces the 3D numerical convection simulations by Miesch et al. (2008) more closely. More specifically, the best fit was found using a sum of Lorentzian and Gaussian functions. The Gaussian shape is found by the authors to reproduce the very low-frequencies while the Lorentzian the highest frequencies, which are of particular interest. There is yet no definite issue, but what is sure is that it has a crucial impact on predicted g-mode amplitudes. As demonstrated by Belkacem et al. (2009), Gaussian and Lorentzian time-correlation functions lead to differences in mode surface velocities of several order of magnitude.

It is worthwhile mentioning that experimental studies of turbulent convection can provide some clues towards the resolution of this issue. In particular, the recent work of Mordant et al. (2004) demonstrates that the two-point second-order time-correlation relevant to our discussion is reasonably well reproduced by an exponential decrease with separation time in the inertial range (see their Fig. 10) which is in agreement with Kolmogorov (1941) phenomenology (see also Sawford 1991). It corresponds to a Lorentzian power spectrum with respect to frequency, which lends support to the use of a Lorentzian in the Sun, even though the Prandtl number in the experiment (6.8) is very far from solar. At frequencies beyond the inertial range dissipation causes the spectrum to decline more rapidly (see Fig 13 of Mordant et al. 2004). It is interesting to record that simulations by Georgobiani et al. (2006) indicate that the spectrum is actually not separable in frequency and wavenumber, as Kraichnan's (1957) had already pointed out, and suggested an empirical improvement.

Another important matter for solar g modes is the way in which the damping rates are computed. Belkacem et al. (2009) did not calibrate their predictions against observations of p modes, because they considered that because the g modes of higher-frequency ($\nu > 110 \mu\text{Hz}$), whose damping rates depend on the uncertain modelling of the interaction with convection, could not be predicted reliably, a meaningful connection with the p-mode regime of current observation could not be made. Instead they restricted attention to low-frequency modes whose damping rates η are dominated by radiative losses, and scale with ν^{-3} , a behaviour which follows from straightforward asymptotic argument (e.g. Belkacem et al. 2009), and which is evident in Fig. 14. But for grave g modes, the situation is less clear. It should perhaps be pointed out in passing that the ϵ mechanism is significant for the grave g modes, and the influence of the dynamically induced thermodynamic perturbations must consistently be taken into account. A predictive description of the interaction between convection and oscil-

lations when both are strongly coupled is mandatory to obtain reliable mode amplitude estimates in this frequency domain.

3.6 Some concluding remarks

Concerning the damping rates, the failure to detect g modes favours that they are linearly stable. Theoretical amplitude estimates investigated by Dziembowski (1983, 1982) and Jordinson & Gough (2000) are well above the current detection threshold, although it must be appreciated that the results are somewhat uncertain.

In the high-order asymptotic regime, radiative diffusion is thought to be the dominant contribution to g-mode damping. For low-order g modes the situation is less clear since those modes are sensitive to the interaction with convection, as are the p modes; there is no consensus about the dominant contribution to the mode line-width (e.g., Houdek 2006). This issue is very important and prevents an unambiguous theoretical determination of low-order g-mode amplitudes.

For the driving mechanism, turbulent convection is thought to be responsible for g-mode excitation (Gough 1980; Kumar et al. 1996; Belkacem et al. 2009), and is probably dominated by the contribution of the Reynolds stresses. Indeed, the so-called entropy contribution to the driving is found in the current theoretical computation to be negligible for both low- and high-order g modes since they are not sensitive to the very upper layers where entropy fluctuations are important.

Quantitative estimates of mode amplitudes differ from each other by orders of magnitude, depending principally on the way the turbulent eddies are time-correlated. While Kumar et al. (1996); Chaplin et al. (2005) favours a Gaussian profile to describe this function, Samadi & Goupil (2001); Samadi et al. (2003a, 2007); Belkacem et al. (2009) used a Lorentzian profile. It should be clear that the eddy correlation function cannot be analytically derived, and therefore is adhoc taken either from 3D simulations or turbulence experiment; as such it is a scale parameter. In fact the truth is probably somewhere in between, the challenge is now to determine where exactly. The detection of g modes would provide a definite answer to this burning question.

4 Detection techniques

In this section, we present different detection techniques that have been applied in searches for g modes. We discuss the conceptual design of each technique using the metaphor of bricks. We consider each *detection technique* to be built or comprised of several bricks or *categories*. An appropriate combination of various bricks constitutes a given *detection technique*. The categories we consider are as follows:

- Observables
- Spatial and temporal filters
- Spectrum estimators
- Statistical testing
- Patterns
- Data combinations

The choice of the solar observable (or perturbation) to be observed plays a key rôle in determining the likely success, or otherwise, of a given technique (i.e., it can affect

sources of noise, observed mode amplitudes etc.). Since we analyse time series, the temporal filter of these series (e.g., low-pass, high-pass, band-pass) also merits careful attention. Observations of the Sun may be made by imaging the surface onto several or many detector pixels, or by observing the “Sun as a star”. When resolved observations are made, it is advisable to apply appropriate spatial masks to extract the signatures of the modes of interest.

The detection of potential frequencies of interest requires that we obtain estimates of the frequency spectrum, using Fourier transform or other techniques. Then, a thorough statistical assessment of what is observed plays a key part in deciding whether or not something of interest has been detected. If the identification of individual frequencies fails, one can then bring more *a priori* information to bear in the detection procedures, for example by searching for signatures of patterns expected from theoretical modelling of the g modes (e.g., near constant spacings in period of modes in the asymptotic regime, rotational frequency splittings etc.). Use of a priori knowledge in this way suggests a Bayesian approach to the analysis. Finally, if the detection is not successful with a single instrument, one can bring data from different instruments to bear, for example by searching for coincidences in the different datasets.

4.1 Observables

Perturbed parameters such as temperature and displacement can be deduced from observables. The displacement can be either physically observed or inferred from the solar radial velocities.

The solar oscillations were first detected in radial velocity observations made by Leighton et al. (1962). This method is now widely used for observing solar p modes. Solar radial velocities can either be measured from resolved images of the Sun (Unno et al. 1989, and references therein), or from full-disc integrated Sun-as-a-star observations. The instrument aboard SOHO all rely on measuring the intensity distribution in an absorption line for deriving the solar radial velocity either locally such as with the SOI/MDI⁶ instrument (Scherrer et al. 1995) or globally with the GOLF⁷ instrument (Gabriel et al. 1995). This set of instrument is also complemented by ground-based networks such as the high-resolution GONG⁸ instrument (Harvey et al. 1996), and the full-disk integrated BiSON⁹ instrument (Chaplin et al. 1996). The lengths of the usable time series are about 14 years for MDI and GOLF, 15 years for GONG and nearly 30 years for BiSON.

Temperature perturbations induce intensity fluctuations that can be detected. Intensity fluctuations may also be induced by changes in the size and shape of the solar surface produced by the oscillation modes (Toutain et al. 1999). Intensity fluctuations were first observed from space by Woodard & Hudson (1983) in solar irradiance data collected by the ACRIM¹⁰ instrument (Willson 1979). Similar observations have been made with sunphotometers from stratospheric balloons (e.g. Fröhlich 1984) which confirmed the ACRIM results. Ground-based observations with the SLOT¹¹ instru-

⁶ Solar Oscillations Investigation / Michelson Doppler Imager

⁷ Global Oscillations at Low Frequency

⁸ Global Oscillations Network Group

⁹ Birmingham Solar Oscillations Network

¹⁰ Active Cavity Radiometer Irradiance Monitor

¹¹ Solar Luminosity Oscillation Telescope

ment produced rather marginal p-mode detections (Jiménez et al. 1987), while rather higher signal-to-noise data were collected by the LOI¹² instrument, observing from El Teide, Tenerife Appourchaux et al. (1997, 1995). Following the success of ACRIM, the IPHIR¹³ instrument onboard the PHOBOS mission lead to the first long-duration intensity measurements of the solar p modes (Toutain & Fröhlich 1992). The ACRIM, SLOT and IPHIR instruments lead to the design of the VIRGO¹⁴ instrument for the SOHO mission, which was composed of two radiometers (DIARAD and PMO6), three Sun PhotoMeters (SPM) and the LOI (Fröhlich et al. 1995). The lengths of the usable time series are about 14 years for VIRGO.

Intensity fluctuations produce a much lower signal-to-noise ratio in the p modes than do solar radial velocity observations. The signal-to-noise ratio for the former is at most 30, while the latter is at most 300; examples of the various signal-to-noise ratios for the different observables can be found in Toutain et al. (1997).

The detection of the physical displacement is more difficult. For instance a putative g-mode amplitude of 1 mm s^{-1} at a frequency of $100 \mu\text{Hz}$ would induce a peak-to-peak variation of $4.3 \mu\text{arcsec}$ as seen from the Earth, whereas for a p-mode amplitude of 30 cm s^{-1} (at a frequency of $3000 \mu\text{Hz}$) would induce a variation of $43 \mu\text{arcsec}$. In the 1970's, the SCLERA¹⁵ instrument was used in an attempt to detect p modes and g modes alike (Oleson et al. 1974; Hill 1985, 1992). The detection of displacement was performed by observing the change in diameter of the Sun (Brown et al. 1978), and signals with typical amplitude of the order of 5 marcsec were observed. These amplitudes were about a factor of 100 larger than the expected amplitudes for p modes, based on high signal-to-noise detections of the p modes made in radial velocity observations (Claverie et al. 1981; Fossat et al. 1981). This discrepancy cast some doubt on the identification of the detected SCLERA peaks as p modes.

The PICARD mission, due for launch in late 2009 (Damé et al. 1999), will be sensitive not only to the displacement, but also to intensity fluctuations induced by temperature perturbations, like those detected by Appourchaux & Toutain (1998) with the VIRGO/LOI or by Toner et al. (1999) with SOI/MDI. PICARD will have the capability of making observations of displacement and intensity fluctuations at the limb of the Sun, where the perturbations appear to have higher amplitude than those observed in the disc. This amplification, theorised by Toutain et al. (1999), is due to the fact that at the solar limb the atmosphere becomes more transparent, providing a larger contribution from the other hemisphere.

Another potential observable is the perturbation of the gravitational field caused by the g modes producing tidal perturbations of the Newtonian fields, and generating detectable gravitational waves (Christensen-Dalsgaard & Gough 1980; Giamperi et al. 2000). The perturbation is non-zero only for modes with $l \geq 2$; for $l = 1$ it is exactly zero. The advantage is that the solar noise caused by convection would have a negligible impact on the perturbation of the gravitational field. Unfortunately, as Christensen-Dalsgaard (2002b) explicitly mentions, signal from galactic binary stars could be the limiting factor for g-mode detection and not the Sun itself.

¹² Luminosity Oscillations Imager

¹³ InterPlanetary Helioseismology by IRradiance measurements

¹⁴ Variability of IRradiance and Gravity Oscillations

¹⁵ Santa Catalina Laboratory for Experimental Relativity by Astrometry

4.2 Spatial and Temporal filters

4.2.1 Temporal filters

The analysis of discretized signals dates back to the start of the telephone and telegraphic system, when Harry Nyquist devised the so-called Nyquist frequency (Nyquist 1924), and when Claude Shannon enunciated the Shannon theorem concerning the sampling of band-limited signals (Shannon 1949). Both worked at Bell Telephone Laboratories.

Although, we do not always follow the Shannon-Nyquist prescription, one should not forget the limitation inherent in the sampling of a band limited signal. The main difficulties encountered in astrophysical applications are as follows:

- the signal is *not* band limited
- the signal is undersampled
- the signal is aliased

These three factors are not unrelated to one another.

In our case, the observations of intensity fluctuations and of solar radial velocities do not present a clear high-frequency cut-off (Kosovichev et al. 1997; Fröhlich et al. 1997). The frequency drop-off of the solar background noise at high frequencies is proportional to ν^2 (Harvey 1985; Aigrain et al. 2004, and references therein), or possibly even a higher power law (Appourchaux et al. 2002). Since the astrophysical signal is *not* band limited, the highest frequencies will not be properly sampled, resulting in an *undersampled* signal. This leads to high-frequency signal leaking back into the spectrum, below the Nyquist frequency, i.e., aliasing of the signal. The imaging effect of aliasing is to produce the Moiré effect when the image is not properly sampled.

It is also worth pointing out that the Shannon theorem states that the signal should not only be properly sampled, but also properly integrated over the sampling interval. In other words, one should have a 100% fill cycle (the fill cycle being the ratio of the integration time to the sampling time). If this is not the case, frequencies from the non-band limited signal above the Nyquist frequency will not be suppressed. It is then very critical to make sure that the fill cycle is as high as possible, thereby helping to reduce the aliasing effects of the high-frequency power contained in the non-band limited signal. The aliasing effects will severely affect the derivation of how the power drops at high frequency, implying that extreme care should be taken when recovering the power law of the background at high frequencies. From this point of view, the VIRGO instrument aboard SOHO has, by design, a fill cycle very close to 100% (Fröhlich et al. 1997), while that of GOLF is 80% (Gabriel et al. 1995).

Last, but not least, since the signal is digitised, it is possible to use digital filters that are routinely used in the electronic world for many digital applications (telephone, images and so forth; Antoniou 1979).

4.2.2 Spatial filters: Sun-as-a-star observations

When the Sun is observed as a star, there is a cancellation effect due to the integration over the disk. The net effect is that not all modes can be detected. The calculation of the attenuation as a function of the degree of the modes is given by Christensen-Dalsgaard & Gough (1982) for solar radial velocities and by Toutain et al. (1999) for intensity; mainly modes with $l \leq 4$ can be detected. To the first order, when

the solar inclination angle is 90 degrees with respect to the line of sight, only the odd $l + m$ modes are detectable. Nevertheless, there is a small effect with the solar inclination angle discussed recently by Gizon & Solanki (2003), rendering all $2l + 1$ singlet modes of a multiplet detectable (See also Ballot et al. 2006, 2008). Indeed, several attempts had already been made to determine from the relative amplitudes of the observed p-mode singlets in the Sun the orientation of the principal axis of rotation (Gough et al. 1995; Gizon et al. 1998) For g modes, the sensitivity to the degree of the modes was derived by Berthomieu & Provost (1990) for both intensity and solar radial velocities. They showed that for g modes, sensitivities of different degrees depends strongly on frequency. The large difference in sensitivities between solar radial velocities and intensities can in principle be exploited to help identify detected g modes.

4.2.3 Spatial filters: spatially resolved solar images

The observation of resolved images of the Sun makes possible the decomposition of the spatial structure of the modes onto functions that are related to the modes. The spatial filters may be classified in terms of different types of mask:

- spherical harmonics masks
- g-mode specific masks
- optimal masks
- time-distance masks

For p modes, the obvious choice for the masks is to use the spherical harmonics that match the spatial dependence of the modes when the star is spherically symmetric (Unno et al. 1989). When the star rotates steadily or has a magnetic field, the spatial dependence becomes more complicated (Gough & Kosovichev 1993; Gizon et al. 1998) partly because the star is no longer spherically symmetrical, and partly because the modes must be referred to a frame of reference, if one exists, in which the state of the star is steady. If no such state exists, a well defined frequency of oscillations does not exist either. One has to bear in mind that such effects could be important for the visibilities of g modes if there is a large magnetic field in the central core (Goode & Thompson 1992; Rashba et al. 2006).

Spherical-harmonic masks correspond to displacement or temperature perturbations (velocity or intensity observations). These masks were applied first in the 1980s by Brown (1985) (using an algorithm based on the Fast Fourier transform). The degree sensitivities of these masks have been derived by Schou (1992), Appourchaux et al. (2000) and Corbard et al. (2008) for imaging instruments such as SOI/MDI, GONG, LOI, or SODISM¹⁶ on the PICARD mission.

Unfortunately, although the spherical-harmonic masks are rather well adapted for most p modes, they are not well adapted for the g modes. For velocity observations, the significant horizontal g-mode displacement must be taken into account (the perturbations induced by p modes are predominantly radial), the spatial dependence of which differs from that of the radial displacement. For intensity observations, the oscillations perturb the figure of the Sun modulating the light emitted from the surface (Berthomieu & Provost 1990; Toutain et al. 1999). For either type of observation, the additional contribution is a non-spherical harmonic function (Unno et al. 1989; Appourchaux & Andersen 1990). Specific g-mode masks can be devised (for intensity

¹⁶ Solar Diameter Imager and Surface Mapper

observations see Appourchaux & Andersen 1990). In some cases inclusion of the most appropriate spatial dependence of the g-mode perturbation still remains to be done. A large uncertainty lies in the way nonadiabatic effects are accounted for.

Masks that are optimal for some specific signals have been developed. For instance, Appourchaux & Andersen (1990) developed p-mode intensity masks that minimise both the leakage from other degrees and also the leakage from other m (see also Christensen-Dalsgaard 1984; Kosovichev 1986a,b). Similar masks have been derived by Gough & Latour (1984), Appourchaux et al. (1998) and by Toutain & Kosovichev (2000). Recently, Wachter et al. (2002) produced g-mode masks optimising (i.e. minimising) the noise contribution from the supergranulation noise across the solar disc (which has a strong horizontal component).

Other kinds of masks derived from the properties of the observations themselves have been used by Vecchio et al. (2005). These masks are based upon a Proper Orthogonal Decomposition (POD) of the velocity field, which is nothing less than the computation of eigenvalues and eigenvectors of that vector field. This POD analysis showed different power spectra at disc centre compared to the solar limb. These differences could be related to the dependence of the perturbation with distance to the centre of the solar disc.

The aforementioned masks are defined for observing perturbations at the surface. With the advent of time-distance helioseismology (Duvall et al. 1993), there is the possibility of constructing special masks that will be sensitive to perturbations located deeper in the Sun, where the motions induced by gravity modes are much larger than at the surface. The idea is to detect motions induced by the g modes on the solar p modes.

4.3 Spectrum estimators

4.3.1 For data with no gaps

The estimation of the spectrum of the time series is of prime importance when one wants to detect eigenmodes. The lifetimes of the modes should be taken into account when using these estimators. The following estimators are at our disposal:

- Fourier spectrum (power spectra)
- Lomb-Scargle periodogram and sine wave fitting
- Average, smoothed and multitapered spectra
- Cross spectrum
- Random Lag Singular (Cross) Spectrum analysis
- Frequency matching (oversampling and bin shifting)
- Time-frequency spectrum
- Varying time base

Fourier spectrum estimation is widely used in helioseismology. Its properties are well known and quite often well understood (Bracewell 2000), as are its statistics (Davenport & Root 1958). In short, the Discrete Fourier spectrum estimation is widely used for time series being sampled at a regular sampling cadence (Δt) during an observing time (T) that is an integer number N of the sampling cadence. The Nyquist frequency of the Discrete Fourier spectrum is then $\nu_{\text{Nyquist}} = 1/\Delta t$, and the so-called frequency bin is the N th part of that or $\Delta\nu = 1/N/\Delta t$. The increase in frequency

resolution makes the detection of sine waves extremely effective because the power spectrum level of any stationary noise decreases like $1/T$. If a sine wave would change many times its phase during the observation time T , it would not be advised to compute the Fourier transform of the whole observation. In that latter case, the optimal computation would be to perform the Fourier transform for the period of constant phase, if these are known, and then to add the power spectra. An other incentive for not computing the whole Fourier transform would be that the frequency of the sine wave changes gradually with time (See later in this Section).

Other tools have been developed for time series that are not evenly sampled. Then, the Fast Fourier Transform should be replaced by an adaptation of the Discrete Fourier Transform, the so-called Lomb-Scargle (LS) periodogram (Scargle 1982). The LS periodogram is widely used in astrophysics for stars having modes with very long lifetimes. The LS periodogram is strictly equivalent to sine-wave fitting, as shown in Appendix C of Scargle (1982). The main difference between the two methods is more in the approach than in the result: with the LS periodogram the frequency of the sine wave is found from the spectrum itself, while for the sine wave fit the frequency is obtained from the fit provided that a proper initial guess is given, coming from the LS periodogram for instance. For speed, the LS periodogram is usually computed using the implementation prescribed by Press & Rybicki (1989) which is an approximation of the LS periodogram based upon *extrapolation*¹⁷ on a regular mesh and the use of the FFT. The prescription is then very close to interpolating onto a regular mesh. It is worth noting that most scientists using the LS periodogram for unevenly sampled data are in fact computing the FFT of the original data resampled onto a regular mesh, but with only a proper normalization as given by Scargle (1982).

Fourier spectrum estimation is well adapted for periodic signals (pure sine waves or stochastic waves) but not necessarily well suited for estimating the spectral density of pink or red noise. For that purpose, one can:

- average the power spectrum over an ensemble of q' sub-series,
- smooth the power spectra over q' frequency bins or,
- use multitapered spectra using the full time series for deriving a similar average.

Fourier spectrum estimation is now being replaced by multitapered spectra that are widely used in geophysics (for a review see Thomson 1982). Multitapered spectra are generated by applying a set of *slepian* tapers to a single time series, and an estimate of the mean power spectrum is derived from an average of these spectra. The multitapered spectra are statistically independent from one another, and the statistics of the mean spectrum follows a χ^2 distribution with $2q$ degrees of freedom (where q is the number of tapers, Thomson 1982). While the statistics of the average power spectrum (or smoothed power spectrum) also follow a χ^2 distribution with $2q'$ degrees of freedom, the resolution of the average spectrum is q' times lower than that of the multitapered spectrum. In helioseismology the use of these *slepian* tapers has been replaced by more practical (but less accurate) sine tapers (Komm et al. 1999). Unfortunately, for long-lived modes, tapers tend to broaden the peaks, as shown by Thomson (1982). Tapers as such provide more benefit for p modes having a lifetime shorter than the observation time.

The use of cross spectrum estimation can also be useful for detecting signals being present in two different time series (Sturrock et al. 2005). This can be done either from

¹⁷ Reverse interpolation or *extrapolation* replaces a function value at any arbitrary point by several function values on a regular mesh

the same observable or from different observables (e.g. intensity and radial velocity). This technique has been used by García et al. (1999) for improving the signal-to-noise ratio in the p-mode region, but it is not useful for g-mode detection as shown by Appourchaux et al. (2007).

Random Lag Singular (Cross) Spectrum analysis is an elaborate technique based on Singular Value Decomposition (RLSSA, RLSCSA Varadi et al. 1999, 2000). Although the technique claimed successful detection of low-frequency p modes (Bertello et al. 2000b; García et al. 2001b), although a proper assessment of its statistical properties is still lacking: i.e. it cannot be excluded that the technique produces large peaks solely due to noise (Couvidat 2002). The spectrum produced by the RLSSA technique can be compared to a power spectrum raised to an unknown power (greater than one). As such, small peaks with a signal-to-noise ratio slightly larger than unity are amplified, while those with a lower signal-to-noise ratio are damped. The fact that this exponentiation is unknown (dependent upon the data) makes the RLSSA and RLSCSA techniques in our view unsuited for robust signal analysis.

Frequency matching has been developed by Gabriel et al. (2002) and by Chaplin et al. (2002) using zero padding and frequency-bin shifting, respectively. When one wants to detect signals from oscillators having a lifetime longer than the observing time, there is a significant chance that the frequency bin will not match the frequency of the oscillator. As a result, power from the signal may be split between frequency bins and the main peak could be reduced in power by up to 60 %, as shown by Gabriel et al. (2002). In order to alleviate this problem one can either oversample the data by using zero padding (Gabriel et al. 2002) or try to tune for the frequency by using frequency-bin shifting (Chaplin et al. 2002). This latter technique involves creating many different time series of similar but slightly different lengths, but without zero padding (Chaplin et al. 2002). In either case, the statistics of the observation are indeed affected. For oversampling, the analytical calculation has been replaced by Monte-Carlo simulation showing that there are typically three independent frequency bins when the Fourier spectrum is oversampled by a factor five or more (Gabriel et al. 2002). The frequency-bin shifting method also produces three independent power spectra from the many spectra generated (Chaplin et al. 2002). Both approaches have the added benefit that they give access to different “realizations” of the noise background, as if we had three actual, independent realizations of the noise available.

Time-frequency spectrum or wavelet analysis has been used by Gabriel et al. (1998), by Finsterle & Fröhlich (2001) and by Jiménez & García (2009) to look for signatures that are affected by the lifetimes of candidate g modes. The statistical properties of these wavelets can be derived from those of the Fourier spectrum. The potential influence of solar activity on the size of the resonant cavity, which would affect the frequency of long-lived modes, has also been studied by Gabriel (2006). If the frequency of the mode changes slowly with time, the frequency of the mode will be spread over several frequency bins. The idea followed by Gabriel (2006) is to change, or distort, the sampling time to follow the variations in the mode frequency induced by solar activity.

4.3.2 For data with gaps

All the estimators described above have different properties when gaps appear in the data. Hereafter, we shall discuss mainly the following:

- Fourier spectrum (power spectra)

- Lomb-Scargle periodogram and sine wave fitting
- Average, smoothed and multitapered spectra
- Frequency matching (oversampling and bin shifting)

The impact of the gaps on the Fourier spectrum has been described by Gabriel (1994) providing as a result that the correlation matrix of the frequency bins is not longer diagonal. The gaps introduce correlation between the frequency bins that require to be taken into account when one wants, for example, to fit the power spectrum (See for applications Stahn & Gizon 2008).

The LS periodogram does not provide a better solution to coping with the presence of gaps. The reason is that although the Fourier transform *explicitly* includes gaps as zeros, adding zeros is also *implicitly* performed with the LS periodogram. As a consequence, correlations between frequency bins also exist with the LS periodogram, but these are frequently ignored.

The impact of the gaps for the average will have the same origin as for the Fourier spectra. As for the smoothed spectra, there is an intrinsic correlation between the q' bins; the number of truly independent frequency bins is then divided by q' . In that latter case, the gaps do not have a large influence on the smoothed spectrum unless the fraction of gaps is about $1/q'$. For multitapered spectra, the influence of gaps can be taken into account for obtaining optimised tapers that match the structure of the gaps (Fodor & Stark 1998). In that case, the correlation between the frequency bins, although reduced, will be not negligible, especially if several tapers are used for the estimation of the mean power spectrum.

4.4 Statistical testing

Statistical testing is essential when one wants to decide: *have we found g modes* or not? This is related to *decision theory*, which can be summarised as *how do we choose between one hypothesis versus another in the presence of uncertainties?* In this area, there are two schools of thought: the frequentist school and the Bayesian school.

The difference between a Bayesian and a frequentist relates to his or her views of *subjective* versus *objective* probabilities. A frequentist thinks that the laws of physics are *deterministic*, while a Bayesian ascribes a belief that the laws of physics are true or *operational*. The *subjective* approach to probability was first coined by De Finetti (1937). For the rest of us, the difference in views can be summarised by this quote from the Wikipedia encyclopaedia: *Whereas a frequentist and a Bayesian might both assign a probability $\frac{1}{2}$ to the event of getting a head when a coin is tossed, only a Bayesian might assign a probability $\frac{1}{1000}$ to personal belief in the proposition that there was life on Mars a billion years ago, without intending to assert anything about any relative frequency.* In short, frequentists assign probability to measurable events that can be measured an infinite number of times, while Bayesians assign probability to events that cannot be measured, like the outcome of sport-related bets, for instance. or the survival time of the human race (Gott 1994).

With this word of caution, one should never forget that we wish to use this armada of statistics because we know that we are at the limit of detection for g modes. In what follows, we will try to give an overview of what *we believe* we know on a subject that is fast evolving; and what we write is certainly *not* gospel.

4.4.1 Frequentist approach

For a frequentist, statistical testing is related to hypothesis testing. In short, we have two types of hypotheses:

- H_0 hypothesis or null hypothesis: what has been observed is pure noise?
- H_1 hypothesis or alternative hypothesis: what has been observed is a signal?

For the H_0 hypothesis, we assume a known statistics for the random variable X observed as x and assumed to be pure noise; and then set a *false alarm probability* that defines the acceptance or rejection of the hypothesis (Scargle 1982). The so-called *detection significance* (or *p-value*, terms not widely used in helioseismology) is the probability of having a value as extreme as *the one actually observed*. There is an on-going confusion because statisticians call *the significance level* what astronomers call the *false alarm probability*; and they call the *p-value* what is set in astronomy as the *detection significance* (which is *not* the significance level). Here we shall use the current vocabulary understood in astronomy. For example, the *false alarm probability* p for the H_0 hypothesis is defined as:

$$p = P_0(T(X) \geq T(x_c)), \quad (29)$$

where T is the statistical test, and P_0 is the probability of having $T(X) \geq T(x_T)$ when H_0 is true; and x_c is the cut-off threshold derived from the test T and the value p . For example, take the case of a random variable X distributed with χ^2 , 2 degrees of freedom (d.o.f) statistics, having a mean of σ . If we further assume that $T(X) = X$, we then have that:

$$p = P_0(X \geq x_c) = e^{-\frac{x_c}{\sigma}}. \quad (30)$$

If one observes a value \tilde{x} of the random variable X that is larger than x_c , the H_0 hypothesis is rejected. The value that is quoted in this case is the *detection significance* \mathcal{D} , i.e.,

$$\mathcal{D} = e^{-\frac{\tilde{x}}{\sigma}}. \quad (31)$$

The H_0 hypothesis was used by Appourchaux et al. (2000) to impose an upper limit on the g-mode amplitudes. The method was based on the knowledge of the statistical distribution of the power spectrum of full-disc integrated instruments, namely the χ^2 distribution with 2 d.o.f.

For the H_1 hypothesis, we assume given statistics both for the noise and for the signal that we wish to detect, and set a level that defines the acceptance or rejection of that hypothesis. The H_1 hypothesis was used in Gabriel et al. (2002) to determine the probability of detecting a sine wave given noise in the GOLF data (Gabriel et al. 2002). In this latter case, the statistics follow a non-centred χ^2 distribution with 2 d.o.f. Both hypotheses have also been used to calculate significance levels for detecting stellar p modes (Appourchaux 2004).

Taking a decision based on the result given by a single test, for either hypothesis, could lead to errors in the decision process. For instance, the null hypothesis could be wrongly rejected when it is true (*false positive* or wrong detection), but could also be wrongly accepted while it is false (*false negative* or no detection in presence of a signal). The *false positive* results in a *Type I* error, while *the false negative* results in a *Type II* error (see Table 2). The ideal case would be to set a test that would minimise the occurrence of both types of errors.

In helioseismology, it has been customary when applying the H_0 hypothesis to set the decision level arbitrarily at 10% (Appourchaux et al. 2000). From the frequentist

Table 2 Types of error obtained for different decisions, based upon the statistical test performed, and how the error relates to the status of the H_0 hypothesis.

		Status of H_0	
		True	False
Decision	Reject	Type I	Correct
	Accept	Correct	Type II

view point there is nothing wrong in setting *a priori* the decision level before the test is applied. There are three types of result we might obtain from the test:

1. H_0 always rejected
2. H_0 rejected or accepted at a level very *close* to 10%
3. H_0 always accepted

Decision 1 will lead to the mention of a *detection being statistically significant* at a level provided by the *detection significance* [from Eq. (31)]. The next step would be the application of a test for the H_1 hypothesis, very likely resulting in the detection of signal. Decision 2 is the more difficult borderline case, forcing us to either accept or reject H_0 . Here, we might ask: are things really that clear-cut? What are the chances that if we accept H_0 is it actually wrong (Type II error), or truly right if rejected (Type I error)? Decision 3 seems straightforward, i.e., noise dominates, but might one then be tempted to lower, *a posteriori*, the decision level?

These potential actions result from the application of a frequentist test trying to answer the following question: what is the likelihood of the observed data set \tilde{x} , given that H_0 is true or $p(\tilde{x}|H_0)$? The *detection significance* mentioned when the test rejects the H_0 hypothesis is nothing but $p(\tilde{x}|H_0)$, when actually what we want to know is the likelihood that H_0 is true given the data, i.e., $p(H_0|\tilde{x}) (\neq \mathcal{D})$. The frequentist view does provide a useful answer when one can repeat the observations ad infinitum. But when we have only one observations, another approach we may apply is the Bayesian approach, which in principle gives access directly to $p(H_0|\tilde{x})$.

4.4.2 Bayesian approach

On the posterior probability We should never forget the *two sides of the coin*: if probability (likelihood) can justify *alone* the rejection or acceptance of an hypothesis, this probability *is not* the significance that the hypothesis is rejected or accepted. The decision levels discussed above are related directly to a well-known controversy in the medical field, concerning improper use of Fisher's p-values as measures of the probability of effectiveness of a medicine or drug (Sellke et al. 2001). The *detection significance* (or p-value) is improperly used as the significance of the evidence against the null hypothesis. It is far from trivial at first sight to understand what is wrong with the *detection significance*. Let us recall the example of a noise with 2 d.o.f statistics. In that case the *detection significance* is given as:

$$\mathcal{D} = e^{-\frac{\tilde{x}}{\sigma}} \neq P_0(X \geq \tilde{x}). \quad (32)$$

The latter statement (\neq) is fundamental. The observation is performed only once providing a value of \tilde{x} . It is not correct to assume that this observation if it were repeated

would provide the same level \tilde{x} . The mistake is to ascribe a significance to a measurement performed only once, i.e., not repeated, and spanning just a very small volume of the space of the parameters (e.g. $X \in [\tilde{x}, \tilde{x} + \delta x]$). If one makes a measurement \tilde{x} of the random variable X which is above x_c , the significance of that measurement is *not* $e^{-\tilde{x}/\sigma}$. In the framework of Bayesian statistics, we are not interested in the *detection significance* but in the posterior probability of the hypothesis, in other words as already stated above $p(\text{H}_0|\tilde{x}) \neq \mathcal{D}$. A similar description of this misunderstanding has been presented by Sturrock & Scargle (2009).

In order to derive the posterior probability $p(\text{H}_0|x)$, let us first recall the Bayes theorem. The posterior probability of a hypothesis H, given the data D and all other prior information I is stated as:

$$P(\text{H}|\text{D}, \text{I}) = \frac{P(\text{H}|\text{I})P(\text{D}|\text{H}, \text{I})}{P(\text{D}|\text{I})}. \quad (33)$$

where $P(\text{H}|\text{I})$ is the prior probability of H given I, or otherwise known as the prior; $P(\text{D}|\text{I})$ is the probability of the data given I, which is usually taken as a normalising constant; $P(\text{H}|\text{I})$ is the direct probability of obtaining the data given H and I. Berger & Sellke (1987) obtained, using the Bayes theorem, $p(\text{H}_0|\tilde{x})$ with respect to $p(\tilde{x}|\text{H}_0)$ and $p(\tilde{x}|\text{H}_1)$, where H_1 is the alternative hypothesis.

$$p(\text{H}_0|\tilde{x}) = \frac{p(\text{H}_0)p(\tilde{x}|\text{H}_0)}{p(\text{H}_0)p(\tilde{x}|\text{H}_0) + p(\text{H}_1)p(\tilde{x}|\text{H}_1)}. \quad (34)$$

We set $p_0 = p(\text{H}_0)$, and since we have $p(\text{H}_1) = 1 - p_0$, they finally obtained:

$$p(\text{H}_0|\tilde{x}) = \left(1 + \frac{(1 - p_0)}{p_0} \mathcal{L} \right)^{-1}, \quad (35)$$

with \mathcal{L} being the likelihood ratio defined as:

$$\mathcal{L} = \frac{p(\tilde{x}|\text{H}_1)}{p(\tilde{x}|\text{H}_0)}. \quad (36)$$

Here, $p(\text{H}_0|\tilde{x})$ is the so-called posterior probability of H_0 given the observed data \tilde{x} . Naturally there is no way to privilege H_0 over H_1 , or vice versa, otherwise our own prejudice would most likely be confirmed by the test, i.e. $p_0 = 0.5$. Subsequently, Berger et al. (1997) recommended to report the following when performing hypothesis testing:

$$\text{if } \mathcal{L} \leq 1, \text{ reject } \text{H}_0 \text{ and report } p(\text{H}_0|\tilde{x}) = \frac{1}{1 + \mathcal{L}}, \quad (37)$$

$$\text{if } \mathcal{L} > 1, \text{ accept } \text{H}_0 \text{ and report } p(\text{H}_1|\tilde{x}) = \frac{1}{1 + \mathcal{L}^{-1}}. \quad (38)$$

The advantage of such a presentation is that even for a borderline case, say when the ratios above are close to unity, it is clear that there is only a 50 % chance that the H_0 hypothesis is wrongly accepted, or wrongly rejected. This presentation is more honest and better encapsulates human judgement and prejudice.

The work of Berger et al. (1997) can be applied to the problem of detecting modes with very long lifetimes, i.e., those modes whose peaks are predominantly restricted to one frequency bin in the frequency spectrum. We can write the likelihood for the H_0 hypothesis as:

$$p(\tilde{x}|\text{H}_0) = \frac{1}{B} e^{-\tilde{x}/B}. \quad (39)$$

where B is the mean noise level. Next, we assume that the mode is stochastically excited with a known amplitude A . The likelihood for H_1 is then:

$$p(\tilde{x}|H_1) = \frac{1}{B+A} e^{-\tilde{x}/(B+A)}. \quad (40)$$

Since the *detection significance* is $p = e^{-\tilde{x}/B}$, we use Eq. (35) to give:

$$p(H_0|x) = \left(1 + \frac{B}{B+A} p^{-A/(B+A)}\right)^{-1}. \quad (41)$$

Figure 16 show the results for two different *detection significances*. When the *detection significance* is 10%, the likelihood ratio can be greater than unity for large values of the mode amplitude, leading to the acceptance of the null hypothesis. This is rather paradoxical, i.e., that large mode amplitude can lead to the rejection of the alternative hypothesis. To resolve the paradox we note that the posterior probability of H_0 is in any case never lower than 40%, or the posterior probability of H_1 is never higher than 60%. This implies that both hypotheses are equally likely when the *detection significance* is as low as 10%. In other words, when we set, a priori, a large mode amplitude and get a low *detection significance*, the alternative hypothesis is as likely as the null hypothesis.

The main conclusion to be drawn from this calculation is that the *detection significance* should be set much lower than 10% in order to avoid misinterpretation of the result. For example, with a *detection significance* of 1%, the posterior probability for H_0 can fall to 10% when the signal-to-noise ratio is above unity. Sellke et al. (2001) showed that the posterior probability can never be lower than the lower bound

$$p(H_0|x) \geq \left(1 - \frac{1}{ep \ln p}\right)^{-1}. \quad (42)$$

The reader may verify for themselves that this lower bound is effectively reached for Eq. (41). In the case, when the amplitude of the mode A is not known, one needs to set, a priori, value for the likely range of amplitude. In the case of a uniform prior, the posterior probability $p(H_0|\tilde{x})$ then does reach a minimum that is higher than the lower bound of Eq. (42).

In summary, the significance level should not be used for justifying a detection (or a non-detection). Instead we recommend to use the prescription of Berger et al. (1997), as given by Eqs. (37) and (38) and to specify the alternative hypothesis H_1 .

On the choice of the prior probability One important question when applying Bayesian statistics is what value should the prior probability of the hypothesis H_0 , i.e., p_0 , take? We define the prior probability as the probability that the H_0 hypothesis is correct. The probability that the alternative H_1 hypothesis is correct can then be defined as $p(H_1) = 1 - p_0$. It is common to set $p_0 = 0.5$ so as to avoid prejudicing one hypothesis over the other. Given current model prejudices, we know that low-frequency p modes have narrow widths typically between 10 and 30 nHz, (Chaplin et al. 2005), which cover a few frequency bins only; and we expect the same to be true for g modes. In which case, would we expect the probability that H_1 and H_0 are true to be the same at all frequencies? Since Bayesian statistics uses a priori knowledge, it is possible to use our knowledge of the properties of modes to tell us which hypothesis is more likely to be true at a given frequency. We can also use this knowledge to then guide the regions we search in frequency (See section 4.5.3).

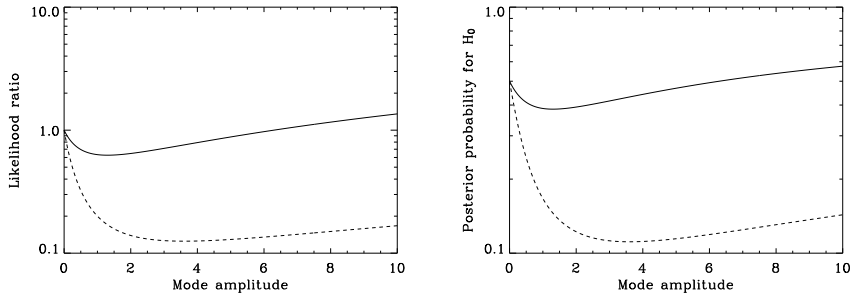


Fig. 16 On the left-hand side, likelihood ratio \mathcal{L} as a function of the mode amplitude for *detection significances* of 10% (solid line), and of 1% (dashed line); the noise is set to unity. On the right-hand side, the posterior probability of H_0 as a function of mode amplitude for *detection significances* of 10% (solid line), and of 1% (dashed line) (from Eq. 41).

4.5 Patterns

4.5.1 Rotational splitting

As shown in Section 2 [see Eq. (19)], the mode degeneracy is lifted by the solar rotation; each (n, l) mode is then split into $2l+1$ components. The collapsogramme technique pioneered by Appourchaux et al. (2000) makes use of the pattern created by the rotational splitting to detect the modes. It has been extensively used by Salabert et al. (2009) for detecting modes below $1000 \mu\text{Hz}$, using resolved-Sun data collected the GONG instrument. It can also be used for full-disc instruments producing a single power spectrum: in this case it is called an *overlapogramme* (For an application see Salabert & Garcia 2008). Chaplin et al. (2002) has devised a statistical technique based on the detection of an ordered multiplet (due to rotational splitting) in the power spectrum of full-disc integrated data. This lowers the detection level, relative to the level for just a single peak, depending on the number of peaks that are found in the multiplet. The derived limit (under the H_0 hypothesis) can be translated into the equivalent σ level in a power spectrum for a one-year observing time (where σ is the mean power spectral density in the neighbourhood of the sought-for modes): 5.9σ , 4.5σ , 3.8σ for a doublet, triplet and a quadruplet, respectively. A similar approach has been used by García et al. (2001a) for the GOLF data. They derived levels for detecting modes of various degrees using Monte-Carlo simulations, which can be translated for a one-year time series to 5.4σ for an $l = 1$ doublet, 5.9σ for an $l = 2$ doublet and 4.3σ for an $l = 2$ triplet.

4.5.2 Asymptotic behaviour

The asymptotic behaviour of g-mode periods may be used to aid detection [see Eq. (11) of Section 2]. Such analyses were pioneered by Delache in 1983, leading to a claimed detection of g modes (Delache & Scherrer 1983). This approach is only of relevance to high-order g modes (i.e., very low-frequency modes below $\sim 100 \mu\text{Hz}$) for which the asymptotic behaviour applies. Unfortunately, the solar noise increases towards lower frequencies, and the mode spacing (in frequency) decreases dramatically. The situation is further complicated by the effects of rotational splitting (Fröhlich & Andersen 1995, see also Section 5.2.1).

The *Exact Fractions Technique* (EFT) was pioneered by van der Raay (1988) and applied by Pallé et al. (1998). The technique is rather similar to the *echelle diagram* devised by Grec (1981). The main difference is that instead of cutting the spectrum into several windows of width $\Delta\nu_0$, the frequency axis is first changed to period, and the spectrum is then cut into several windows of width $P_0/\sqrt{l(l+1)}$. The full EFT procedure is described in more detail in Pallé et al. (1998).

The EFT uses the property that the modes, if they exist, are regularly spaced in period. The same property has been used by García et al. (2007). They compute the periodogram of the frequency power spectrum expressed in period, i.e., the periodogram of the periodogram. The regular comb-like pattern expected in the first periodogram then manifests as another comb-like pattern in the second periodogram. Unlike the technique devised by Delache & Scherrer (1983) or the EFT, the statistical understanding is far from trivial, requiring Monte-Carlo simulations to derive the likelihood of structures appearing above a given threshold.

4.5.3 Guided search

An artificial way of reducing the detection limit is to reduce the size of the frequency windows over which we wish to search for modes, e.g., by looking in windows centred around theoretical g-mode frequencies. Denison & Walden (1999) provided a simple formula to derive the number of peaks due to noise that one can find in a power spectrum, given a list of frequencies and a window containing these frequencies. Under the H_0 hypothesis, it is written as follows:

$$N = N_1(1 - (1 - p_{\text{det}})^{N_w}). \quad (43)$$

Here, N_1 is the number of frequencies guiding the search, p_{det} is the probability level needed for identifying a peak and N_w is the window size in units of frequency bins. When $N_w p_{\text{det}}$ is much smaller than unity, we can rewrite Eq (43) as:

$$N \approx N_1 N_w p_{\text{det}}. \quad (44)$$

This simple formula is quite useful, in that it allows us to realise that the number of identified peaks will increase with the size of the window and the number of frequencies guiding the search. This is the drawback of such a method: spurious peaks will be detected that are likely to be wrongly identified as g modes. Here we should also remind the reader that theoretical p-mode frequencies showed systematic errors of the order of several μHz , which came from our inability to model properly the surface of the Sun (Christensen-Dalsgaard 1990). Therefore care should be exercised when using theoretical frequencies as a guideline for searching for g modes.

The sensitivity of g-mode frequency predictions to solar models is of the order of 1% (see Section 2.2.3). This error estimate can be used to produce an inverted top-hat prior probability distribution that can be used to guide Bayesian searches for g modes. The centres of each hat were determined by the mode frequencies predicted by the M1 model of Provost et al. (2000) and the width of each hat was 2% of the mode frequency. Frequencies where modes are expected to be observed have been given a prior probability that the H_0 hypothesis is true (p_0 in equation 36) of 0.5 and elsewhere the prior probability is unity. Figure 17 shows such a distribution, where all components that will be visible in Sun-as-a-star data (when $l + m$ is even) have been plotted for $l = 1$ and $l = 2$ g modes. We have assumed that the different m components are

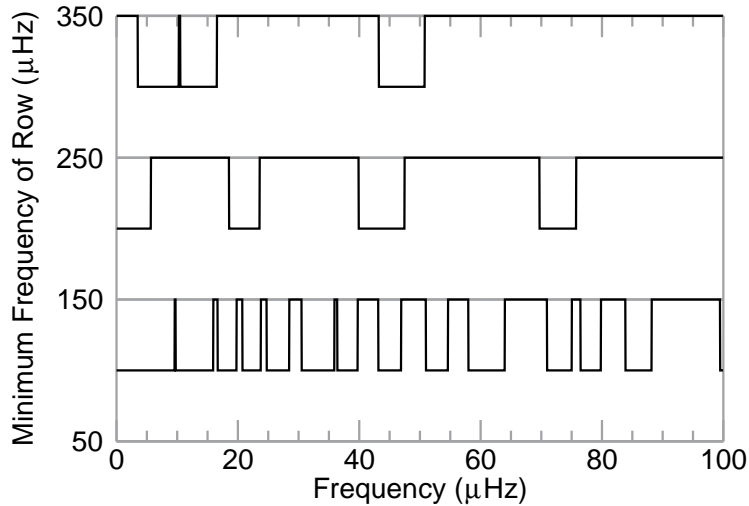


Fig. 17 An Echelle diagram showing the variation of the of the prior probability for g modes. The prior probability, p_0 , was either 1.0, at frequencies where modes are not expected to be observed, or 0.5 at frequencies where modes are expected.

separated by $0.4 \mu\text{Hz}$. However, as we do not know the rotation rate of the solar core this assumption may not be valid (see Section 2.2.4). Notice that despite the large number of g modes that are present at low frequencies the prior is not uniform with frequency and so this approach should limit the number of false detections.

4.6 Data combination

The signal from solar oscillations will be common to contemporaneous data observed by different instruments. It is, therefore, pertinent to search spectra constructed from contemporaneous data for statistically significant prominent concentrations of power, which lie significantly above the local noise background and that are coincident in frequency in the different datasets. The use of different data sets related to different observables and/or wavelengths could very well be the solution to the g-mode detection. There is no doubt that the combination of more than two signals could considerably lower our detection limit. Observables such as radial velocity, intensity fluctuations, limb displacement and/or brightening are polluted by different sources of noise, such as supergranulation and active regions, that produce different signatures. We can list the possible combinations as follows:

- use of one instrument
- use of more than one instrument

In terms of the analysis techniques we might apply to exploit such data, autocorrelation falls into the first category. The collapsogramme technique used by Appourchaux et al. (2000) also belongs to the first category. Another technique developed by García et al. (1999) used a longer sampling time (e.g., 80 sec instead of 40 sec) to create two overlapping, independent timeseries of the GOLF data. The first time series used all the even-sample data points, while the other used the odd-sample data points. The combination of the two resulting Fourier spectra can be used to improve the signal-to-noise

ratio of modes with a lifetime shorter than the observation time (Appourchaux et al. 2007).

The Multivariate Spectral Regression Analysis (MSRA) belongs to the second category (Koopmans 1974; Appourchaux et al. 2000). It assumes that the modes are predominantly coherent over the observing time. The basic assumption is that low-degree p modes and g modes will have lifetimes that are significantly longer than the observing time. The MSRA has been applied to data from the different SPM channels of the VIRGO data by Finsterle & Fröhlich (2001).

A derivation of the joint probability, p , of the occurrence of coincident prominent features in two spectra is given in Broomhall et al. (2007). Various statistical tests are derived in Chaplin et al. (2002) that determine the probability of observing prominent structures in a single spectrum. These tests can be easily adapted so they can be used to compare two spectra if the probability of observing a single prominent spike at the same frequency in each of the spectra can be calculated (Broomhall et al. 2007). The technique works best when the signal-to-noise ratio is similar in the different instruments. These tests were originally designed to detect p modes, however, the underlying theory is still applicable when searching for g modes.

5 Applications of detection techniques

As outlined in the previous section, the building of a detection is made of an assemblage of various elementary bricks. It is essential that a *detection technique* be segmented in different categories. The key category is *statistical testing* because it exemplifies that the potential biases of a detection technique can indeed be understood.

Hereafter, we will try to review the application of detection techniques, and their associated results.

5.1 Statistical thresholding

5.1.1 Radial velocity

The first reported g-mode detection was made by Delache & Scherrer (1983). They analysed differences in the solar radial velocity recorded at disc centre, and further out toward the limb. Observations were made at the Stanford Solar Observatory (Scherrer et al. 1979), and at the Crimean Astrophysical Observatory (Severnyi et al. 1976). The length of the time series was 105 days, but with a duty cycle of only 10%. After computing the power spectrum, they constructed the cumulative power distribution in the frequency range [45-105] μHz . Delache & Scherrer (1983) calculated the cumulative distribution of the power spectrum in this range, and ascribed the strongest peaks as being due to g modes.

The cut-off used to tag prominent peaks was 2.5σ which, given the assumed χ^2 with 2 d.o.f statistics, means that in the window considered about 5 ± 2.5 “detections” will have been due solely to noise (there are about 55 independent frequency bins in the window given the 10% duty cycle). Fourteen possible modes were identified, at least half of which are likely due to noise. In addition, they did not take into account that the power spectrum has a $1/\nu$ dependence implying that the mean varies with

frequency; this explains the departure observed from the expected statistical distribution. The minimum amplitude of the detected peaks was 25 cm s^{-1} . Since this paper appeared, no independent confirmation of the results has appeared in the literature. Indeed, as we shall see we below, quoted upper limits on g-mode amplitudes, given by analyses of modern datasets, lie some two orders of magnitude below the claimed Delache & Scherrer (1983) amplitudes.

A similar approach was used by Appourchaux et al. (2000) for setting an upper limit to the amplitude of the g modes, which lay significantly below the amplitudes claimed by Delache & Scherrer (1983). The canonical figure for H_0 was given for a threshold of 10 % for a $100 \mu\text{Hz}$ window, providing a minimum posterior probability for H_0 of 38% (See Section 4.2.2). As shown in Fig. 17, a threshold of 1 % would provide a lower posterior probability for H_0 of typically 15 % for mode amplitude at a signal-to-noise ratio less than 10 (but greater than unity). The 1 % threshold would increase by a factor two the upper limit quoted by Appourchaux et al. (2000).

Gabriel et al. (2002) also used a statistical thresholding approach. They used oversampling in an attempt to increase the detectability of long-lived signals. They reported the detection of three g-mode candidates below $290 \mu\text{Hz}$ with a significance level of 4%, or a posterior probability for H_0 of 25%. They could not tag the candidates as being g modes, and then set an upper limit to the amplitude of g modes, based upon the H_1 hypothesis, of 7 mm s^{-1} .

Turck-Chièze et al. (2004) applied thresholding for various kinds of features: for singlets (as Appourchaux et al. 2000), for doublets and for triplets. The latter application of the thresholding is more akin to *searching for pattern of g-mode peaks*, which is described below. Several candidate detections were flagged at a threshold of 10 % (implying a lower bound on the posterior probability of 38%). But none appeared in all their test observation periods.

5.1.2 Solar diameter

Observations of the solar diameter have also been used in the search for g modes, e.g., in observations by the SCLERA instrument. The lowest amplitude detected corresponded to a radius change of 1 mas for p modes, and to 0.1 mas for g modes; assuming that these radius changes were real physical changes, they would have been equivalent to radial velocities of 50 km s^{-1} and 250 m s^{-1} , respectively. As outlined by Brown (1979), the observed oscillation signals were more likely due to brightness effects than to physical radius changes. This latter fact was also confirmed by Appourchaux & Toutain (1998) and Toner et al. (1999) using space-borne instrumentation. The amplification is due to a geometrical effect, which makes optical thickness changes dominate temperature changes. The rms amplitudes of the modes detected by Appourchaux & Toutain (1998) were typically of the order of 8 ppm, corresponding to a radius change of 1 mas. Toner et al. (1999) showed that the oscillation signal increases as the distance to the limb decreases. This property will be used by the SODISM instrument on the PICARD mission to try to detect modes at the limb (Damé et al. 1999; Corbard et al. 2008).

5.1.3 Solar wind data

Thomson et al. (1995) used magnetic field and particle data collected by the Ulysses mission. They used different spectral estimators (based on multi tapers; see Thomson

(1982)) and different statistical tests (based on the F -test), with a threshold of 5%¹⁸. They claimed the detection of several g-mode frequencies. However, these claimed detections were not confirmed by Denison & Walden (1999) or by Hoogeveen & Riley (1998), who both argued that the chosen threshold was too weak and gave rise to false detections. By making use of the work of Berger et al. (1997), we can now understand in retrospect that this threshold will have lead to a posterior probability of H_0 being true of at least 29% [from Eq. (42)]: the applied F -test threshold was clearly not low enough.

5.2 Searching for patterns of g-mode peaks

5.2.1 Asymptotic properties of periods

The first attempt to use the asymptotic properties of the g-mode frequencies dates back to Fröhlich & Delache (1984a,b). They used the asymptotic formula [see Eq. (11)], corrected for rotational splitting, to compute g-mode frequencies as a function of P_0 and $\overline{\Omega}_0$ ($\overline{\Omega}_0$ being the mean rotation as defined by Eq. 19). They then calculated the coherence between the calculated g-mode frequencies and the observed power spectrum, and drew maps of coherence as a function of $(P_0, \overline{\Omega}_0)$. No detections were made. The same procedure was applied by Fröhlich & Andersen (1995) also without success.

Fröhlich & Andersen (1995) concluded that either the g modes were not present or that the solar noise was too high. This method has also recently been extended to include also g-mode frequencies excluded by the normal asymptotic equation. The models shown in Table 1 cover a sufficient range of P_0 rendering an interpolation scheme as function of P_0 possible. This allows to include g modes with $l = 1$ and $l = 2$ down to $n = 1$. The results are not yet conclusive, possibly due to the precision of the frequencies and/or the interpolation scheme. Another reason may have been that the range for the rotation in the core was too small. One of the major drawbacks of the technique is that the computation of g-mode frequencies needs to be very accurate.

5.2.2 Rotational splitting

Turck-Chièze et al. (2004) applied statistical thresholding to search for patterns of peaks induced by rotational splitting. They derived, using Monte-Carlo simulation, pattern rejection thresholds for doublets and triplets at the 10% level for a 20- μ Hz window (posterior probability greater than 38%); similar levels were analytically derived by Chaplin et al. (2002) for p modes. Given the appearance, and disappearance, in different observation periods of the various detected peaks, Turck-Chièze et al. (2004) concluded that some patterns *were due to noise*, thereby supporting the posterior probability of H_0 being greater than 38%. The analysis was further pursued by Mathur et al. (2007) who confirmed detection at a 2% level for a 10 μ Hz window (corresponding to a 4% level for a 20 μ Hz window, or posterior probability greater than 26%). Chaplin et al. (2002) also searched for similar patterns, reporting possible detections of p modes as low as 700 μ Hz. A similar technique was used by Salabert et al. (2009) to detect low-order p modes, of higher degree, in resolved-Sun observations made by

¹⁸ The F -test is used for comparing two random variables having a χ^2 distribution with 2 d.o.f

the GONG network. They detected modes below 1000 μHz , with typical lifetimes of the order of 3 years.

5.2.3 Periodogram of Fourier space

García et al. (2007) found a very interesting peak in the periodogram of the periodogram of GOLF data (See also García et al. 2008a). They claimed that this peak is due to the superposition of g modes that lie in the asymptotic region, where the separation in period is approximately constant. The likelihood that the peak is not due to noise is $99.5 \pm 0.13\%$, with a posterior for H_0 greater than 3.4 %. The peak is positioned close to the period predicted by standard solar models. The peak can be produced in several ways, all related to clusters of peaks being equally spaced in period. For instance, the power of the g modes could be spread onto several adjacent peaks like the presence of a deep magnetic field or changes in the propagation cavity (a displacement of the tachocline as a consequence of the activity cycle). Other possibilities were also discussed by García et al. (2007). They used artificial data to show that, if this peak is evidence of g modes, the modes could have widths in a frequency-power spectrum that are commensurate with damping times of several months, with a possible signal-to-noise ratio not greater than five in power. If this is the case, and given that the data searched here are 3071 d in length, the width of these modes would be resolved in the spectrum. For example, if the mode damping time was 122 d the power of the modes in the spectrum would be spread across eight frequency bins. Appourchaux (2004) showed that it is possible to detect short-lived modes by smoothing the power spectrum over several frequency bins. For example, the detection probability is higher than 90 % for modes spanning at least eight frequency bins with a signal-to-noise ratio greater than three. Therefore, we have searched the contemporaneous, very low-frequency ($\nu < 500 \mu\text{Hz}$) BiSON¹⁹, GOLF and SOI/MDI data for evidence of prominent peaks with various widths. We searched for clusters containing 2, 3, 4 and 5 spikes. We allowed a cluster to be spread over twice the width of the mode and took the widths of the modes to be the number of frequency bins covered if the mode lifetimes were 1 month, 2 months and 4 months, respectively (i.e., 32 bins, 16 bins and 8 bins, respectively). However, no statistically significant peaks were found within 4 μHz of the model g-mode frequencies.

5.3 Innovative methods using a single set of data

5.3.1 Time-distance analysis

Duvall (2004) devised a method for detecting g modes using time-distance helioseismology of p mode signals. The idea is to detect the small flows induced by the g modes on the travel times of the p modes. He used deep-focusing rays to create travel-time maps for detecting perturbations at about 100 Mm below the solar surface, and then applied regular spherical harmonics masks on these maps to obtain power spectra of these travel times. While this method has not yielded any potential detections, plenty of work is need to develop the technique.

¹⁹ Birmingham Solar Oscillation Network, Chaplin et al. (1996)

5.3.2 Cross spectra of GOLF data

Very recently, Grec et al. (2009) used about 13 years of GOLF data to search for g modes using cross spectra. The idea is to use about 22 sub-series, each of 7-month's duration, to create cross spectra that are calculated by pair-by-pair. In total, this provides more than 253 cross spectra (i.e., $22 \times 23/2$). The averaged cross spectrum is then normalised to *remove* the low frequency dependence, and then an autocorrelation of the cross spectrum is calculated. The autocorrelation of the cross spectrum shows a maximum at a value that is tentatively identified as being the g-mode *rotational splitting*. In addition, they also tried to detect in the 253 cross spectra the signature of peaks having the same phase. They compared their result with computed g-mode frequencies of a solar model, but found no convincing detections.

5.4 Use of contemporaneous data

5.4.1 A signal at 220.7 μHz ?

At the beginning of the SOHO mission, there were several reports of the detection of a signal close to 220.7 μHz , that might possibly be identified as the $l=2$, $n = -3$ g mode (Gabriel et al. 1999; Finsterle & Fröhlich 2001). Very recently, Jiménez & García (2009) and García et al. (2008a) reported again on the presence of this signal in data from the different intensity instruments comprising the VIRGO package on SOHO. There is a trace of the signal in GOLF (but not with the same quality), in GONG (but at the level of the noise) and nothing in SOI/MDI. However, it seems that the signal has no obvious instrumental or SOHO-related origin. It is possible that the origin of the signal is related to the noise created in intensity by convection close to a g-mode frequency, or in fact could be a component of a g-mode.

5.4.2 Coincidence search

Statistical tests have been used to search contemporaneous BiSON, GOLF and SOI/MDI data for low-frequency p modes, g modes and mixed modes using a frequentist approach. To take advantage of the availability of contemporaneous data from different instruments frequency-amplitude spectra were searched for prominent spikes or patterns of spikes that were positioned in the same frequency bin or bins in any two of the three spectra. Details of the statistical tests can be found in Broomhall et al. (2007). Amplitude threshold levels were calculated for a 1% probability of detecting a prominent feature by chance at least once in a frequency range of 100 μHz .

Figure 18 shows visually, in the form of an echelle diagram, the locations in frequency where prominent spikes or patterns of spikes were observed. Also plotted on Figure 18 are the mode frequencies predicted by solar models. Detections were only considered as possible mode candidates if they were positioned within 1 μHz of a predicted mode frequency and such candidates are highlighted by a green square in Figure 18.

In the p-mode frequency range all of the candidates correspond to previously claimed detections of p modes (See Toutain et al. 1998; Bertello et al. 2000a; García et al. 2001b; Chaplin et al. 2002; García et al. 2004; Broomhall et al. 2007). Some of the detections in the g-mode range lie close to the predicted frequencies. However, it should

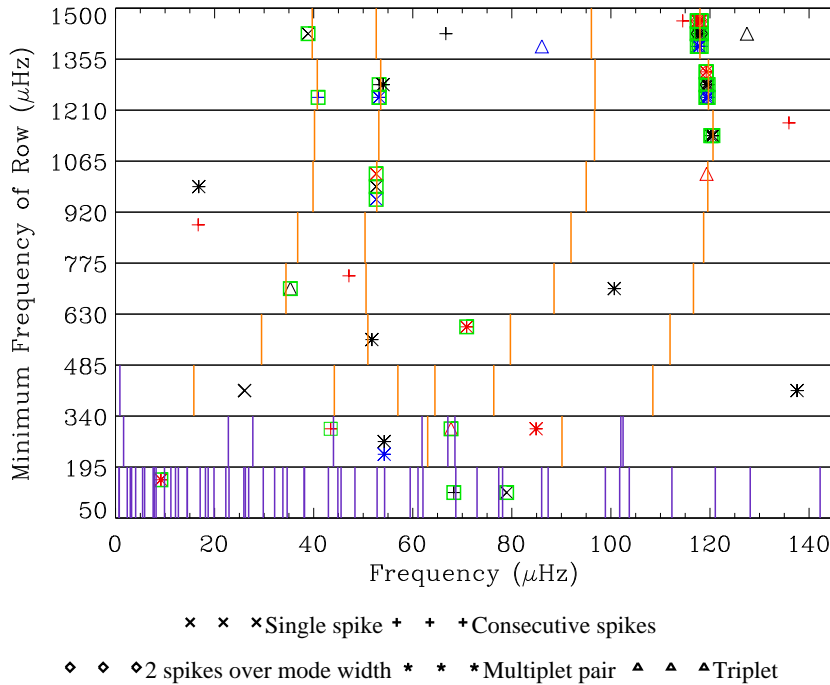


Fig. 18 An Echelle plot, modulo $145 \mu\text{Hz}$, marking locations in frequency of occurrences uncovered by the test searches. Locations in frequency where spikes, or patterns of spikes, were found in the same frequency bin, or bins, in BiSON and GOLF spectra at levels sufficient to record $p \leq 1\%$ are marked by the black symbols in the middle of each row. A different symbol has been used for each test (see figure legend). We have also recorded prominent spikes or patterns of spikes found by comparing either the BiSON and SOI/MDI spectra (red symbols at top of each row) or the GOLF and SOI/MDI spectra (blue symbols at bottom of each row). The orange vertical lines mark locations of the frequencies of p modes predicted by the Saclay seismic model (Turck-Chièze et al. 2001). The vertical purple lines mark locations of the $m = 0$ frequencies of g modes predicted by the M1 model (Provost et al. 2000).

be noted that, since the number of g modes that lie in the frequency range searched is large, the chances of mistaking a false detection for a g mode candidate is large. Therefore, to improve confidence in the detections we required that each mode candidate passed more than one of the statistical tests, thus significantly reducing the number of false detections. This extra requirement discounts all of the detections in the g-mode range and some of the detections in the p-mode range.

It is apparent from Figure 18 that the analysis has uncovered several occurrences of $p \leq 1\%$ that lie well away from the predicted mode frequencies. The number of these detections exceeds the number expected given the range in frequencies searched and the threshold probability. This possibly indicates that the statistical distribution in the noise is slightly different from the Gaussian distribution, which was assumed when deriving the statistical tests. Alternatively it could be due to the misleading significance levels assigned when adopting a frequentist approach (see Section 4.4.2).

6 Discussion and Conclusion

Figure 15 shows the comparison of the best observational measurements with theoretical amplitudes of the g modes. The theoretical g-mode amplitudes range from $10^{-2} \text{ mm s}^{-1}$ to a few mm s^{-1} . The most optimistic theoretical mode amplitudes could be collectively detectable, after the collection of more than 10 years of observations of the solar radial velocity. Unfortunately, the detection of individual peaks is very far from being feasible since the only possibility would be to have the most optimistic amplitude larger by 50%, or twice as much in power (Belkacem et al. 2009). Since the noise reduction scales with the observing time T like $\log(T)/\sqrt{T}$, another 80 years or so of data would be required to reduce the actual detection limit by a factor two. The limit does not scale like $1/\sqrt{T}$ because the probability limit is kept constant in a given detection window while the number of frequency bins in that window increases like T (Appourchaux 1998). At the time of writing, there is indeed a consensus amongst the authors of this review that *there is currently no undisputed detection of solar g modes*.

Despite this state of affairs, the search is not over yet. What can be done to turn our fortunes around? First of all, some of the detection techniques presented in this review paper that rely on the theoretical knowledge presented in Sections 2 and 3. Several are yet to exploit fully the theoretical information: this calls for the application of full Bayesian statistical inference on the data (yet to be done).

The observation of signals from the the solar limb will hopefully offer another way of improving the potential visibility of the g modes. These observations will be carried out by PICARD, which is due to be launched in 2009.

Because the solar atmosphere is relatively noisy, reductions of noise levels can potentially be achieved by making multiple observations that are sensitive to perturbations at different heights in the atmosphere. Here, one would seek to rely on changes in the coherence of the noise with height. The GOLF-NG instrument recently put in operation uses this principle for measuring solar radial velocities in 8 different heights of the solar atmosphere (Turck-Chièze et al. 2006; Salabert et al. 2008).

Development of methods based on time-distance helioseismology offer promises not only for detecting directly the g modes, but also for probing the solar core by making observations from two widely separated point of view. The technique is called stereoscopic seismology, and may provide the structure and the dynamics of the core with a completely different approach with the Solar Orbiter mission (Kosovichev & Duvall 2003; Gizon 2006).

Finally, we could try to detect the perturbation of the gravitational potential created by the g modes. For instance, the LISA²⁰ mission may provide a lower detection limit than the current classical helioseismic techniques. Polnarev et al. (2009) deduced a lower detection limit for LISA that is about a factor five lower in amplitude than the actual GOLF limit for modes of $m = \pm 2$ (see Figure 15). This limit would be low enough to detect g modes if they had amplitudes as high as those predicted by Belkacem et al. (2009). The variations in the potential can be also detected by using laser ranging, e.g., the ASTROD mission (Ni 2007; Appourchaux et al. 2009). As shown by Burston et al. (2008), the capability of ASTROD would be sufficient to allow the detection of g modes even if their amplitudes were to be as low as those predicted by Kumar et al. (1996).

²⁰ The ESA/NASA gravitational wave laser interferometric space antenna

We conclude with an optimistic comment. It is superficially unfortunate that we may not yet have detected g modes in the Sun. On the brighter side, on which we always prefer to be, it shows that we have before us a greater challenge which will yield greater satisfaction when we overcome it. We are all now much more prepared to continue the search.

Acknowledgements The whole Phoebus group would like to thank the long-time support provided by the European Space Agency, in particular we thank Clare Bingham, Cecilia Nillson, Mylene Riemens, Birgit Schroeder for secretarial support, and Martin Huber, Peter Wenzel and Bernard Foing for political and financial support; and the support provided by the International Space Science Institute, in particular we thank Brigitte Schutte, Saliba Saliba, Vittorio Manno and Roger-Maurice Bonnet for supporting our program. SOHO is a mission of international collaboration between ESA and NASA. The Phoebus group would like also to thank Boris Dintrans for setting the CVS server at the Observatoire Midi-Pyrénées which allows for the parallel writing of the review.

A Nonlinear amplitude limitation

A.1 Illustrative case of one-dimensional acoustic wave

Consider a toy acoustic mode in a uniform medium in which Eulerian perturbations, denoted by a prime, to pressure, p , density, ρ , and temperature, T , are related by the perturbed equation of state at first order:

$$p' = c^2 \rho' + \widehat{\alpha} T'. \quad (45)$$

Acoustic modes confined between two values, 0 and 1, of a spatial variable x are slowly damped by viscosity and excited by a thermal process which we model crudely, and approximately, by

$$\frac{\partial T'}{\partial t} = -\widehat{\beta} u, \quad (46)$$

where u is velocity. The following equation then governs the wave motion:

$$\frac{\partial^2 \rho'}{\partial t^2} - c^2 \frac{\partial^2 \rho'}{\partial x^2} - \frac{\partial}{\partial t} \left(\lambda \rho' + \nu \frac{\partial^2 \rho'}{\partial x^2} \right) = \frac{\partial}{\partial x} \left(\rho u \frac{\partial u}{\partial x} \right), \quad (47)$$

where c^2 , ρ , $\lambda = \widehat{\alpha} \widehat{\beta} / c \rho$ and the kinematic viscosity ν are all constants. We have also introduced the device of replacing $\partial/\partial x$ by $c^{-1} \partial/\partial t$ in the thermal term, which is now $\lambda \partial \rho' / \partial t$, to ensure that it excites both forward and backward propagating components of the mode. A more physically realistic model not requiring that artificial device for the excitation could easily have been adopted, but the governing equation would have been unnecessarily more complicated.

The Eulerian density perturbation may be represented as a sum of normal modes:

$$\rho' = \sum_n \frac{1}{2} \left(A_n e^{-i\omega_n t} + A_n^* e^{i\omega_n t} \right) \cos k_n x \quad (48)$$

with $n = 0$ corresponding to the parent mode and $n = 1, 2$ to the daughter modes, where the complex amplitude $A_n(t)$ is slowly varying and the asterisk denotes complex conjugate. The wavenumber k_n is determined by the boundary conditions, and the real frequency ω_n satisfies $\omega_n = c k_n$, so that the amplitude of a linearized unforced mode grows exponentially with time at rate $\sigma_n = (\lambda - \nu k_n^2) / 2$, whose magnitude we consider to be small compared with ω_n . It is now straightforward to show that when the weak nonlinear interactions between the parent and the two low-amplitude daughters are taken into account as a small perturbation, by substituting the linear eigenfunctions of Eq. (48) into Eq. (47), keeping only second-order terms, and integrating over x , the resulting equations for the amplitudes are given approximately by

$$\frac{dA_0}{dt} - \sigma_0 A_0 = \frac{4iA\omega_0}{I_0} A_1 A_2 e^{i\Delta\omega t} \quad (49)$$

and

$$\frac{dA_{1,2}}{dt} - \sigma_{1,2}A_{1,2} = \frac{iA\omega_0^2}{I_{1,2}\omega_{1,2}}A_0A_{2,1}^*e^{-i\Delta\omega t} \quad (50)$$

in which $I_n = \langle \rho'_n \rho_n'^* \rangle$ is a measure of the inertia of mode, the angular brackets denoting integration over x , and $A = [\cos \Delta k x]_0^1 / 4\Delta k$ is a mode coupling constant which is an integral of terms trilinear in eigenfunctions; also $-\sigma_{1,2}$ are the intrinsic damping rates of the daughters, and are presumed to be positive, $\Delta\omega = \omega_0 - \omega_1 - \omega_2$ is the frequency mismatch, and $\Delta k = k_0 - k_1 - k_2$ depends on the chosen boundary conditions. These equations are very similar to those derived by Dziembowski (see 1982) for stellar g modes.

Equation (50) describes the pulchral²¹ dynamics: if it is accepted that the daughters dissipate much more rapidly than the parent can grow, then the variation of A_0 may at first be neglected; the equations are linear in $A_{n \neq 0}$, and admit solutions $A_n = Q_n \exp(-i\Delta\omega t/2)$ with $Q_n \propto \exp(st)$ in which $s \geq 0$ if $|A_0|^2 \geq A_c^2$, where

$$A_c^2 = \frac{I_1 I_2 \omega_1 \omega_2}{A^2 \omega_0^4} \left\{ \sigma_1 \sigma_2 + \frac{1}{4} \left[1 + \left(\frac{\sigma_2 - \sigma_1}{\sigma_2 + \sigma_1} \right)^2 \right] (\Delta\omega)^2 \right\}. \quad (51)$$

As we discuss later, A_c estimates the limiting amplitude of the parent. Note that for a given coupling constant A and close resonance ($\Delta\omega$ very small), the amplitude above which the parent excites her daughters is approximately proportional to the (harmonic) mean of their damping rates, and inversely proportional to the coupling constant. It is independent of the intrinsic growth rate of the parent (of course), provided that the growth rate is small compared with the damping rates $-\sigma_n$. A state of steady amplitudes exists when $|A_0| = A_c$. In that case, other things being equal, the amplitude of the main mode would decrease if the viscosity were to be reduced, a result which at first sight might seem counterintuitive.

To proceed further we need to apply these results to solar g modes, which requires considering the g-mode frequency spectrum in spherical symmetry. Not surprisingly, for a nontrivial coupling constant one needs $m_1 + m_2 = m_0$, and also $l_2 - l_1 = l_0$ or $l_0 - 2$, where m and l are azimuthal order and degree. These selection rules come from the integral of spherical harmonics that appears as a factor of the coupling coefficient (see Dziembowski 1982, for details)

$$Z = \int Y_0^* Y_1 Y_2 \sin \theta d\theta d\phi \quad (52)$$

where $Y_{0,1,2}$ denotes the spherical harmonic associated to the modes $(0, 1, 2)$, and (θ, ϕ) are spherical polar angles. If the coupling constant is not to be small, one needs the orders n_1, n_2 not to be very different, so that the product of the daughter eigenfunctions varies on a scale similar to that of their parent. These conditions, together with the resonance condition $|\Delta\omega| \ll \omega_0$, are most likely to be satisfied when l_1 and l_2 are large, requiring $l_2 \simeq l_1$ and consequently $\omega_2 \simeq \omega_1 \simeq \frac{1}{2}\omega_0$, because when l is large the frequency distribution is dense, as can be seen from the approximate asymptotic eigenfrequency equation derivable from Eq. (4):

$$\pi^{-1} \int \left(\frac{N^2}{\omega^2} - 1 \right)^{1/2} d \ln r \simeq \frac{n - \frac{1}{2}}{l + \frac{1}{2}}, \quad (53)$$

the integral being between two radii at which $N = \omega$. From that relation it follows that the frequency difference $\delta\omega$ between two modes of consecutive order satisfies $\delta\omega \simeq \mu\omega l^{-1}$ with μ of order unity. Also the damping rates of the daughters satisfy $-\sigma_2 \simeq -\sigma_1$, which, for convenience, we here denote simply by η .

A.2 Effect of frequency mismatches

The scenario proposed by Dziembowski (1983) is that an ‘equilibrium’ state of steady oscillations is reached (ignoring temporal variation of the background state of the Sun) in which

²¹ derived from Appius Claudius Pulcher, Roman politician of the 1st century BC who had several daughters and grand-daughters all named Claudia.

twin daughters of high degree extract energy nonlinearly from the parent and subsequently dissipate it at the same rate that the parent extracts energy linearly from the background state. Following a similar study by Wersinger et al. (1980), Dziembowski also demanded that the equilibrium be stable, which requires $\Delta\omega > 2\eta$. Then, not knowing the structure of the Sun precisely enough to calculate the resonances, he considered instead the probable amplitude of the parent, making certain assumptions about the probability distribution of frequencies: the probability of being within $\Delta\omega$ of resonance is proportional to $\Delta\omega/\delta\omega$, and since $\delta\omega \simeq l^{-1}$ one might expect to find amplitude limitation to be most likely amongst daughters with greatest l . But also one must recognise that damping rates increase with l , according to $\eta \simeq \eta_0 l^2$ (for a damping dominated by radiative losses), rendering the energy-extraction process at high l less effective and thereby permitting more freedom for the parent to grow. The outcome is a compromise. Dziembowski estimated the probability P that the parent has its amplitude limited to A to be

$$P = 1 - \exp\left(-\frac{\pi A^2}{16\mu\eta} \sum_i \Lambda_i^2\right), \quad (54)$$

the summation being over all pairs i of twins (having coupling constants Λ_i). Of course, the formula for the coupling constant, which depends on the precise way in which one chooses to define A , is much more complicated than that for the simple acoustic interaction discussed at the beginning of the section.

References

- Adelberger, E. G., Austin, S. M., Bahcall, J. N., et al. 1998, *Reviews of Modern Physics*, **70**, 1265
- Aerts, C., Eyer, L., & Kestens, E. 1998, *A&A*, **337**, 790
- Aigrain, S., Favata, F., & Gilmore, G. 2004, *A&A*, **414**, 1139
- Andersen, B. N. 1994, *Sol. Phys.*, **152**, 241
- Andersen, B. N. 1996, *A&A*, **312**, 610
- Andersen, B. N., Andreassen, O., Wasberg, C. E., & Leifsen, T. 1993, in *Astronomical Society of the Pacific Conference Series*, Vol. 42, GONG 1992. *Seismic Investigation of the Sun and Stars*, ed. T. M. Brown, 49
- Ando, H. 1986, *Astrophysics and Space Science*, **118**, 177
- Andreassen, O., Andersen, B. N., & Wasberg, C. E. 1992, *A&A*, **257**, 763
- Antia, H. M. & Basu, S. 2006, *ApJ*, **644**, 1292
- Antoniou, A. 1979, *Digital Filters: Analysis and Design* (McGraw-Hill, New York)
- Appourchaux, T. 1998, in ‘Structure and Dynamics of the Interior of the Sun and Sun-like Stars’, ed. S. Korzennik & A. Wilson (ESA SP-418, ESA Publications Division, Noordwijk, The Netherlands), 37–46
- Appourchaux, T. 2004, *A&A*, **428**, 1039
- Appourchaux, T. & Andersen, B. N. 1990, *Sol. Phys.*, **128**, 91
- Appourchaux, T., Andersen, B. N., Fröhlich, C., et al. 1997, *Sol. Phys.*, **170**, 27
- Appourchaux, T., Andersen, B. N., & Sekii, T. 2002, in *From Solar Min to Max: half a solar cycle with SOHO*, ed. C. Fröhlich & A. Wilson (ESA SP-508, ESA Publications Division, Noordwijk, The Netherlands), 47
- Appourchaux, T., Fröhlich, C., Andersen, B. N., et al. 2000, *ApJ*, **538**, 401
- Appourchaux, T., Gizon, L., & Rabello-Soares, M. C. 1998, *A&A Sup. Series*, **132**, 107
- Appourchaux, T., Leibacher, J., & Boumier, P. 2007, *A&A*, **463**, 1211
- Appourchaux, T., Liewer, P., Watt, M., et al. 2009, *Experimental Astronomy*, **23**, 1079
- Appourchaux, T. & Toutain, T. 1998, in *Sounding Solar and Stellar Interiors*, IAU 181, Poster volume, ed. J. Provost & F.-X. Schmider (Kluwer Academic Publishers, Dordrecht), 5
- Appourchaux, T., Toutain, T., Telljohann, U., et al. 1995, *A&A*, **294**, L13
- Asplund, M., Grevesse, N., & Sauval, A. 2005, in *Cosmic Abundances as Records of Stellar Evolution and Nucleosynthesis*, ed. T. B. III & F. Bash, Vol. **336** (Astronomical Society of the Pacific), 25
- Asplund, M., Grevesse, N., Sauval, A. J., & Scott, P. 2009, *ArXiv e-prints*, 0909.0948
- Auré, J.-L. 1971, *A&A*, **11**, 345
- Bahcall, J. N., Basu, S., & Serenelli, A. M. 2005, *ApJ*, **631**, 1281
- Bahcall, J. N., Serenelli, A. M., & Pinsonneault, M. 2004, *ApJ*, **614**, 464

- Baker, N. H. & Gough, D. O. 1979, *ApJ*, **234**, 232
- Ballot, J., Appourchaux, T., Toutain, T., & Guittet, M. 2008, *A&A*, **486**, 867
- Ballot, J., García, R. A., & Lambert, P. 2006, *MNRAS*, **369**, 1281
- Balmforth, N. J. 1992a, *MNRAS*, **255**, 639
- Balmforth, N. J. 1992b, *MNRAS*, **255**, 603
- Basu, S. & Antia, H. 2008, *Physics Reports*, **457**, 217
- Basu, S. & Antia, H. M. 2004, *ApJ*, **606**, L85
- Batchelor, G. 1953, *Homogeneous Turbulence* (Cambridge University Press)
- Baturin, V. A., Däppen, W., Gough, D. O., & Vorontsov, S. V. 2000, *MNRAS*, **316**, 71
- Baudin, F., Samadi, R., Goupil, M.-J., et al. 2005, *A&A*, **433**, 349
- Belkacem, K., Samadi, R., Goupil, M.-J., & Dupret, M.-A. 2008, *A&A*, **478**, 163
- Belkacem, K., Samadi, R., Goupil, M. J., et al. 2009, *A&A*, **494**, 191
- Belkacem, K., Samadi, R., Goupil, M.-J., & Kupka, F. 2006a, *A&A*, **460**, 173
- Belkacem, K., Samadi, R., Goupil, M.-J., Kupka, F., & Baudin, F. 2006b, *A&A*, **460**, 183
- Berger, J., Boukai, B., & Wang, Y. 1997, *Statistical Science*, **12**, 133
- Berger, J. & Sellke, T. 1987, *Journal of the American Statistical Association*, **82(397)**, 112
- Bertello, L., Henney, C. J., Ulrich, R. K., et al. 2000a, *ApJ*, **535**, 1066
- Bertello, L., Varadi, F., Ulrich, R. K., et al. 2000b, *ApJ Letters*, **537**, L143
- Berthomieu, G., Gonczi, G., Graff, P., Provost, J., & Rocca, A. 1978, *A&A*, **70**, 597
- Berthomieu, G. & Provost, J. 1990, *A&A*, **227**, 563
- Berthomieu, G. & Provost, J. 1991, *Sol. Phys.*, **133**, 127
- Böhm-Vitense, E. 1958, *Zeitschrift für Astrophysik*, **46**, 108
- Bonnet, R. M., Crommelynck, D., Delaboudinière, J. P., et al. 1981, DISCO assessment study, ESA SCI(81)3, Tech. rep., European Space Agency, Paris
- Boury, A., Gabriel, M., Noels, A., Scuflaire, R., & Ledoux, P. 1975, *A&A*, **41**, 279
- Bracewell, R. N. 2000, *The Fourier transform and its applications* (Boston : McGraw Hill (McGraw-Hill series in electrical and computer engineering. Circuits and systems))
- Broomhall, A. M., Chaplin, W. J., Elsworth, Y., & Appourchaux, T. 2007, *MNRAS*, **379**, 2
- Brown, T. M. 1979, *ApJ*, **230**, 255
- Brown, T. M. 1985, *Nature*, **317**, 591
- Brown, T. M., Stebbins, R. T., & Hill, H. A. 1978, *ApJ*, **223**, 324
- Brun, A. S., Turck-Chièze, S., & Morel, P. 1998, *ApJ*, **506**, 913
- Brun, A. S., Turck-Chièze, S., & Zahn, J. P. 1999, *ApJ*, **525**, 1032
- Burgers, J. M. 1969, *Flow Equations for Composite Gases* (New York: Academic Press)
- Burston, R., Gizon, L., Appourchaux, T., Ni, W.-T., & the ASTROD I team. 2008, *Journal of Physics Conference Series*, **118**, 012043
- Caffau, E., Ludwig, H.-G., Steffen, M., et al. 2008, *A&A*, **488**, 1031
- Caffau, E., Maiorca, E., Bonifacio, P., et al. 2009, *A&A*, **498**, 877
- Canuto, V. M. & Mazzitelli, I. 1991, *ApJ*, **370**, 295
- Castro, M., Vauclair, S., & Richard, O. 2007, *A&A*, **463**, 755
- Caughlan, G. R. & Fowler, W. A. 1988, *Atomic Data and Nuclear Data Tables*, **40**, 283
- Chaplin, W. J., Elsworth, Y., Howe, R., et al. 1996, *Sol. Phys.*, **168**, 1
- Chaplin, W. J., Elsworth, Y., Isaak, G. R., et al. 2002, *MNRAS*, **336**, 979
- Chaplin, W. J., Houdek, G., Elsworth, Y., et al. 2005, *MNRAS*, **360**, 859
- Christensen-Dalsgaard, J. 1980, *A&A*, **190**, 765
- Christensen-Dalsgaard, J. 1984, in *Solar Seismology from Space*, ed. R. K. Ulrich, J. Harvey, E. J. Rhodes, Jr., & J. Toomre, 219–253
- Christensen-Dalsgaard, J. 1990, in *IAU Colloq. 121: Inside the Sun*, 305
- Christensen-Dalsgaard, J. 2002a, *Reviews of Modern Physics*, **74**, 1073
- Christensen-Dalsgaard, J. 2002b, *International Journal of Modern Physics D*, **11**, 995
- Christensen-Dalsgaard, J. & Berthomieu, G. 1991, in *Solar interior and atmosphere* (University of Arizona Press, Tucson, AZ, USA), 401
- Christensen-Dalsgaard, J., Däppen, W., Ajukov, S., et al. 1996, *Science*, **272**, 1286
- Christensen-Dalsgaard, J., Dilke, F. W. W., & Gough, D. O. 1974, *MNRAS*, **169**, 429
- Christensen-Dalsgaard, J. & Frandsen, S. 1983, *Sol. Phys.*, **82**, 469
- Christensen-Dalsgaard, J. & Gough, D. O. 1975, *Mémoires of the Société Royale des Sciences de Liège*, **8**, 309
- Christensen-Dalsgaard, J. & Gough, D. O. 1980, in *Lecture Notes in Physics*, Berlin Springer Verlag, Vol. 125, *Nonradial and Nonlinear Stellar Pulsation*, ed. H. A. Hill & W. A. Dziembowski, 369–380

- Christensen-Dalsgaard, J. & Gough, D. O. 1982, *MNRAS*, **198**, 141
- Christensen-Dalsgaard, J., Proffitt, C. R., & Thompson, M. J. 1993, *ApJ*, **403**, L75
- Claverie, A., Isaak, G., McLeod, C., van der Raay, H., & Roca Cortés, T. 1979, *Nature*, **282**, 591
- Claverie, A., Isaak, G. R., McLeod, C. P., van der Raay, H. B., & Roca Cortes, T. 1981, *Sol. Phys.*, **74**, 51
- Corbard, T., Berthomieu, G., Morel, P., et al. 1997, *A&A*, **324**, 298
- Corbard, T., Blanc-Féraud, L., Berthomieu, G., & Provost, J. 1999, *A&A*, **344**, 696
- Corbard, T., Boumier, P., Appourchaux, T., et al. 2008, *Astronomische Nachrichten*, **329**, 508
- Couvidat, S. 2002, *Rôle de l'héliosismologie dans la dynamique interne du Soleil et dans le problème des neutrinos solaires*, PhD thesis (Université Paris VII, Paris)
- Couvidat, S., Turck-Chièze, S., & Kosovichev, A. 2003, *ApJ*, **599**, 1434
- Cowling, T. G. & Newing, R. A. 1949, *ApJ*, **109**, 149
- Cox, A. N. & Guzik, J. A. 2004, *ApJ*, **613**, L169
- Cox, A. N., Guzik, J. A., & Kidman, R. B. 1989, *ApJ*, **342**, 1187
- Cox, J. P., Cox, A. N., Olsen, K. H., King, D. S., & Eilers, D. D. 1966, *ApJ*, **144**, 1038
- Damé, L., Hersé, M., Thuillier, G., et al. 1999, *Advances in Space Research*, **24**, 205
- Davenport, W.B., J. & Root, W. 1958, *An introduction to the theory of random signals and noise* (International Student Edition, McGraw-Hill Book company, Inc., New York)
- De Finetti, B. 1937, *Annales de l'Institut Henri Poincaré*, **7**, 1, 1
- Delache, P. & Scherrer, P. H. 1983, *Nature*, **306**, 651
- Denison, D. G. T. & Walden, A. T. 1999, *ApJ*, **514**, 972
- Deubner, F.-L. 1975, *A&A*, **44**, 371
- Deubner, F.-L. & Gough, D. 1984, *Ann. Rev. Astron. Astrophys.*, **22**, 593
- Dikpati, M., Corbard, T., Thompson, M. J., & Gilman, P. A. 2002, *ApJ*, **575**, L41
- Dilke, F. W. W. & Gough, D. O. 1972, *Nature*, **240**, 262
- Dintrans, B., Brandenburg, A., Nordlund, Å., & Stein, R. F. 2005, *A&A*, **438**, 365
- Dintrans, B. & Rieutord, M. 2000, *A&A*, **354**, 86
- Domingo, V., Fleck, B., & Poland, A. I. 1995, *Sol. Phys.*, **162**, 1
- Dupret, M.-A., Barban, C., Goupil, M.-J., et al. 2006a, in *ESA Special Publication*, Vol. 624, *Proceedings of SOHO 18/GONG 2006/HELAS I, Beyond the spherical Sun*
- Dupret, M.-A., Goupil, M.-J., Samadi, R., Grigahcène, A., & Gabriel, M. 2006b, in *ESA Special Publication*, Vol. 624, *Proceedings of SOHO 18/GONG 2006/HELAS I, Beyond the spherical Sun*
- Dupret, M.-A., Samadi, R., Grigahcène, A., Goupil, M.-J., & Gabriel, M. 2006c, *Communications in Asteroseismology*, **147**, 85
- Duvall, Jr., T. L. 2004, in *ESA Special Publication*, Vol. 559, *SOHO 14 Helio- and Asteroseismology: Towards a Golden Future*, ed. D. Danesy, 412
- Duvall, Jr., T. L., Jefferies, S. M., Harvey, J. W., & Pomerantz, M. A. 1993, *Nature*, **362**, 430
- Dyson, J. & Schutz, B. F. 1979, *Royal Society of London Proceedings Series A*, **368**, 389
- Dziembowski, W. 1982, *Acta Astronomica*, **32**, 147
- Dziembowski, W. 1983, *Sol. Phys.*, **82**, 259
- Dziembowski, W. & Kosovichev, A. 1987, *Acta Astronomica*, **37**, 313
- Dziembowski, W. A. 1977, *Acta Astronomica*, **27**, 203
- Dziembowski, W. A. & Pamiatnykh, A. A. 1993, *MNRAS*, **262**, 204
- Dziembowski, W. A., Paterno, L., & Ventura, R. 1985, *A&A*, **151**, 47
- Dziembowski, W. A. & Sienkiewicz, R. 1973, *Acta Astronomica*, **23**, 273
- Eckart, C. 1960, *Hydrodynamics of oceans and atmospheres* (Pergamon Press, Oxford, New York)
- Eisenfeld, J. 1969, *J. Math. Analysis Appl.*, **26**, 357
- Elliott, J. R. & Gough, D. O. 1999, *ApJ*, **516**, 475
- Ellis, A. N. 1986, in *Seismology of the Sun and the Distant Stars*, 173
- Elsworth, Y. P., Baudin, F., Chaplin, W., et al. 2006, in *ESA Special Publication*, Vol. 624, *Proceedings of SOHO 18/GONG 2006/HELAS I, Beyond the spherical Sun*
- Finsterle, W. & Fröhlich, C. 2001, *Sol. Phys.*, **200**, 393
- Fodor, I. K. & Stark, P. B. 1998, in *ESA Special Publication*, Vol. 418, *Structure and Dynamics of the Interior of the Sun and Sun-like Stars*, ed. S. Korzenik, 171
- Fossat, E., Grec, G., & Pomerantz, M. 1981, *Sol. Phys.*, **74**, 59
- Frandsen, S., Carrier, F., Aerts, C., et al. 2002, *A&A*, **394**, L5
- Fröhlich, C. 1984, *Mem.S.A.It*, **55**, 237

- Fröhlich, C. & Andersen, B. N. 1995, in *Helioseismology*, ESA SP-376, Vol 1, ed. B. J.T.Hoeksema, V.Domingo & B.Batrick (ESA Publications Division, Noordwijk, The Netherlands), 137
- Fröhlich, C., Andersen, B. N., Appourchaux, T., et al. 1997, *Sol. Phys.*, **170**, 1
- Fröhlich, C. & Delache, P. 1984a, in *Solar Seismology from Space*, JPL 84-84, ed. R. K. Ulrich, J. Harvey, E. J. Rhodes, Jr., & J. Toomre, 183-193
- Fröhlich, C. & Delache, P. 1984b, *Memorie della Società Astronomica Italiana*, **55**, 99
- Fröhlich, C., Romero, J., Roth, H., et al. 1995, *Sol. Phys.*, **162**, 101
- Gabriel, A. H. 2006, in *ESA Special Publication*, Vol. 624, *Proceedings of SOHO 18/GONG 2006/HELAS I, Beyond the spherical Sun*
- Gabriel, A. H., Baudin, F., Boumier, P., et al. 2002, *A&A*, **390**, 1119
- Gabriel, A. H., Grec, G., Charra, J., et al. 1995, *Sol. Phys.*, **162**, 61
- Gabriel, A. H., Turck-Chièze, S., García, R., et al. 1998, in *Structure and Dynamics of the Interior of the Sun and Sun-like Stars*, ESA SP-418, ed. S. Korzennik & A. Wilson (ESA Publications Division, Noordwijk, The Netherlands), 61
- Gabriel, A. H., Turck-Chièze, S., García, R. A., et al. 1999, *Advances in Space Research*, **24**, 147
- Gabriel, M. 1994, *A&A*, **287**, 685
- Gabriel, M. 1996, *Bulletin of the Astronomical Society of India*, **24**, 233
- Gabriel, M. 1997, *A&A*, **327**, 771
- Gabriel, M., Scufflaire, R., Noels, A., & Boury, A. 1975, *A&A*, **40**, 33
- Garaud, P. 2002, *MNRAS*, **329**, 1
- García, R. A., Bertello, L., Turck-Chièze, S., et al. 2001a, in *Structure and Dynamics of the Interior of the Sun and Sun-like Stars*, ESA SP-464, ed. P.L.Pallé & A.Wilson (ESA Publications Division, Noordwijk, The Netherlands), 473
- García, R. A., Corbard, T., Chaplin, W. J., et al. 2004, *Sol. Phys.*, **220**, 269
- García, R. A., Jefferies, S. M., Toner, C. G., & Pallé, P. L. 1999, *A&A*, **346**, L61
- García, R. A., Jiménez, A., Mathur, S., et al. 2008a, *Astronomische Nachrichten*, **329**, 476
- García, R. A., Mathur, S., Ballot, J., et al. 2008b, *Sol. Phys.*, **251**, 119
- García, R. A., Régulo, C., Turck-Chièze, S., et al. 2001b, *Sol. Phys.*, **200**, 361
- García, R. A., Turck-Chièze, S., Jiménez-Reyes, S. J., et al. 2007, *Science*, **316**, 1591
- Gautschy, A. & Saio, H. 1995, *Ann. Rev. Astron. Astrophys.*, **33**, 75
- Gautschy, A. & Saio, H. 1996, *Ann. Rev. Astron. Astrophys.*, **34**, 551
- Georgobiani, D., Stein, R. F., & Nordlund, Å. 2006, in *Astronomical Society of the Pacific Conference Series*, Vol. 354, *Solar MHD Theory and Observations: A High Spatial Resolution Perspective*, ed. J. Leibacher, R. F. Stein, & H. Uitenbroek, 109-+
- Giamperi, G., Polnarev, A., Roxburgh, I., & Vorontsov, S. 2000, *Astrophysics and Space Science*, **261**, 35
- Gizon, L. 2006, in *ESA Special Publication*, Vol. 641, *Proceedings of the Second Solar Orbiter workshop*, Athens, Greece
- Gizon, L., Appourchaux, T., & Gough, D. O. 1998, in *IAU Symposium*, Vol. 185, *New Eyes to See Inside the Sun and Stars*, ed. F.-L. Deubner, J. Christensen-Dalsgaard, & D. Kurtz, 37
- Gizon, L. & Solanki, S. K. 2003, *ApJ*, **589**, 1009
- Goldreich, P. & Keeley, D. A. 1977, *ApJ*, **211**, 934
- Goldreich, P. & Keeley, D. A. 1977b, *ApJ*, **212**, 243
- Goldreich, P. & Kumar, P. 1990, *ApJ*, **363**, 694
- Goldreich, P. & Kumar, P. 1991, *ApJ*, **374**, 366
- Goldreich, P., Murray, N., & Kumar, P. 1994, *ApJ*, **424**, 466
- Goldreich, P. & Nicholson, P. D. 1977, *Icarus*, **30**, 301
- Goode, P. R. & Thompson, M. J. 1992, *ApJ*, **395**, 307
- Gott, J. R. I. 1994, *Nature*, **368**, 108
- Gough, D. O. 1965, in *Woods Hole Oceanographic Institution*, Vol. II, *Geophysical Fluid Dynamics*, 49
- Gough, D. O. 1969, *Journal of Atmospheric Sciences*, **26**, 448
- Gough, D. O. 1977a, *ApJ*, **214**, 196
- Gough, D. O. 1977b, in *Lecture Notes in Physics*, Berlin Springer Verlag, Vol. 71, *Problems of Stellar Convection*, ed. E. A. Spiegel & J.-P. Zahn, 15-56
- Gough, D. O. 1980, in *Lecture Notes in Physics*, Berlin Springer Verlag, Vol. 125, *Nonradial and Nonlinear Stellar Pulsation*, ed. H. A. Hill & W. A. Dziembowski, 273

- Gough, D. O. 1985, in *Future Missions in Solar, Heliospheric and Space Plasma Physics* (ESA Publication Division), 183–197
- Gough, D. O. 1993, in *Astrophysical Fluid Dynamics - Les Houches 1987*, 399–560
- Gough, D. O. 2004, in *American Institute of Physics Conference Series*, Vol. 731, *Equation-of-State and Phase-Transition in Models of Ordinary Astrophysical Matter*, ed. V. Celebonović, D. Gough, & W. Däppen, 119
- Gough, D. O. 2007, *Astronomische Nachrichten*, **328**, 273
- Gough, D. O. 2009, in *Astr. Sp. Sci. Proc.*, Heidelberg, Vol. in press, *Magnetic coupling between the interior and the atmosphere of the Sun*, ed. S. S. Hasan & R. Rutten
- Gough, D. O. & Kosovichev, A. G. 1993, in *Astronomical Society of the Pacific Conference Series*, Vol. 40, *IAU Colloq. 137: Inside the Stars*, ed. W. W. Weiss & A. Baglin, 566
- Gough, D. O., Kosovichev, A. G., Toomre, J., et al. 1996, *Science*, **272**, 1296
- Gough, D. O., Kosovichev, A. G., & Toutain, T. 1995, in *Astronomical Society of the Pacific Conference Series*, Vol. 76, *GONG 1994. Helio- and Astro-Seismology from the Earth and Space*, ed. R. K. Ulrich, E. J. Rhodes Jr., & W. Däppen, 55
- Gough, D. O. & Latour, J. 1984, *Astronomy Express*, **1**, 9
- Gough, D. O. & McIntyre, M. E. 1998, *Nature*, **394**, 755
- Grec, G. 1981, PhD thesis, Université de Nice
- Grec, G., Fossat, E., & Pomerantz, M. 1980, *Nature*, **288**, 541
- Grec, G., Provost, J., & Renaud, C. 2009, in *Solar-stellar dynamos as revealed by helio- and asteroseismology*, Vol. In press (European Space Agency, Noordwijk, The Netherlands)
- Green, E. M., Fontaine, G., Reed, M. D., et al. 2003, *ApJ Letters*, **583**, L31
- Grevesse, N. & Noels, A. 1993, in *Origin and Evolution of the elements*, ed. N. Prantzos, E. Vangioni-Flam, & M. Cassé (Cambridge Univ. press), 15–25
- Grevesse, N. & Sauval, A. 1998, *Space Science Reviews*, **85**, 161
- Grigahcène, A., Dupret, M.-A., Gabriel, M., Garrido, R., & Scuflaire, R. 2005, *A&A*, **434**, 1055
- Guenther, D. B. & Demarque, P. 1984, *ApJ Letters*, **277**, L17
- Guenther, D. B., Demarque, P., Kim, Y.-C., & Pinsonneault, M. H. 1992, *ApJ*, **387**, 372
- Guzik, J. A. 2006, in *Beyond the spherical Sun*, ed. K. Fletcher & M. Thompson, Vol. ESA SP-624 (ESA Publications Division), 17.1
- Guzik, J. A., Watson, L., & Cox, A. 2005, *ApJ*, **627**, 1049
- Harvey, J. 1985, in *Future missions in solar, heliospheric and space plasma physics*, ESA SP-235, ed. E. Rolfe & B. Battrick (ESA Publications Division, Noordwijk, The Netherlands), 199–208
- Harvey, J. W., Hill, F., Hubbard, R., et al. 1996, *Science*, **272**, 1284
- Hill, H. A. 1985, *ApJ*, **290**, 765
- Hill, H. A. 1992, *ApJ Supplement Series*, **78**, 283
- Holweger, H. 2001, in *American Institute of Physics Conference Series*, Vol. 598, *Joint SOHO/ACE workshop "Solar and Galactic Composition"*, ed. R. F. Wimmer-Schweingruber, 23
- Hoogeveen, G. W. & Riley, P. 1998, *Sol. Phys.*, **179**, 167
- Houdek, G. 2003, in *Astronomical Society of the Pacific Conference Series*, Vol. 305, *Astronomical Society of the Pacific Conference Series*, ed. L. A. Balona, H. F. Henrichs, & R. Medupe, 45
- Houdek, G. 2006, in *ESA Special Publication*, Vol. 624, *Proceedings of SOHO 18/GONG 2006/HELAS I, Beyond the spherical Sun*
- Houdek, G., Balmforth, N. J., & Christensen-Dalsgaard, J. 1995, in *ESA Special Publication*, Vol. 376, *Proceedings of the 4th SOHO Workshop, Helioseismology*, ed. J. Hoeksma, V. Domingo, B. Fleck, & B. Battrick, 447
- Houdek, G., Balmforth, N. J., Christensen-Dalsgaard, J., & Gough, D. O. 1999, *A&A*, **351**, 582
- Houdek, G. & Gough, D. O. 2002, *MNRAS*, **336**, L65
- Hughes, D., Rosner, R., & Weiss, N. 2005, *Astronomy and Geophysics*, **46**, 040000
- Jeffreys, H. 1925, *Proceeding of the London Mathematical Society*, **23**, 428
- Jiménez, A. & García, R. A. 2009, *ApJ*, **184**, 288
- Jiménez, A., Palle, P. L., Roca Cortes, T., Domingo, V., & Korzennik, S. 1987, *A&A*, **172**, 323
- Jordinson, C. & Gough, D. O. 2000, in *Astronomical Society of the Pacific Conference Series*, Vol. 203, *IAU Colloq. 176: The Impact of Large-Scale Surveys on Pulsating Star Research*,

- ed. L. Szabados & D. Kurtz, 390
- Kolmogorov, A. 1941, *Akademiia Nauk SSSR Doklady*, **30**, 301
- Komm, R. W., Gu, Y., Hill, F., Stark, P. B., & Fodor, I. K. 1999, *ApJ*, **519**, 407
- Koopmans, L. 1974, *The Spectral Analysis of Time Series* (Academic Press, Inc., London, United Kingdom)
- Kosovichev, A. G. 1986a, *Izvestiya Ordena Trudovogo Krasnogo Znameni Krymskoj Astrofizicheskoy Observatorii*, **75**, 22
- Kosovichev, A. G. 1986b, *Bulletin Crimean Astrophysical Observatory*, **75**, 19
- Kosovichev, A. G. 1996, *ApJ Letters*, **469**, L61
- Kosovichev, A. G. & Duvall, Jr., T. L. 2003, in *Society of Photo-Optical Instrumentation Engineers (SPIE) Conference Series*, ed. S. L. Keil & S. V. Avakyan, Vol. 4853, 327
- Kosovichev, A. G., Schou, J., Scherrer, P. H., et al. 1997, *Sol. Phys.*, **170**, 43
- Kosovichev, A. G. & Severny, A. B. 1985, *Bulletin Crimean Astrophysical Observatory*, **72**, 162
- Kraichnan's, R. H. 1957, *Phys. Rev.*, **107**, 1485
- Kumar, P., Quataert, E. J., & Bahcall, J. N. 1996, *ApJ Letters*, **458**, L83
- Kupka, F. & Robinson, F. J. 2007, *MNRAS*, **374**, 305
- Lebreton, Y., Monteiro, M., Montalbán, J., et al. 2008, *Astrophysics and Space Science*, **316**, 1
- Ledoux, P. 1951, *ApJ*, **114**, 373
- Ledoux, P. & Sauvenier-Goffin, E. 1950, *ApJ*, **111**, 611
- Ledoux, P. & Walraven, T. 1958, *Handbuch der Physik*, **51**, 353
- Leighton, R. B., Noyes, R. W., & Simon, G. W. 1962, *ApJ*, **135**, 474
- Lighthill, M. J. 1952, *Royal Society of London Proceedings Series A*, **211**, 564
- Mathis, S., Talon, S., Pantillon, F.-P., & Zahn, J.-P. 2008, *Sol. Phys.*, **251**, 101
- Mathis, S. & Zahn, J.-P. 2005, *A&A*, **440**, 653
- Mathur, S., Eff-Darwich, A., García, R. A., & Turck-Chièze, S. 2008, *A&A*, **484**, 517
- Mathur, S., Turck-Chièze, S., Couvidat, S., & García, R. A. 2007, *ApJ*, **668**, 594
- Michaud, G. & Proffitt, C. R. 1993, in *Inside the stars*, ed. A. Baglin & W. Weiss, Vol. ASP Conf Series **40** (ASP, San Francisco), 246
- Miesch, M. S., Brun, A. S., DeRosa, M. L., & Toomre, J. 2008, *ApJ*, 673, 557
- Montalbán, J., Miglio, A., Noels, A., Grevesse, N., & di Mauro, M. P. 2004, in *Helio- and Asteroseismology: Towards a Golden Future*, ed. D. Danesy. (ESA SP-559, ESA Publications Division, Noordwijk, The Netherlands), 574
- Montalbán, J., Miglio, A., Theado, S. and Noels, A., & Grevesse, N. 2006, *Communications in Asteroseismology*, **147**, 80
- Montalbán, J. & Schatzman, E. 2000, *A&A*, **354**, 943
- Monteiro, M. J. P. F. G. 2009, *Evolution and Seismic Tools for Stellar Astrophysics* (Springer)
- Mordant, N., Lévêque, E., & Pinton, J.-F. 2004, *New Journal of Physics*, **6**, 116
- Morel, P. 1997, *A&A Sup. Series*, **124**, 597
- Morel, P., Provost, J., & Berthomieu, G. 1997, *A&A*, **327**, 349
- Morel, P., Provost, J., & Berthomieu, G. 1998, in *Structure and Dynamics of the Interior of the Sun and Sun-like Stars*, ed. S. Korzennik & A. Wilson, Vol. ESA-SP418 (ESA Publications Division), 499
- Moya, A., Christensen-Dalsgaard, J., Charpinet, S., et al. 2008, *Astrophysics and Space Science*, **316**, 231
- Musielak, Z. E., Rosner, R., Stein, R. F., & Ulmschneider, P. 1994, *ApJ*, **423**, 474
- Ni, W.-T. 2007, *Nuclear Physics B Proceedings Supplements*, **166**, 153
- Noels, A., Boury, A., Scuflaire, R., & Gabriel, M. 1974, *A&A*, **31**, 185
- Nyquist, H. 1924, *Bell Syst. Tech. Journal*, **3**, 324
- Oleson, J. R., Zaroni, C. A., Hill, H. A., et al. 1974, *Applied Optics*, **13**, 206
- Olver, F. W. J. 1956, *Royal Society of London Philosophical Transactions Series A*, **249**, 65
- Osaki, Y. 1975, *Publication of the Astronomical Society of Japan*, **27**, 237
- Osaki, Y. 1990, in *Lecture Notes in Physics*, Berlin Springer Verlag, Vol. 367, *Progress of Seismology of the Sun and Stars*, ed. Y. Osaki & H. Shibahashi, 75
- Pallé, P. L., Roca Cortés, T., Gelly, B., Pérez-Hernández, F., & the GOLF Team. 1998, in *ESA Special Publication*, Vol. 418, *Structure and Dynamics of the Interior of the Sun and Sun-like Stars*, ed. S. Korzennik, 279
- Pamyatnykh, A. A. 1999, *Acta Astronomica*, **49**, 119
- Pinsonneault, M. H., Kawaler, S. D., Sofia, S., & Demarque, P. 1989, *ApJ*, **338**, 424

- Polnarev, A. G., Roxburgh, I. W., & Baskaran, D. 2009, *Phys. Review D*, **79**, 082001
- Poyet, J.-P. 1983, *Sol. Phys.*, **82**, 267
- Press, W. H. 1981, *ApJ*, **245**, 286
- Press, W. H. & Rybicki, G. B. 1989, *ApJ*, **338**, 277
- Proffitt, C. R. & Michaud, G. 1991, *ApJ*, **380**, 238
- Provost, J. 2008, *Astrophysics and Space Science*, **316**, 135
- Provost, J. & Berthomieu, G. 1986, *A&A*, **165**, 218
- Provost, J., Berthomieu, G., & Morel, P. 2000, *A&A*, **353**, 775
- Rashba, T. I., Semikoz, V. B., Turck-Chièze, S., & Valle, J. W. F. 2007, *MNRAS*, **377**, 453
- Rashba, T. I., Semikoz, V. B., & Valle, J. W. F. 2006, *MNRAS*, **370**, 845
- Richard, O., Vauclair, S., Charbonnel, C., & Dziembowski, W. A. 1996, *A&A*, **312**, 1000
- Rogers, T. M. & Glatzmaier, G. A. 2005, *MNRAS*, **364**, 1135
- Rogers, T. M., MacGregor, K. B., & Glatzmaier, G. A. 2008, *MNRAS*, **387**, 616
- Rosenbluth, M. N. & Bahcall, J. N. 1973, *ApJ*, **184**, 9
- Rosenthal, C. S. 1998, *ApJ*, **508**, 864
- Saio, H. 1980, *ApJ*, **240**, 685
- Salabert, D. & Garcia, R. A. 2008, *ArXiv e-prints*, 0810.1696
- Salabert, D., Leibacher, J., Appourchaux, T., & Hill, F. 2009, *ApJ*, **696**, 653
- Salabert, D., Turck-Chièze, S., Barriere, J. C., et al. 2008, *ArXiv e-prints*, 0810.3393
- Samadi, R., Belkacem, K., Goupil, M.-J., Dupret, M.-A., & Kupka, F. 2008, *ArXiv e-prints*, 806
- Samadi, R., Georgobiani, D., Trampedach, R., et al. 2007, *A&A*, **463**, 297
- Samadi, R. & Goupil, M.-J. 2001, *A&A*, **370**, 136
- Samadi, R., Goupil, M.-J., Alecian, E., et al. 2005, *J. Astrophys. Atr.*, **26**, 171
- Samadi, R., Nordlund, Å., Stein, R. F., Goupil, M.-J., & Roxburgh, I. 2003a, *A&A*, **404**, 1129
- Samadi, R., Nordlund, Å., Stein, R. F., Goupil, M.-J., & Roxburgh, I. 2003b, *A&A*, **403**, 303
- Sawford, B. L. 1991, *Physics of Fluids*, **3**, 1577
- Scargle, J. D. 1982, *ApJ*, **263**, 835
- Schatzman, E. 1993, *A&A*, **279**, 431
- Schatzman, E. 1996, *Sol. Phys.*, **169**, 245
- Scherrer, P. H., Bogart, R. S., Bush, R. I., et al. 1995, *Sol. Phys.*, **162**, 129
- Scherrer, P. H., Wilcox, J. M., Kotov, V. A., Severny, A. B., & Tsap, T. T. 1979, *Nature*, **277**, 635
- Schou, J. 1992, PhD thesis, Århus Universitet, Denmark
- Scuffaire, R. 1974, *A&A*, **36**, 107
- Sellke, T., Bayarri, M. J., & Berger, J. 2001, *The American Statistician*, **55**, 62
- Serenelli, A. M., Bahcall, J. N., Basu, S., & Pinsonneault, M. H. 2004, in *Helio- and Asteroseismology: Towards a Golden Future*, ed. D. Danesy. (ESA SP-559, ESA Publications Division, Noordwijk, The Netherlands), 624
- Severnyi, A. B., Kotov, V. A., & Tsap, T. T. 1976, *Nature*, **259**, 87
- Shannon, C. E. 1949, *Proceedings of the IRE*, **37**, 10
- Shibahashi, H., Osaki, Y., & Unno, W. 1975, *Publication of the Astronomical Society of Japan*, **27**, 401
- Spiegel, E. A. & Zahn, J.-P. 1992, *A&A*, **265**, 106
- Stahn, T. & Gizon, L. 2008, *Sol. Phys.*, **251**, 31
- Stein, R., Georgobiani, D., Trampedach, R., Ludwig, H.-G., & Nordlund, Å. 2004, *Sol. Phys.*, **220**, 229
- Stein, R. F. 1966, PhD thesis, Goddard Space Flight Center & Columbia University, N.Y.
- Stein, R. F. 1967, *Sol. Phys.*, **2**, 385
- Stein, R. F. & Nordlund, Å. 2001, *ApJ*, **546**, 585
- Sturrock, P. A. & Scargle, J. D. 2009, *ArXiv e-prints*, 0904.1713
- Sturrock, P. A., Scargle, J. D., Walther, G., & Wheatland, M. S. 2005, *Sol. Phys.*, **227**, 137
- Takata, M. 2006, *Publication of the Astronomical Society of Japan*, **58**, 893
- Talon, S. & Charbonnel, C. 2003, *A&A*, **405**, 1025
- Talon, S., Kumar, P., & Zahn, J.-P. 2002, *ApJ Letters*, **574**, L175
- Talon, S. & Zahn, J.-P. 1998, *A&A*, **329**, 315
- Tassoul, M. 1980, *ApJS*, **43**, 469
- Thompson, M. J., Toomre, J., Anderson, E., et al. 1996, *Science*, **272**, 1300
- Thomson, D. J. 1982, in *Proc. IEEE*, Vol. **70**, 1055
- Thomson, D. J., MacLennan, C. G., & Lanzerotti, L. J. 1995, *Nature*, **376**, 139

- Thoul, A., Bahcall, J. N., & Loeb, A. 1994, *ApJ*, **421**, 828
- Toner, C. G., Jefferies, S. M., & Toutain, T. 1999, *ApJ Letters*, **518**, L127
- Toutain, T., Appourchaux, T., Baudin, F., et al. 1997, *Sol. Phys.*, **175**, 311
- Toutain, T., Appourchaux, T., Fröhlich, C., et al. 1998, *ApJ*, **506**, L147
- Toutain, T., Berthomieu, G., & Provost, J. 1999, *A&A*, **344**, 188
- Toutain, T. & Fröhlich, C. 1992, *A&A*, **257**, 287
- Toutain, T. & Kosovichev, A. G. 2000, *ApJ Letters*, **534**, L211
- Turck-Chièze, S., Carton, P.-H., Ballot, J., et al. 2006, *Advances in Space Research*, **38**, 1812
- Turck-Chièze, S., Couvidat, S., Kosovichev, A. G., et al. 2001, *ApJ*, **555**, L69
- Turck-Chièze, S., Couvidat, S., Piau, L., et al. 2004, *Phys. Rev. Letters*, **93**, 211102
- Turck-Chièze, S., Däppen, W., Fossat, E., et al. 1993, *Physics Reports*, **230**, 57
- Turck-Chièze, S., García, R. A., Couvidat, S., et al. 2004, *ApJ*, **604**, 455
- Unno, W. 1966, *Transactions of the International Astronomical Union, Series B*, **12**, 555
- Unno, W. 1967, *Publication of the Astronomical Society of Japan*, **19**, 140
- Unno, W., Osaki, Y., Ando, H., Saio, H., & Shibahashi, H. 1989, *Nonradial oscillations of stars* (University of Tokyo Press, 1989, 2nd ed.)
- van der Raay, H. B. 1988, in *Seismology of the Sun and Sun-Like Stars*, ed. V. Domingo & E. Rolfe (ESA SP-286, ESA Publications Division, Noordwijk, The Netherlands), 339
- Vandakurov, Y. V. 1968, *Soviet Astronomy*, **11**, 630
- Varadi, F., Pap, J. M., Ulrich, R. K., Bertello, L., & Henney, C. J. 1999, *ApJ*, **526**, 1052
- Varadi, F., Ulrich, R. K., Bertello, L., & Henney, C. J. 2000, *ApJ Letters*, **528**, L53
- Vecchio, A., Carbone, V., Lepreti, F., et al. 2005, *Physical Review Letters*, **95**, 061102
- Wachter, R., Schou, J., Kosovichev, A., & Scherrer, P. H. 2002, in *Symposium on From Solar Min to Max: Half a Solar Cycle with SOHO*, SOHO-11, A symposium dedicated to Roger M. Bonnet, ESA SP-508, ed. C. Fröhlich & A. Wilson (ESA Publications Division, Noordwijk, The Netherlands), 115
- Waelkens, C. 1991, *A&A*, **246**, 453
- Wentzel, D. G. 1987, *ApJ*, **319**, 966
- Wersinger, J.-M., Finn, J. M., & Ott, E. 1980, *Phys. Fluids*, **23**, 1142
- Willson, R. C. 1979, *Applied Optics*, **18**, 179
- Winget, D. E. & Kepler, S. O. 2008, *Ann. Rev. Astron. Astrophys.*, **46**, 157
- Wolff, C. L. & O'Donovan, A. E. 2007, *ApJ*, **661**, 568
- Woodard, M. & Hudson, H. 1983, *Sol. Phys.*, **82**, 67
- Yang, W. M. & Bi, S. L. 2007, *ApJ*, **658**, L67
- Zaatri, A., Provost, J., Berthomieu, G., Morel, P., & Corbard, T. 2006, in *Beyond the spherical Sun*, ed. K. Fletcher & M. Thompson (ESA SP-624, ESA Publications Division, Noordwijk, The Netherlands), 92.1
- Zaatri, A., Provost, J., Berthomieu, G., Morel, P., & Corbard, T. 2007, *A&A*, **469**, 1145
- Zahn, J.-P. 1991, *A&A*, **252**, 179